

University of Warwick institutional repository: <http://go.warwick.ac.uk/wrap>

A Thesis Submitted for the Degree of PhD at the University of Warwick

<http://go.warwick.ac.uk/wrap/56347>

This thesis is made available online and is protected by original copyright.

Please scroll down to view the document itself.

Please refer to the repository record for this item for information to help you to cite it. Our policy information is available from the repository home page.

Library Declaration and Deposit Agreement

1. STUDENT DETAILS

Please complete the following:

Full name: RUTH MIRANDA SANDERSON

University ID number: 9532816

2. THESIS DEPOSIT

2.1 I understand that under my registration at the University, I am required to deposit my thesis with the University in BOTH hard copy and in digital format. The digital version should normally be saved as a single pdf file.

2.2 The hard copy will be housed in the University Library. The digital version will be deposited in the University's Institutional Repository (WRAP). Unless otherwise indicated (see 2.3 below) this will be made openly accessible on the Internet and will be supplied to the British Library to be made available online via its Electronic Theses Online Service (EThOS) service.

[At present, theses submitted for a Master's degree by Research (MA, MSc, LLM, MS or MMedSci) are not being deposited in WRAP and not being made available via EThOS. This may change in future.]

2.3 In exceptional circumstances, the Chair of the Board of Graduate Studies may grant permission for an embargo to be placed on public access to the hard copy thesis for a limited period. It is also possible to apply separately for an embargo on the digital version. (Further information is available in the *Guide to Examinations for Higher Degrees by Research*.)

2.4 If you are depositing a thesis for a Master's degree by Research, please complete section (a) below. For all other research degrees, please complete both sections (a) and (b) below:

(a) Hard Copy

I hereby deposit a hard copy of my thesis in the University Library to be made publicly available to readers (please delete as appropriate) EITHER immediately OR after an embargo period of FIVE months/years as agreed by the Chair of the Board of Graduate Studies.

I agree that my thesis may be photocopied. YES / ~~NO~~ (Please delete as appropriate)

(b) Digital Copy

I hereby deposit a digital copy of my thesis to be held in WRAP and made available via EThOS.

Please choose one of the following options:

EITHER My thesis can be made publicly available online. YES / NO (Please delete as appropriate)

OR My thesis can be made publicly available only after.....[date] (Please give date) 05/02/2018
YES / ~~NO~~ (Please delete as appropriate)

OR My full thesis cannot be made publicly available online but I am submitting a separately identified additional, abridged version that can be made available online.

YES / NO (Please delete as appropriate)

OR My thesis cannot be made publicly available online.

YES / NO (Please delete as appropriate)

3. GRANTING OF NON-EXCLUSIVE RIGHTS

Whether I deposit my Work personally or through an assistant or other agent, I agree to the following:

Rights granted to the University of Warwick and the British Library and the user of the thesis through this agreement are non-exclusive. I retain all rights in the thesis in its present version or future versions. I agree that the institutional repository administrators and the British Library or their agents may, without changing content, digitise and migrate the thesis to any medium or format for the purpose of future preservation and accessibility.

4. DECLARATIONS

(a) I DECLARE THAT:

- I am the author and owner of the copyright in the thesis and/or I have the authority of the authors and owners of the copyright in the thesis to make this agreement. Reproduction of any part of this thesis for teaching or in academic or other forms of publication is subject to the normal limitations on the use of copyrighted materials and to the proper and full acknowledgement of its source.
- The digital version of the thesis I am supplying is the same version as the final, hard-bound copy submitted in completion of my degree, once any minor corrections have been completed.
- I have exercised reasonable care to ensure that the thesis is original, and does not to the best of my knowledge break any UK law or other Intellectual Property Right, or contain any confidential material.
- I understand that, through the medium of the Internet, files will be available to automated agents, and may be searched and copied by, for example, text mining and plagiarism detection software.


(b) IF I HAVE AGREED (in Section 2 above) TO MAKE MY THESIS PUBLICLY AVAILABLE DIGITALLY, I ALSO DECLARE THAT:

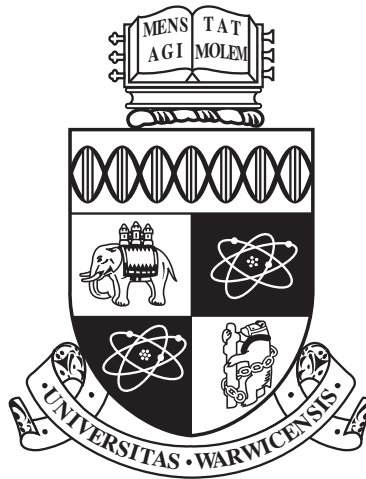
- I grant the University of Warwick and the British Library a licence to make available on the Internet the thesis in digitised format through the Institutional Repository and through the British Library via the EThOS service.
- If my thesis does include any substantial subsidiary material owned by third-party copyright holders, I have sought and obtained permission to include it in any version of my thesis available in digital format and that this permission encompasses the rights that I have granted to the University of Warwick and to the British Library.

5. LEGAL INFRINGEMENTS

I understand that neither the University of Warwick nor the British Library have any obligation to take legal action on behalf of myself, or other rights holders, in the event of infringement of intellectual property rights, breach of contract or of any other right, in the thesis.

Please sign this agreement and return it to the Graduate School Office when you submit your thesis.

Student's signature:  Date: 05/02/2013



Quantitative Studies in Guided Wave Inspection of Pipelines

by

Ruth Sanderson

Thesis

Submitted to the University of Warwick

for the degree of

Doctor of Philosophy

Engineering

October 2012

THE UNIVERSITY OF
WARWICK

Contents

List of Tables	v
List of Figures	vi
Acknowledgments	xvi
Declarations	xvii
Abstract	xviii
Chapter 1 Introduction	1
1.1 Overview	1
1.2 Motivation	1
1.3 Advantages and current limitations of long-range guided wave inspection	2
1.4 Research methodology	3
1.5 Organisation of thesis	4
Chapter 2 Fundamentals of Guided Waves in Pipes	5
2.1 Introduction	5
2.2 Guided waves	5
2.3 Nomenclature of guided wave modes	6
2.4 Wave mode displacement characteristics	7
2.5 Time and frequency domain	9
2.6 Excitation and bandwidth	9
2.7 Phase and group velocity	11
2.8 Dispersion and dispersion curves	13
2.9 Transduction	14

Chapter 3	Review of Guided Wave Inspection of Pipes	16
3.1	Introduction	16
3.2	Early research into guided waves in pipes	16
3.3	Commercial implementation of guided wave pipe inspection	18
3.4	Recent research into guided wave inspection	19
3.5	Modelling of guided wave inspection	21
3.6	Flaw sizing and characterisation using guided waves	23
3.7	Interactions between multiple flaws	24
3.8	Interaction of guided waves with pipe bends	25
Chapter 4	Analytical Model for Straight Pipe	27
4.1	Introduction	27
4.2	Guided wave inspection optimisation	28
4.3	Approach	29
4.3.1	Excitability	29
4.3.2	Application to pipes	33
4.3.3	Analytical model formulation	34
4.4	Comparison with finite element modelling results	36
4.5	Experimental validation	41
4.6	Discussion	44
4.6.1	Potential applications	44
4.6.2	Potential enhancements	44
4.7	Conclusions	46
Chapter 5	Flaw Sizing	48
5.1	Introduction	48
5.2	Acknowledgements	49
5.3	Flaw sizing procedure	49
5.3.1	General Method	49
5.3.2	Enhancement and practical application	53
5.4	Characteristics of real corrosion flaws	54
5.5	Finite element analysis	55
5.5.1	Regular shaped flaws	55
5.5.2	Real corrosion flaws	57
5.6	Experimental measurements	60
5.6.1	Overview	60
5.6.2	6" pipe	60
5.6.3	8" pipe	63

5.6.4	12" pipe	64
5.6.5	16" pipe	67
5.6.6	18" pipe	67
5.6.7	24" pipe	69
5.6.8	Assessment of limitations	71
5.7	Discussion	74
5.8	Conclusions	76
Chapter 6	Multiple Flaws	77
6.1	Introduction	77
6.2	Analytical model concept	78
6.3	Analytical model for a single flaw	78
6.3.1	Reflection coefficients for a single flaw	78
6.3.2	Calculation of R_f	82
6.3.3	Transmission coefficients for a single flaw	82
6.4	Analytical model for multiple flaws	83
6.5	Experimental validation	87
6.6	Dependence of R_f and T_f	88
6.7	Verification of analytical model for multiple flaws	91
6.8	Limitations of analytical model	93
6.9	Conclusions	96
Chapter 7	Behaviour of Guided Waves in Pipe Bends	98
7.1	Introduction	98
7.2	Behaviour in pipe bends	99
7.2.1	Approach	99
7.2.2	Finite element modelling results	101
7.2.3	Effect of wall thickness variation in the bend	103
7.3	Experimental validation	109
7.4	Analytical model	112
7.4.1	Concept	112
7.4.2	Formulation for a pipe bend example	112
7.4.3	Verification	114
7.5	Reconstructing signals from flaws beyond pipe bends	118
7.6	Generation of pure axisymmetric wave modes beyond pipe bends	121
7.7	Discussion	121
7.8	Conclusions	123

Chapter 8	Conclusions and Recommendations for Future Work	125
8.1	Conclusions	125
8.2	Recommendations for future work	127

List of Tables

5.1	Summary of features from ApplusRTD laser profilometry database .	54
5.2	Details of the real corrosion flaws that were modelled	58
5.3	Experimental flaw sizing results for 6" pipe, showing dimensions measured using guided waves.	61
5.4	Approximate dimensions of flaws in the 8" pipe.	64
5.5	Approximate dimensions of flaws in the 12" pipe.	65
5.6	Flaw sizing guided wave measurements for flaws in a 323.8mm outer diameter, 10.31mm wall thickness pipe.	66
7.1	Wall thickness measurements in the middle of the bend	106

List of Figures

2.1	Illustration of bulk wave characteristics using a finite element prediction of the von-Mises stress field for a 3-cycle 4MHz pulse.	6
2.2	Guided wave modes in an 88.9mm outer diameter, 5.49mm wall thickness steel pipe around 40kHz.	8
2.3	10-cycle 40kHz Hann-windowed pulse	10
2.4	Illustration of phase and group velocity for a 10-cycle 70kHz pulse example.	12
2.5	Dispersion curves for an 88.9mm outer diameter, 5.49mm wall thickness steel pipe for 0 to 25kHz.	13
2.6	Dispersion curves for an 88.9mm outer diameter, 5.49mm wall thickness steel pipe for 0 to 80kHz.	14
2.7	Photograph of the Teletest multimode transducer array.	15
3.1	Illustration of the interaction of guided waves with a flaw in a pipe. .	17
3.2	Schematic of the three main commercial guided wave inspection systems that are currently available.	19
4.1	Frequency spectrum for 4-cycle 1MHz Hann-windowed excitation . .	30
4.2	Schematic of the 2D model used to calculate excitability in a 1mm thick Aluminium plate.	31
4.3	Comparison between existing technique (points) and new broadband FFT method (lines) for calculation of excitability in 1mm aluminium plate	32
4.4	Ratio of received amplitude to excited amplitude for a range of excitation frequencies around 56kHz in an 88.9mm outer diameter, 5.49mm wall thickness pipe arising from a single node excitation in the torsional direction.	35

4.5	Comparison of analytical model and transient finite element result for torsional displacement history 0.5m away from 28-cycle 56kHz excitation.	37
4.6	Comparison of analytical model and transient finite element result for torsional displacement history 1m away from 28-cycle 56kHz excitation.	38
4.7	Comparison of analytical model and transient finite element result for torsional displacement history 1.5m away from 28-cycle 56kHz excitation.	38
4.8	Comparison of analytical model and transient finite element result for torsional displacement history 2m away from 28-cycle 56kHz excitation.	38
4.9	Comparison of analytical model and transient finite element result for torsional displacement history 2.5m away from 28-cycle 56kHz excitation.	39
4.10	Comparison of analytical formulation using MathCAD and transient finite element result for torsional displacement along the length of an 88.9mm outer diameter, 5.49mm wall thickness steel pipe at 500 μ s (immediately after a 28-cycle 56kHz pulse has been introduced).	39
4.11	Comparison of analytical formulation using MathCAD and transient finite element result for torsional displacement along the length of an 88.9mm outer diameter, 5.49mm wall thickness steel pipe at 1000 μ s.	40
4.12	Polar plot of analytically predicted displacement distribution around the circumference of the pipe at 1.5m from source.	40
4.13	Experimental layout.	41
4.14	Photograph of experimental setup.	42
4.15	Measured amplitude against time 1.5m from excitation, in line with excitation.	43
4.16	Measured amplitude against time 1.5m from excitation, at 30° circumferential location from excitation.	43
4.17	Comparison of measured amplitude along the length pipe in line with the excitation.	43
4.18	Phase velocity dispersion curves for an 88.9mm outer diameter, 5.49mm wall thickness steel pipe over frequency range of main lobe for a 28-cycle 56kHz toneburst excitation.	46
5.1	Flaw prediction amplitude responses from various flaw through wall extent models over increasing flaw circumferential extent.	50

5.2	Reflection of the first four wave modes with respect to flaw circumferential extent.	51
5.3	Illustration of the procedure for determination of the circumferential extent of a flaw using the ratio of the reflected axisymmetric wave mode to the sum of the reflected flexural wave modes.	52
5.4	Schematic of a notch-like flaw in cross section.	52
5.5	Gradient of flaw sizing trendline against number of flexural wave modes included in the equation for three flaw sizes.	53
5.6	Finite element model used to predict reflections from a flaw in a 168.3mm outer diameter, 7.11mm wall thickness steel pipe.	56
5.7	Through wall extent measurement from procedure applied to FE predictions against actual through wall extent for a range of flaws, test parameters and pipe dimensions.	57
5.8	Close up isometric image of finite element mesh and plan view of Image 27 from the real corrosion flaw database.	58
5.9	Predicted time waveforms for the first four wave modes reflecting from Image 26 from the real corrosion flaw database.	59
5.10	Actual flaw circumferential extent against flaw sizing parameter, P for the real corrosion flaws modelled.	59
5.11	Layout of flaw sizing experiments in 6" pipe.	61
5.12	Actual flaw circumferential extent against flaw sizing parameter, P for the flaws measured in 6inch pipe.	62
5.13	Experimentally measured amplitude of T(0,1) family wave modes reflected from flaw 6-1.	63
5.14	Layout of flaw sizing experiments in 8" pipe.	63
5.15	Actual flaw circumferential extent against flaw sizing parameter, P for the flaws measured in 8 inch pipe.	64
5.16	Layout of flaw sizing experiments in 12" pipe.	65
5.17	Actual flaw circumferential extent against flaw sizing parameter, P for the flaws measured in 12 inch pipe.	66
5.18	Layout of flaw sizing experiments in 16" pipe.	67
5.19	Layout of flaw sizing experiments in 18" pipe.	68
5.20	The flaw assessed in the 24 inch pipe.	69
5.21	Layout of flaw sizing experiments in 24" pipe.	70
5.22	Actual flaw circumferential extent against flaw sizing parameter, P for the flaws measured in 24 inch pipe.	70

5.23	Actual flaw circumferential extent against enhanced flaw sizing parameter for the flaws measured in 24 inch pipe.	71
5.24	Experimentally measured through wall extent measurement against actual through wall extent for a range of flaws, test parameters and pipe dimensions (11 results plotted).	72
5.25	Experimentally measured circumferential extent measurement against actual circumferential extent for a range of flaws, test parameters and pipe dimensions (11 results plotted).	73
5.26	Error in through wall extent measurement against circumferential extent of the flaw.	75
6.1	Nomenclature for calculation of reflectivity with respect to flaw circumferential extent.	79
6.2	Reflection coefficients against flaw circumferential extent for a 100% wall thickness flaw.	81
6.3	Nomenclature for calculation of transmission with respect to flaw circumferential extent.	82
6.4	Transmission coefficients against flaw circumferential extent for a 100% wall thickness flaw.	84
6.5	Simplified example showing the four different ways in which $T(0,1)$ is received at the excitation location.	85
6.6	Comparison between finite element results (lines) and experiment (points) for a range of flaws normalised by through wall extent. . . .	88
6.7	Finite element predicted variation of R_f and T_f values with frequency in a 168.3mm outer diameter steel pipe with 7.11mm wall thickness.	89
6.8	Finite element predicted variation of R_f values with through wall extent in a 168.3mm outer diameter steel pipe with 7.11mm wall thickness.	90
6.9	Finite element predicted variation of R_f values with axial extent in a 168.3mm outer diameter steel pipe with 7.11mm wall thickness. . .	90
6.10	Schematic of finite element model used to predict the guided wave response for two flaws at different axial locations.	91
6.11	Comparison between analytical model for single flaw analytical model predictions for a 50% wall thickness flaw seen through a 180°, 50% wall thickness flaw and finite element results for the two flaw example. . .	92

6.12	Comparison between analytical model and finite element analysis for a 50% wall thickness flaw seen through a 30° flaw 50% wall thickness flaw with the second flaw at an angle of 45°	94
7.1	Layout of finite element model and pipe bend experiment.	100
7.2	Finite element predictions of wave modes after propagation of T(0,1) around a 90° bend with a 229mm mean bend radius in an 88.9mm outer diameter, 5.49mm wall thickness steel pipe.	102
7.3	Finite element predictions of wave modes after propagation of F(1,2) at 60° around a 90° bend with a 229mm mean bend radius in an 88.9mm outer diameter, 5.49mm wall thickness steel pipe.	104
7.4	Orientation of wave modes received after an excitation of F(1,2) before a 90° bend with a 229mm mean bend radius in an 88.9mm outer diameter, 5.49mm wall thickness steel pipe.	105
7.5	Amplitude of T(0,1) after a 229mm mean radius, 90° bend in an 88.9mm outer diameter, 5.49mm wall thickness steel pipe from excitation of flexural waves modes at different orientations before the bend.	105
7.6	Schematic of cross section of centre of pipe bend showing how the wall thickness was varied in the model to approximate the wall thickness changed caused by induction bending.	106
7.7	Finite element predictions of wave modes after propagation of T(0,1) around a 90° bend with a 229mm mean bend radius in an 88.9mm outer diameter, 5.49mm wall thickness steel pipe with thickness variations in the bend.	108
7.8	Experimentally measured wave modes after propagation of T(0,1) around a 90° bend with a 229mm mean bend radius in an 88.9mm outer diameter, 5.49mm wall thickness steel pipe.	110
7.9	Experimentally measured versus finite element predicted F(1,2) wave mode received after propagation of F(1,2) around a 90° bend with a 229mm mean bend radius in an 88.9mm outer diameter, 5.49mm wall thickness steel pipe.	111
7.10	Experimentally measured versus finite element predicted F(2,2) wave mode received after propagation of F(1,2) around a 90° bend with a 229mm mean bend radius in an 88.9mm outer diameter, 5.49mm wall thickness steel pipe.	111

7.11	Layout of finite element model of an 88.9mm outer diameter, 5.49mm wall thickness steel pipe with a 229mm bend radius used to test the analytical model.	115
7.12	Comparison between analytical model and FEA for T(0,1) response from a 150° flaw beyond a 229mm pipe bend in an 88.9mm outer diameter, 5.49mm wall thickness steel pipe for a flaw at 0°.	116
7.13	Comparison between analytical model and FEA for F(1,2) response from a 150° flaw beyond a 229mm pipe bend in an 88.9mm outer diameter, 5.49mm wall thickness steel pipe for a flaw at 0°.	116
7.14	Comparison between analytical model and FEA for T(0,1) response from a 150° flaw beyond a 229mm pipe bend in an 88.9mm outer diameter, 5.49mm wall thickness steel pipe for a flaw at 90°.	117
7.15	Comparison between analytical model and FEA for F(1,2) response at 90° from a 150° flaw beyond a 229mm pipe bend in an 88.9mm outer diameter, 5.49mm wall thickness steel pipe for a flaw at 90°.	117
7.16	Comparison between analytically reconstructed T(0,1) signals from a 150° flaw beyond a pipe bend with finite element for T(0,1) signals from a 150° flaw in straight pipe.	119
7.17	Comparison between analytically reconstructed F(1,2) signals from a 150° flaw beyond a pipe bend with finite element for F(1,2) signals from a 150° flaw in straight pipe.	120
7.18	Predicted von-Mises stress field just after time reversed pulse has propagated around the bend. The signal beyond the bend is observed to be close to pure axisymmetric.	121

Publications Arising From the Doctorate

- RMS1** R Sanderson and P P Catton. Flaw Sizing in Pipes Using Long-Range Guided Wave Testing. *Review of Progress in Quantitative Nondestructive Evaluation*, 2010.
- RMS2** R Sanderson and J Gao. Guided wave inspection of pipes containing bends. *BINDT conference*, 2010.
- RMS3** P Mudge, A Haig, Y Gharaibeh, P Catton, R Sanderson. Developments in Guided Wave Testing of Pipelines for Integrity Assessment. *The American Society for Non-destructive Testing (ASNDT) Fall Conference and Quality Testing Show.*, 2010.
- RMS4** P Mudge, A Haig, P Catton, Y Gharaibeh, R Sanderson. Developments in Long Range Ultrasonic testing for Pipes Using Guided Waves for Enhanced Detection and Evaluation of Metal Loss Defects. *The 10th European Conference of Non-Destructive Testing (ECNDT)*, 2010.
- RMS5** R Sanderson and P P Catton. An Analytical Model for Guided Wave Array Design for Structures of Any Cross Section. *IEEE Transactions on Ultrasonics, Ferroelectrics and Frequency Control*, 58(5), pp1016-1026, 2011.
- RMS6** R Sanderson, D Hutchins, D Billson and P Mudge. The investigation of guided wave propagation around a pipe bend using an analytical modelling approach. *Journal of the Acoustical Society of America* (submitted May 2012).
- RMS7** R Sanderson and P P Catton. The reflection of guided waves from multiple flaws in pipes. *IEEE Transactions on Ultrasonics, Ferroelectrics and Frequency Control* (submitted August 2012).

RMS8 R Sanderson. Inspection of pipe networks containing bends using long range guided waves. *BINDT conference*, 2012.

Symbols

A	Amplitude of a pulse
A_i	Amplitude of a pulse for i^{th} wave mode
B	Integer equal to 1 or 2
C	Cross sectional area loss as a ratio of pipe cross sectional area
d	Flaw through wall extent
E	Excitability
f	Frequency in Hz
f_c	Central frequency in Hz
f_{range}	Frequency bandwidth (maximum or minimum)
f_{ref}	Reference pulse
F	Fourier transform
H	Multiplier to apply effects of a pipe bend
i	Index
I	Incident pulse
j	The square root of -1
m	Wave mode index
n	Wave mode order
n_R	Order of reflected wave mode
n_I	Order of incident wave mode
n_i	Wave mode order for i^{th} wave mode
n_c	Number of cycles
P	Flaw sizing parameter
r_o	Pipe outer radius
r_i	Pipe inner radius
R	Reflection coefficient
R_f	Reflection coefficient scaling factor
S	Pulse
SF	Scaling factor for mode filtering

t	Time
T	Transmission coefficient
T_f	Transmission coefficient scaling factor
u	Displacement
U	Total displacement
v	Velocity
v_{ph}	Phase velocity
v_g	Group velocity
x, y	Distance
α, β	Angle between flaws
ϕ_f	Flaw circumferential extent
θ	Circumferential location
ω	Frequency in radians

Acknowledgments

The author would like to extend her immense gratitude to all those who have contributed to the project at Warwick University and TWI. The guidance and supervision of Prof David Hutchins, Dr Duncan Billson, Mr Peter Mudge and Dr Phil Catton has been especially valuable.

The author would also like to thank her fellow Fellows with The Royal Commission for the Exhibition of 1851. Their camaraderie was invaluable and their approach to their own work has inspired me. My friends and family have also been an unfaltering source of support and encouragement and that will always be appreciated.

Finally, the project would not have been possible without the funding provided by The Royal Commission for the Exhibition of 1851, The ERA Foundation and TWI and its industrial members. The author is eternally grateful to the individuals at those organisations who believed in me and gave me the opportunity to carry out the research presented here.

Declarations

The material presented in the thesis is the candidate's own work and the thesis has not been submitted for a degree at another university.

Abstract

Long-range guided wave inspection is a relatively new and exciting non-destructive testing technique for the detection of corrosion in pipes and pipelines. The technique has the potential to increase the extent and cost effectiveness of industrial examinations for degradation which may be unpredictable and widespread, such as corrosion. The current commercial equipment has the ability to screen 100% of the volume of tens of metres of straight pipe from a single test location. However, the technique is yet to be taken up on a large scale relative to competing technologies such as intelligent pigs. Operators generally need quantitative information, yet it is principally a screening tool. It is also suited to straight pipe and inspection beyond common features such as pipe bends can be problematic. There is therefore a need to advance guided wave technology to the point where quantitative information can be obtained from lengths of straight pipe and beyond pipe bends.

The work presented here starts with the development of an analytical model for straight pipe which can be used to design arrays and predict the propagation of guided waves. Then, existing techniques for the sizing of flaws have been built upon and practical inspection procedures developed. These procedures have been validated for a range of pipe sizes and flaw types. Next, formulae for the prediction of reflection and transmission coefficients from single flaws have been derived and used in the development of an analytical model for pipes containing multiple flaws. Finally, the effect of the presence of geometrical features such as a pipe bend has been studied. Inspection procedures have been developed that allow the signal distortion caused by a pipe bend to be corrected. This means that flaw sizing methods have the potential to be used beyond bends and in complex pipe networks.

Chapter 1

Introduction

1.1 Overview

In this chapter, the motivation behind the work is briefly explained and then the potential advantages and current limitations of guided wave inspection are discussed. Next, the approach taken for the research is described and, finally, a summary of the organisation of the thesis is provided.

1.2 Motivation

Pipelines are arguably the most efficient way to transport large amounts of oil products or natural gas over land, and as a result there are millions of kilometres of pipelines all over the world. In many cases these are aging assets. The integrity of pipelines is threatened by internal and external corrosion, environmental cracking such as stress corrosion cracking (SCC), manufacturing flaws and third party damage. Pipeline leakages or bursts are clearly a public safety, economic and environmental concern. In the United States alone, there are several pipeline accidents reported every year [PHMSA, 2012]. One high profile example is the oil spill at Prudhoe Bay in 2006 which is thought to have been caused by undetected corrosion [Meggert, 2008].

In order to ensure the safety of pipelines, regulatory bodies such as the USA's Department of Transportation's Pipeline and Hazardous Materials Safety Administration (PHMSA), require periodic inspections to be carried out. During manufacture a more thorough inspection is possible but once the pipeline is in service, access can be limited making inspection more challenging. Most pipelines are inspected using devices called pigs [Tiratsoo, 1999]. A pig is an in line inspection

(ILI) tool. It carries on-board non-destructive inspection equipment and travels inside the pipe, collecting data on the condition of the pipe as it goes.

However, there are certain situations where pigs cannot be used. For example, if the pipeline has certain types of valves, no pig launching stations or tight bends. Alternative inspection techniques are therefore of interest. Long range guided wave inspection is one option. The technique has the potential to detect corrosion-like flaws remotely from a single tool location whilst the pipe is still in service.

1.3 Advantages and current limitations of long-range guided wave inspection

Guided waves, by their nature, travel along the pipe and occupy the full volume of the pipe wall. This means that corrosion in any location within the pipe wall has the potential to be detected. The basic concept of the technique is to excite guided waves at a single tool location. The waves then propagate along the length of the pipe and reflect from features such as corrosion or welds. These reflections are received back at the tool and from knowledge of the velocity of the wave modes, the location of the feature can be determined [Viktorov, 1967].

Sound waves are attenuated within the material in which they propagate and by their surroundings. However, the attenuation of guided waves can be relatively low [Alleyne & Cawley, 1996]. In ideal conditions (i.e. uncoated pipe) guided waves can propagate over 100 metres in either direction, making it possible to screen 200 metres of pipeline from one position. Leakage could also occur into the fluid contents of the pipe. One way to overcome this is to use torsional excitations. This works best for relatively non-viscous fluids as they transfer minimal shear stress.

The main challenge in the implementation of guided wave inspection is that there are numerous possible wave modes that can propagate and, at the relatively low frequencies used, dispersion is common. This makes interpretation of the inspection results complicated. Moreover, the wavelengths are also relatively long and can be similar in size or larger than typical corrosion patches. Therefore, finding small flaws and achieving good resolution is challenging. For these reasons, the technique has so far been used commercially as a screening procedure where the results of an inspection are interpreted to give an indication of the location and approximate cross sectional area loss of the flaw. However, this is not sufficient information to allow operators to make a clear decision. For example, a uniform circumferential thinning can have the same cross sectional area loss as a deep corrosion pit and the

latter is clearly more critical than the former. Therefore, methods for transforming guided wave inspection from a screening procedure to a quantitative technique are required.

1.4 Research methodology

Finite element analysis has been used extensively as a tool for predicting and understanding the propagation and interaction of guided waves with flaws and other features. This knowledge then allowed new signal processing techniques and testing procedures to be developed. However, finite element analyses require bespoke software and take minutes or hours to process a single case. Therefore throughout the work, analytical or semi-analytical solutions were sought that would have short computation times and therefore the potential to be used on a laptop in the field. Multiple experiments were carried out in order to validate the modelling techniques.

A number of current challenges in guided wave inspection have been addressed. Firstly, an analytical model for the simulation of guided wave excitation and propagation in straight pipe was developed. The method uses finite element analysis to extract key information about the excitability of wave modes (which can be determined relatively quickly) and combines this with an analytical formula to provide fast solutions to three-dimensional guided wave problems. The method can potentially be applied to any prismatic cross section and could therefore be useful for the development of inspection procedures for structures for which guided waves are not currently fully understood. The output of the analytical model compared favourably with both transient finite element predictions and experimental data.

Next, methods for determining the through wall and circumferential extent of flaws in a range of pipe sizes were established. This is an important advancement as it potentially allows operators to make informed decisions about the fitness-for-service of the pipeline without the expense of further inspection and potentially unnecessary excavation.

There has been considerable research into the reflections and detection of guided waves from single flaws (e.g. [Demma *et al.* \[2003\]](#)) but very little has been done on the interactions between multiple flaws for commercial guided wave applications. Therefore, work was carried out into investigating the interactions between two flaws and the effect on the newly developed flaw characterisation procedures. A methodology for taking account of the presence of multiple flaws has been proposed. This allows the aforementioned flaw sizing techniques to be used on each flaw without interference from any preceding flaw.

Finally, the presence of a tight pipe bend often means it is not possible to use intelligent pigs to inspect the pipe. However, guided wave inspection of pipes with tight bends is also known to be problematic since the waves are distorted as they propagate around the bend [Demma *et al.*, 2005]. The distortion will have some effect on screening but the accuracy of flaw characterisation techniques are highly dependent on the relative amplitudes and phase relationships of wave modes, both of which are distorted by the presence of a pipe bend. Therefore, the effect of pipe bends on guided wave propagation was investigated and an analytical modelling method was developed that allows prediction and correction of the signal distortion to be made.

1.5 Organisation of thesis

Chapter 2 provides an overview to the fundamentals of long-range guided wave inspection and introduces some key topics to aid explanation of the research. A review of relevant published literature is presented in Chapter 3, which includes the state of the art in commercial application of long-range guided wave inspection. Chapter 4 describes the analytical model for straight pipe and its uses in improving and developing new inspection procedures. The development of flaw sizing procedures for a range of pipe sizes is presented in Chapter 5. This Chapter also investigates the use of guided wave flaw sizing measurement in fitness-for-service assessments of pipeline. Chapter 6 describes the research carried out into the reflection and transmission coefficients of flaws of different sizes and shapes and presents a method for determining and correcting for the interaction between two or more flaws. Chapter 7 first introduces the research into the propagation of guided waves around pipe bends and discusses their likely effects on standard inspection procedures. This Chapter goes on to present an analytical modelling method for removing the distortion caused by propagation of guided waves around pipe bends and therefore allowing the measurement of flaw size and shape beyond a pipe bend. Chapter 8 then draws conclusions on the research presented and the contributions to knowledge are critically reviewed in the context of the published literature. Finally, recommendations are made for further work resulting from the research.

Chapter 2

Fundamentals of Guided Waves in Pipes

2.1 Introduction

This Chapter is designed to introduce the reader to the characteristics of guided waves compared with conventional ultrasonic testing with which engineers are generally more familiar. Specific nomenclature and concepts such as dispersion, phase and group velocity, and wave mode types are presented. These concepts are fundamental to the understanding of guided wave behaviour and the development of new guided wave inspection methods.

2.2 Guided waves

In order to introduce the concept of guided waves, it is worth first considering the waves used in conventional ultrasonic inspection. Conventional ultrasonic inspection (which is effective over short distances), is typically used in structures which are large relative to the wavelength of the wave. In practice, the waves propagate as discrete packets within the volume, occupying a small region. The relatively high frequency waves used are commonly known as bulk waves. In a solid there are two modes of vibration, namely, compression and shear. These are illustrated in Figure 2.1 with a finite element prediction of the von-Mises stress for a 3-cycle 4MHz Hann-windowed pulse. At these frequencies, other waves also exist which propagate along the surface such as Rayleigh and Love waves [Rayleigh, 1910; Love, 1911] and these are also used for inspection (e.g. Hutchins *et al.* [1991]).

However, when the wavelength of the wave is similar to that of the dimensions

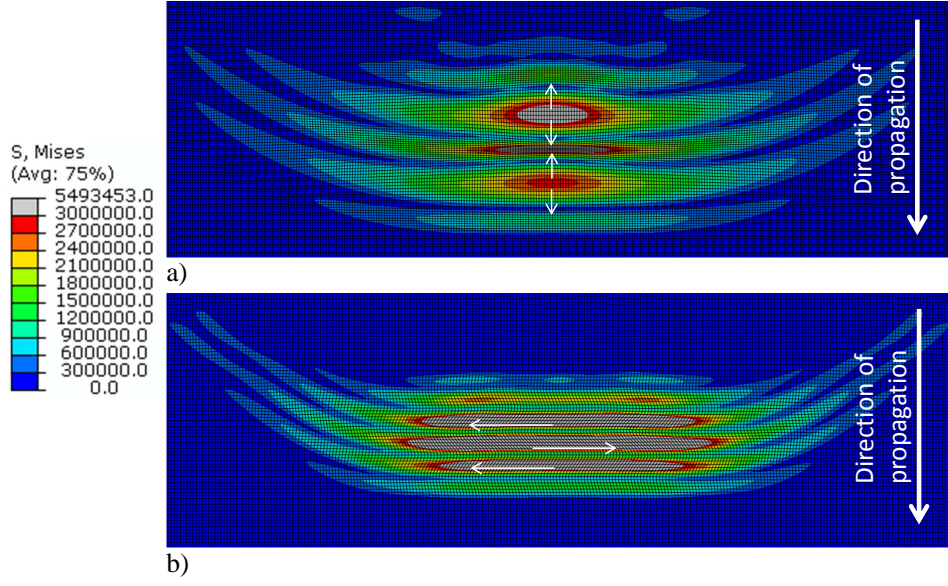


Figure 2.1: Illustration of bulk wave characteristics using a finite element prediction of the von-Mises stress field for a 3-cycle 4MHz pulse: a) Compression wave with regions of contraction and rarefaction; b) Shear wave with transverse motion.

of the cross section, the sound waves will tend to occupy the full volume of the structure and propagate along its length. These types of sound waves are commonly known as guided waves. The advantage of guided waves is full volume coverage and the ability to propagate over long distances with minimal attenuation. This means whole sections of large structures can be inspected from one tool location. One of the main disadvantages is the complexity caused by the numerous types of vibrational modes.

2.3 Nomenclature of guided wave modes

Unlike bulk waves which only have two types of vibration (shear and compression), guided waves have many possible modes of vibration. The nomenclature for these adopted throughout this thesis is that used by [Silk & Bainton \[1979\]](#) for pipes which came from earlier work done by [Meitzler \[1961\]](#).

The nomenclature uses a letter ‘T’ to stand for axisymmetric torsional displacement characteristics, ‘L’ for axisymmetric longitudinal displacement characteristics and an ‘F’ to denote wave modes with flexural displacement characteristics. After the letter, two numbers in brackets are given. The first number describes the circumferential variation of the wave mode and the second number is an index

which counts wave modes as they come into existence with increasing frequency. For example $T(0,1)$ is an axisymmetric mode with torsional displacements and it is the first of its kind, $L(0,2)$ is an axisymmetric wave mode with mainly longitudinal displacements and it's the second of its kind. $F(2,3)$ is a flexural wave mode which is the third of its kind to have a variation of two cycles around the circumference.

2.4 Wave mode displacement characteristics

At the relatively low frequencies used for guided wave testing ($< 100kHz$) and in pipe sizes commonly used for process pipework and transmission pipelines, there are three possible axisymmetric wave modes ($L(0,1)$, $T(0,1)$ and $L(0,2)$). The wave mode $L(0,1)$ generally has mainly radial displacements, $T(0,1)$ has torsional displacements and $L(0,2)$ has mainly axial displacements. Each of the three axisymmetric wave modes has a set of associated non-axisymmetric wave modes, otherwise known as flexural wave modes that have similar displacement characteristics to their respective axisymmetric wave mode. These groups of associated wave modes are often referred to as families. The velocity of the flexural wave modes in each family tends to that of the corresponding axisymmetric wave mode. Figure 2.2 shows examples of a selection of key wave modes in a section of 88.9mm outer diameter, 5.49mm wall thickness steel pipe.

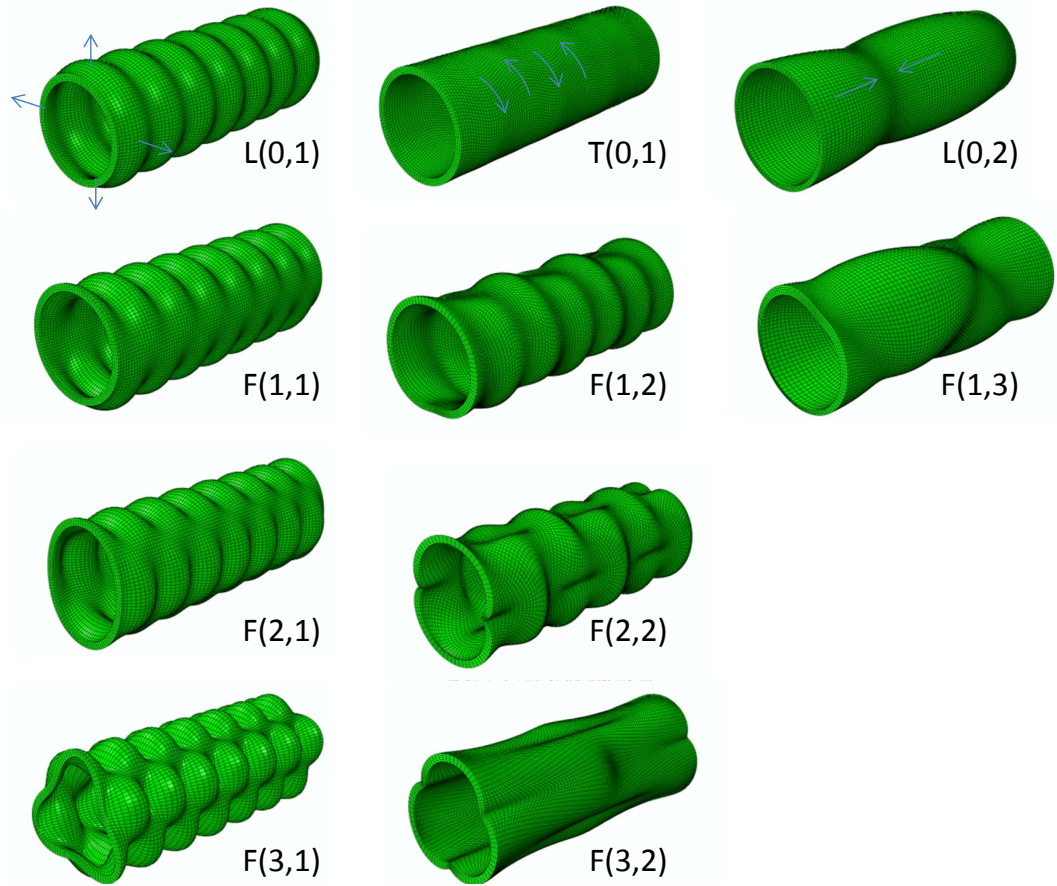


Figure 2.2: Selection of displaced shapes of guided wave modes around 40kHz illustrated through the prediction of standing waves in a section of 88.9mm outer diameter, 5.49mm wall thickness steel pipe.

2.5 Time and frequency domain

The output of most guided wave or ultrasonic inspections is a plot of amplitude of the received signals against time. This is known as a time domain waveform or A-scan. However, it is sometimes useful to convert the A-scan or parts of the A-scan into plots of amplitude against frequency. This is because the frequency components of guided wave pulses can be strongly affected by features such as flaws and therefore examining the results in the frequency domain can provide further information. The conversion is achieved using a Fourier transform or Fast Fourier transform (FFT) which is a more computationally efficient digital version of the Fourier transform. The Fourier transform is defined as follows [Croft *et al.*, 1992]:

$$F(f(t)) = F(\omega) = \int_{-\infty}^{+\infty} f(t)e^{-j\omega t}, \quad (2.1)$$

where F represents the Fourier transform operation, ω is frequency in rad/s, j is the square root of -1 and t is time.

2.6 Excitation and bandwidth

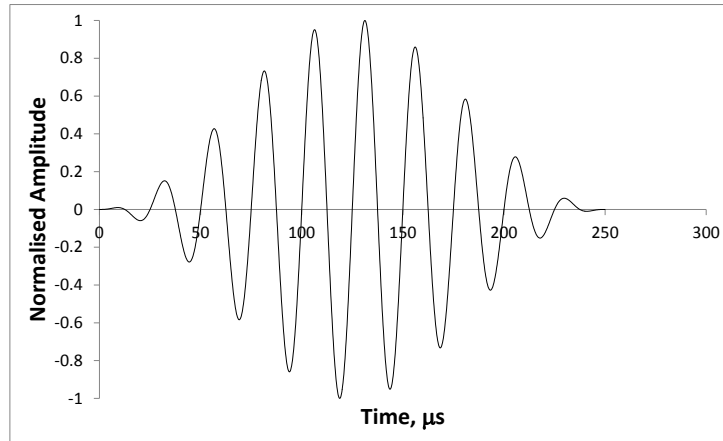
In order to clearly detect reflections from features, the excitation used in ultrasonic testing is usually a modulated toneburst or pulse with a few cycles. This is done to limit the number of cycles so that reflections can be clearly identified. An example of a 10-cycle 40kHz pulse in the time and frequency domain is shown in Figure 2.3.

This particular example is of a Hann windowed pulse with the following formula [Priemer, 1991]:

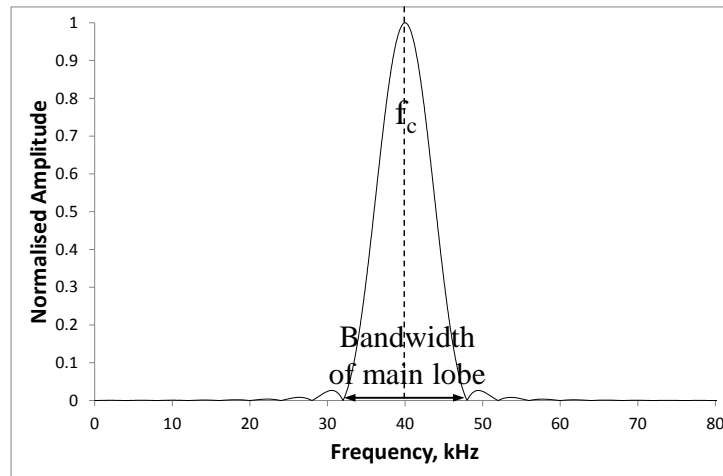
$$u = 0.5[1 - \cos(\frac{2\pi f_c t}{n_c})] \sin(2\pi f_c t), \quad (2.2)$$

where u is the displacement, f_c is the central frequency of excitation, t is time and n_c is the number of cycles.

The Hann window is a common window function and has therefore been used throughout this thesis but other similar window functions such as the Hamming, Gaussian could be used. The frequency spectrum of a Hann-windowed pulse has a main lobe centred about the central frequency of the excitation and an infinite number of side lobes decreasing in amplitude as the frequency moves away from the central frequency. The range of frequencies that the pulse occupies is called the bandwidth. There are many definitions of bandwidth. Throughout this thesis, the following formula has been used to define the frequency range of the bandwidth of



a)



b)

Figure 2.3: 10-cycle 40kHz Hann-windowed pulse: a)time domain; b)frequency domain.

the pulse:

$$f_{range} = f_c \pm \frac{(2+i)f_c}{n_c}, \quad (2.3)$$

where f_{range} is the value of the minimum or maximum possible frequency of the lobe and $i = 0$ corresponds to the main lobe and higher integers values of i correspond to the side lobes.

Finding a balance between the number of cycles and the bandwidth is important since the more cycles, the longer the pulse, and the less resolution in the time domain. The fewer cycles, the shorter the pulse and greater the resolution in the time domain but the bandwidth is increased and therefore a wider range of frequencies are excited. This is not a problem if the velocity of the wave mode is relatively constant with frequency but it becomes a potential problem if this is not the case and the wave mode is dispersive.

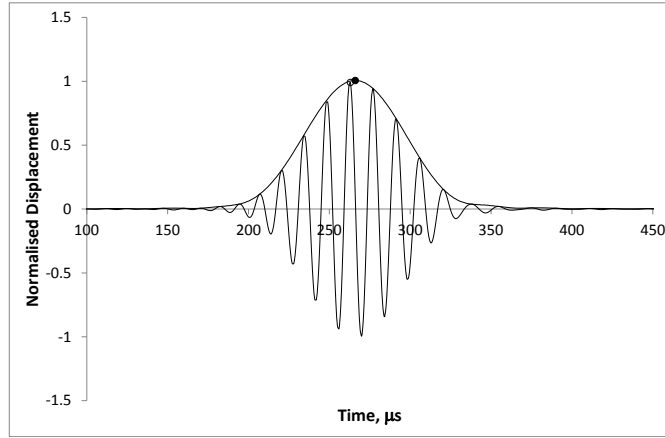
2.7 Phase and group velocity

An input with an infinite number of cycles and therefore infinitely small bandwidth will excite a wave at a single frequency. The velocity of this wave is known as the phase velocity. However, a pulse with a finite number of cycles contains a number of different frequencies. Dispersive wave modes will have a different velocity at each frequency in the bandwidth. This can cause the pulse to spread out and/or change shape as it propagates. The group velocity is the speed of the overall pulse. Figure 2.4 illustrates phase and group velocity for a 10-cycle 70kHz dispersive pulse.

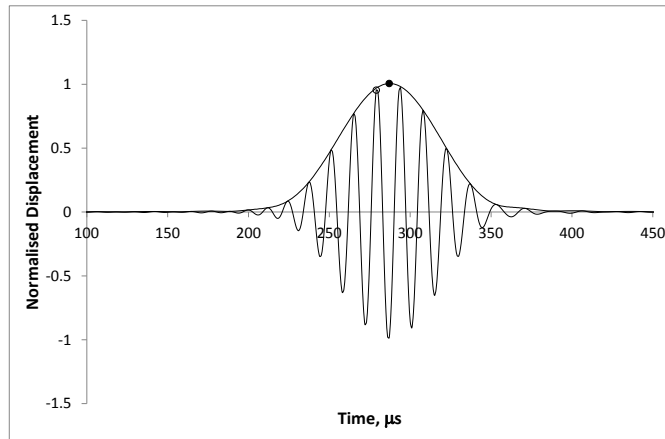
For non-dispersive wave modes the phase velocity and group velocity are equal. The phase and group velocities are related to each other through the following equation [Cheeke, 2002]:

$$v_g = \frac{v_{ph}}{1 - \frac{f}{v_{ph}} \frac{dv_{ph}}{df}}, \quad (2.4)$$

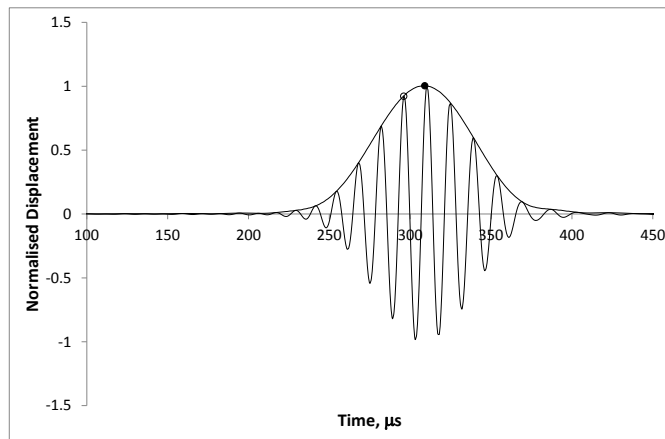
where v_g is the group velocity, v_{ph} is the phase velocity and f is frequency.



a)



b)



c)

Figure 2.4: Illustration of phase and group velocity for a 10-cycle 70kHz pulse example: a) After 0.75m propagation; b) After 0.81m propagation; c) After 0.87m propagation. The open circles represent the phase and the closed circles, the group.

2.8 Dispersion and dispersion curves

A concise way to represent the characteristics of guided wave modes is through a dispersion curve diagram. Each curve describes the relationship between the velocity and frequency of a particular wave mode. Figure 2.5 shows an example set of dispersion curves for an 88.9mm outer diameter, 5.49mm wall thickness steel pipe at low frequencies (0-25kHz). These were calculated using the ‘Disperse’ software [Pavlakovic *et al.*, 1997]. The L(0,1) family is represented by dashed lines, the T(0,1) family by continuous lines and the L(0,2) family by grey lines. The F(1,1), T(0,1) and L(0,1) wave modes exist at all frequencies. Other wave modes appear at a frequency commonly called the cut-off frequency. Figure 2.6 shows the same dispersion curves over a wider frequency range (up to 80kHz). Many more modes now exist and it is noticeable that the velocity of the flexural wave modes in each family tends to that of the corresponding axisymmetric wave mode.

Wave modes which exhibit a change in velocity with frequency are dispersive and hence their pulse shape will change as they propagate. Guided wave inspections are commonly designed to excite wave modes which have no or little dispersion [Alleyn & Cawley, 1996]. This means that their pulse shape is well-defined and the axial location of features can be more easily determined.

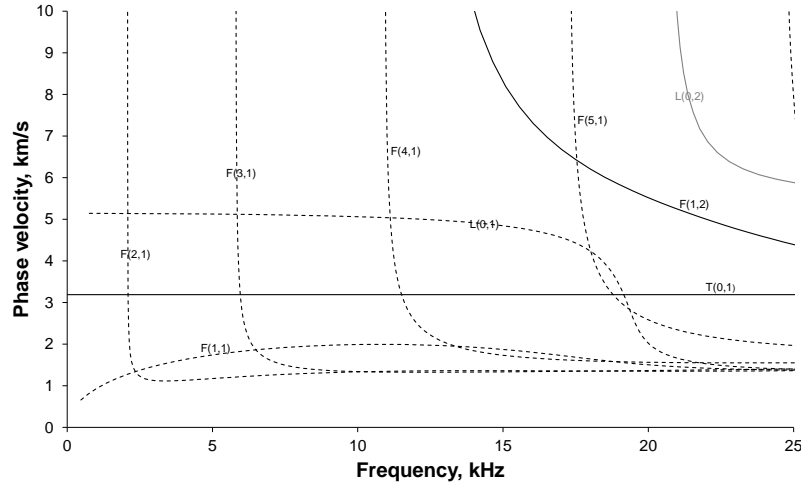


Figure 2.5: Dispersion curves for an 88.9mm outer diameter, 5.49mm wall thickness steel pipe for 0 to 25kHz.

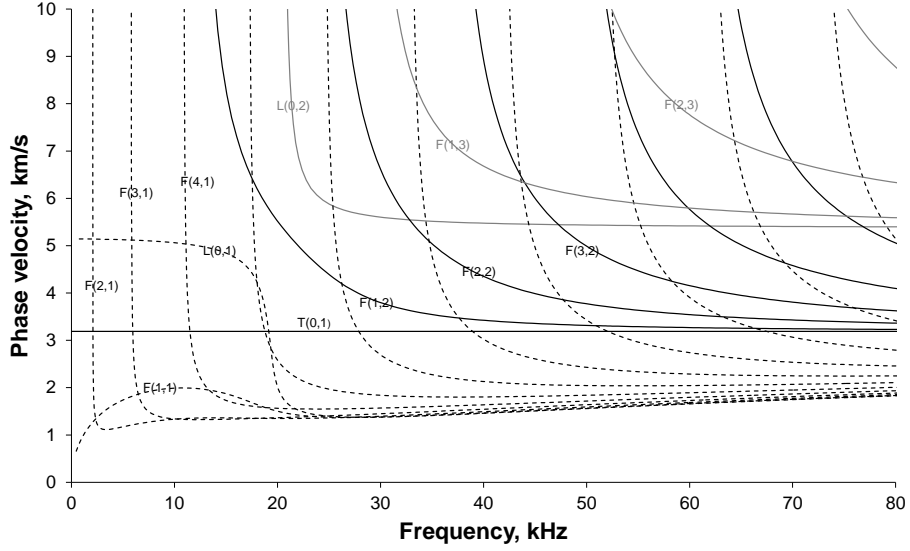


Figure 2.6: Dispersion curves for an 88.9mm outer diameter, 5.49mm wall thickness steel pipe for 0 to 80kHz.

2.9 Transduction

Sound waves can be introduced into structures in a number of ways. One of the most commonly used methods is piezoelectric elements [Cheeke, 2002]. These materials strain when a voltage is applied. The coupling of these devices to the structure is an important issue and can significantly affect array performance [Drinkwater *et al.*, 1997]. Other methods include Electromagnetic Acoustic Transducers (EMATs) and laser heating. The experimental work in this thesis was conducted using piezoelectric elements.

In order to control the excitation of guided waves in pipes, rings of transducers are typically used. The ring contains a number of individual transducers around the circumference of the pipe. This allows selective excitation or suppression of certain wave modes by applying displacement patterns that match that of the desired wave mode. Usually two or more rings are used along the length of the pipe to allow additional selective excitation or suppression of certain wave modes and control over the propagation direction. This is achieved by matching the spacing of the rings to the wavelength and the use of time delays. Figure 2.7 shows the Teletest multimode transducer array where three rings of longitudinally aligned transducers are used to excite the $L(0,2)$ wave mode in one direction and suppress the $L(0,1)$ wave mode. Then, two rings of interspersed circumferentially aligned transducers are used to

excite the $T(0,1)$ in one direction.

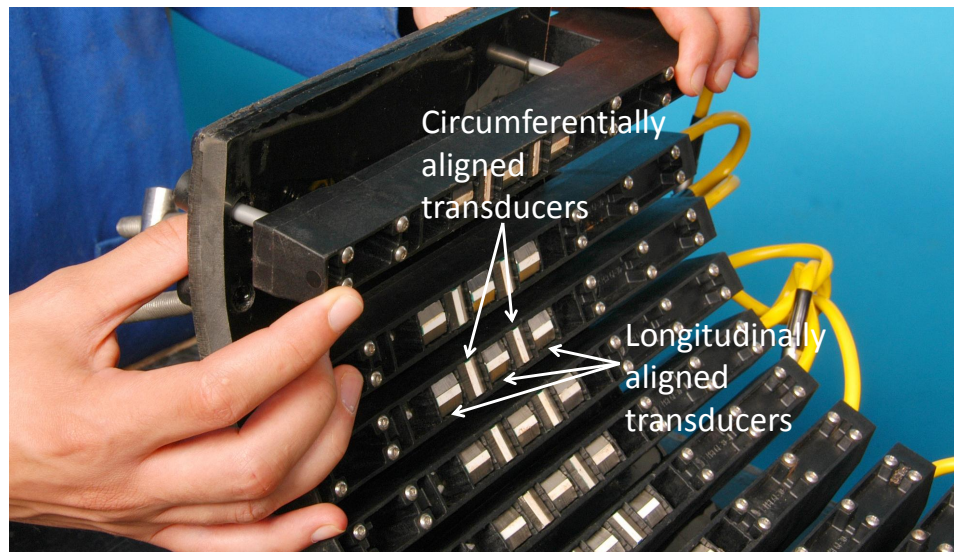


Figure 2.7: Photograph of the Teletest multimode transducer array showing three rings of longitudinally aligned transducers and two rings of circumferentially aligned transducers.

Chapter 3

Review of Guided Wave Inspection of Pipes

3.1 Introduction

Over the last two centuries, sound propagation in solids has been studied by famous physicists such as [Rayleigh \[1885\]](#) and [Lamb \[1910\]](#). In the last 20 years, the use of long range guided waves for the inspection of structures has received considerable interest from academia and industry. This chapter reviews the most significant works in relation to the present research, starting with a general overview of the guided wave inspection technique both past and more recent, and its commercial implementation. The subsequent sections then concentrate on the specific areas to which contributions have been made by this thesis. Published works are critically discussed which address modelling of guided wave propagation, the use of guided waves for flaw characterisation and the interaction of guided waves with complex features such as multiple flaws and pipe bends.

3.2 Early research into guided waves in pipes

Some early work on guided wave propagation in pipes was done by [Ghosh \[1923\]](#). He studied the propagation of longitudinal waves in isotropic hollow cylinders and formulated equations assuming axisymmetry. In the 1950s, Herrmann and Mirsky worked on solutions to the dispersion relation for axisymmetric waves. They suggested both a 3D and a shell theory and obtained good agreement between the two [[Herrmann & Mirsky, 1956](#); [Mirsky & Herrmann, 1958](#)]. Then in 1959, [Gazis \[1959\]](#) presented a generalised three-dimensional linear elastic theory. He used an early

computer to provide numerical solutions of dispersion curves for all three types of wave modes found in pipes (longitudinal, flexural and torsional) and compared his results to Herrmann and Mirsky's shell theory. He found good agreement for lower order modes but commented that the shell theory approximation would not be so appropriate for higher order modes.

Further work on propagation of guided waves in cylinders was done in the 1960s by a number of authors [Meeker & Meitzler, 1964; Fitch, 1963; Pao & Mindlin, 1960]. Meitzler [1961] studied the propagation of guided waves in wires and suggested a simplified naming system for guided waves in cylindrical structures. One of the key publications of the time was that of Viktorov [1967] who published equations for the displacement patterns and propagation characteristics of Lamb waves. He also highlighted the idea of using guided waves for the detection of flaws in engineering structures. Figure 3.1 illustrates the concept for pipes. The amplitudes of the reflection and transmission are affected by a number of variables such as frequency, wave mode type and flaw size.

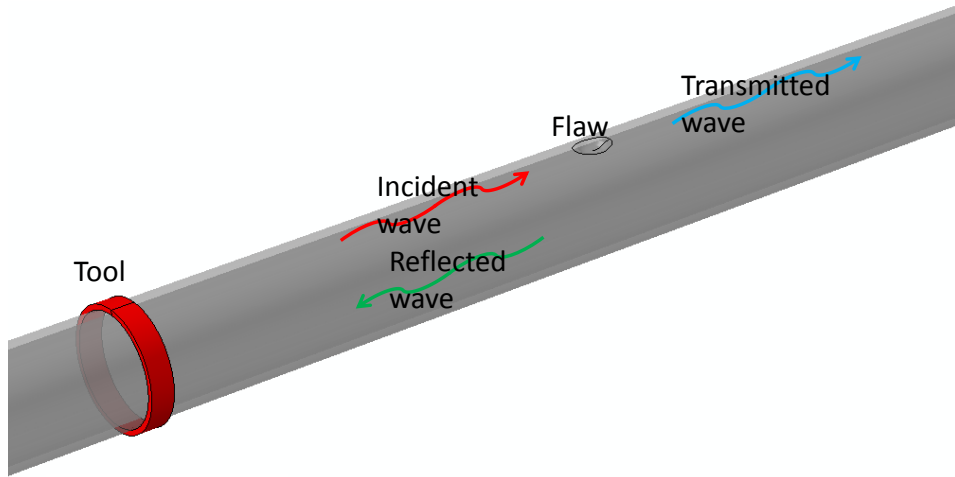


Figure 3.1: Illustration of the interaction of guided waves with a flaw in a pipe.

A few years later, Mead [1973] put forward a modelling technique specific to the periodic nature of guided wave propagation including simulation of attenuation. This was an important contribution since engineering structures such as pipes are often coated to protect them from the environment. Mohr & Holler [1976] investigated the inspection of small diameter (a few centimetres) thin walled tubes using non-contact electrodynamic transducers, and Zemanek [1972] published a substantial paper on the propagation, through thickness displacement and reflection characteristics of longitudinal guided waves in pipes.

Further research was done into using guided waves for flaw detection in the 1970s and 1980s. [Silk & Bainton \[1979\]](#) investigated the inspection of small diameter tubes with an application of heat exchanger tubes. Meanwhile, [Thompson *et al.* \[1972\]](#) suggested the use of electromagnetically excited guided waves for inspection of gas pipelines and [Morgan & Crosse \[1978\]](#) presented an instrument for the detection of blockages and holes in pipes. However, this involved the use of waves that travel in the fluid inside the pipe rather than the walls of the pipe. [Böttger *et al.* \[1987\]](#) published work on the use of an Electromagnetic Acoustic Transducer (EMAT) for the inspection of pipes and studied the reflections from flaws experimentally.

3.3 Commercial implementation of guided wave pipe inspection

In the late 1990s, perhaps partly due to the existence of affordable, relatively fast computers, the commercial implementation of guided waves began. A system using magnetostrictive sensors was investigated [[Kwun & Holt, 1995](#); [Kwun *et al.*, 2001](#)]. Between 1994 and 1996, TWI Ltd. managed a project which resulted in the development of an inspection system using piezoelectric transducers [[Mudge *et al.*, 1996](#); [Lowe *et al.*, 1998b](#); [Mudge, 2001](#); [Alleyne *et al.*, 2001](#)]. The L(0,2) wave mode was selected as being suitable since it was relatively non-dispersive at the frequencies used (20-80kHz). However, since the L(0,1) wave mode also exists at these frequencies it was necessary to use a number of rings of transducers to suppress it as well as allowing control over the direction of the excited wave modes. Around the same time, different transduction techniques were also investigated by [Rose *et al.* \[1996\]](#).

The use of the torsional mode, T(0,1) was also investigated [[Alleyne & Lowe, 1998](#)] and its sensitivity to flaws was investigated by [Demma *et al.* \[2003\]](#) and [Liu *et al.* \[2006\]](#). The use of this mode is now also implemented in some commercial systems. The systems that are well-established on the market now are as follows:

- Teletest sold by Plant Integrity Ltd. (a subsidiary of TWI Ltd., website: www.plantintegrity.co.uk)
- Wavemaker sold by Guided Ultrasonics Ltd. (a spin-off company from Imperial College, website: www.guided-ultrasonics.com)
- MsSR 3030R developed by South West Research Institute (website: www.swri.org).

A schematic illustrating each of these systems is shown in Figure 3.2. The Teletest system is made up of five rings of transducers. The three rings of longitudi-

nally oriented piezoelectric transducers are used to excite the $L(0,2)$ wave mode in one direction whilst suppressing the $L(0,1)$ wave mode. The other two rings of torsionally oriented piezoelectric transducers are used to excite the $T(0,1)$ wave mode in one direction. The Wavemaker system normally uses two rings of torsionally oriented piezoelectric transducers to excite the $T(0,1)$ wave mode in one direction. Finally, the MsSR 3030R system excites guided waves using magnetostriction. The system has two or three rings of ferromagnetic strips and ribbon cables in order to excite either torsional or longitudinal waves and control their direction.

Recently, some new systems have been developed such as the PowerFocus system developed by FBS (a spin-off company from Penn State University) and sold by Structural Integrity Associates Inc.

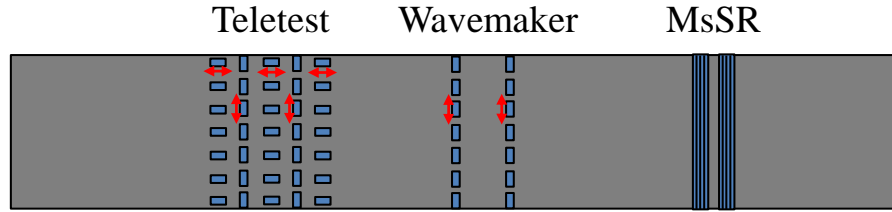


Figure 3.2: Schematic of the three main commercial guided wave inspection systems that are currently available.

3.4 Recent research into guided wave inspection

Since the potential for guided wave inspection of pipes was first realised, a number of researchers have been working on improving the technique. The technique started as a simple screening procedure for relatively large corrosion flaws. However, recent research suggests that it can be used to provide more detail about the flaws that are detected and be used to find smaller flaws.

Different transduction methods including generalised solutions for variable applied surface tractions have been investigated by [Ditri & Rose \[1992\]](#), [Shin & Rose \[1999\]](#) and [Li & Rose \[2001a\]](#). The issue of attenuation into the surroundings has also received some attention by authors such as [Kwun *et al.* \[2004\]](#) and [Long *et al.* \[2003\]](#).

One advanced technique that has received a lot of interest is the idea of focusing the sound energy on predetermined regions of the pipe. Some of the earliest work on this topic involved the idea of using both non-axisymmetric modes and axisymmetric modes to inspect pipes [[Shin & Rose, 1998](#)]. The idea of applying dif-

ferent amplitudes and delays to individual transducers was investigated by authors such as Li & Rose [2002], Rose *et al.* [2003], Barshinger *et al.* [2002]. Hayashi used the semi-analytical finite element method (SAFEM) to simulate focusing [Hayashi *et al.*, 2003a, 2005a]. Since then a number of authors investigated focusing further for different situations such as pipe size [Li & Rose, 2006], viscoelastic coatings [Luo & Rose, 2007] and beyond welds [Zhang & Rose, 2006]. The idea of ‘total focusing’, where the focusing algorithm is applied at every location, was investigated by Velichko & Wilcox [2009b] for relatively high frequencies with the aim of detecting relatively small flaws. The idea of synthetic focusing, where an image of the pipe is formed using post processing techniques was also investigated by Hayashi & Murase [2005] and later by Davies & Cawley [2009].

Another topic of recent interest has been the application of guided wave inspection to other structures. Much work has been done on the inspection of plates by authors such as Alleyne [1991] and this work is still on-going. For example, some recent work by Fromme *et al.* [2006] has looked at detecting a range of different flaw types in a plate and Li & Rose [2001b] has studied guided wave propagation in plates with the application to inspection in the nuclear industry. Railway rails are also a potential candidate for guided wave inspection and have received quite a lot of recent interest. Gavric [1995] used semi-analytical finite element analysis to calculate dispersion curves in rail for relatively low frequencies ($< 5kHz$). Later, Sanderson & Smith [2002] published a 3D finite element analysis technique for calculating dispersion curves for prismatic structures of any cross section. The 3D method was used to calculate dispersion curves for rails at typical guided wave testing frequencies of up to 50kHz. Around the same time Rose *et al.* [2002] carried out some experimental studies into the ability of guided waves to detect a saw cut in a rail, and Wilcox *et al.* [2002] published a 2D finite element analysis method for calculating approximate dispersion curves for structures of any cross section. Then, Hayashi *et al.* [2003b] published a semi-analytical finite element method for dispersion curve calculation for structures of any cross section, giving a rod and a rail as an example and Mace *et al.* [2005] published a similar technique termed Waveguide FE. The inspection of rail was investigated further by others such as Wilcox *et al.* [2003] who used a combination of experiments and finite element analysis to study the reflections from a range of flaws in rails, and Hayashi *et al.* [2007] who developed methods for detecting flaws in the bottom edge of the rail. Other structures have also been investigated such as grouted tendons and bolts [Beard, 2002] and the technique has been applied to steam generator tubing [Rose *et al.*, 1994a,b]. Kwun & Bartels [1996] used a Short Time Fourier transform to measure dispersion curves

in various structures including a square rod and a seven wire strand.

A number of authors such as [Pei *et al.* \[1996\]](#), [Leonard & Hinders \[2003\]](#) and [Leonard & Hinders \[2005\]](#) have also investigated the use of higher frequencies and the use of tomographic techniques to detect flaws through imaging sections of pipe over relatively short distances. The idea of using time reversed, experimentally measured signals as inputs to a numerical model has also been investigated by [Leutenegger & Dual \[2004\]](#). This required the use of a 3D laser vibrometer to accurately record displacements on the surface of the pipe. Wavelets have also been investigated to either give an automatic flaw or no-flaw assessment [[Tucker *et al.*, 2003](#)] or to increase the signal to noise ratio [[Siqueira *et al.*, 2004](#); [Mallett *et al.*, 2007](#)].

Finally, a useful textbook on the topic of ultrasonic waves including some information on guided waves was published by [Cheeke \[2002\]](#) and Rose also published a number of useful review papers [[Rose, 2000, 2002b,a](#); [Rose *et al.*, 2007](#)] and a text book on ultrasonic waves [[Rose, 1999](#)].

In summary, a number of concepts have been developed that improve the inspection of guided waves in pipes and techniques such as focusing have enhanced the ability of guided waves to detect smaller flaws. However, the challenge of deriving a sufficient level of quantitative information on detected flaws in pipes still remains.

3.5 Modelling of guided wave inspection

Analytical equations describing the motion of guided waves such as those presented by [Viktorov \[1967\]](#) were immensely useful in advancing our understanding. However, with increasing complexity in geometry, material properties, loads and boundary conditions, there is a limit to the suitability of analytical models and for more complex situations numerical modelling becomes advantageous. Finite element analysis was developed in an early form in the 1940s and became commonplace in industry in the 1980s [[Zienkiewicz & Taylor, 2000](#)]. One early use of finite element modelling for simulation of wave propagation was the simulation of Lamb wave scattering in plates by [Koshiha *et al.* \[1984\]](#). They recognised the advantages of finite element analysis in being able to simulate irregular flaw shapes and used a combined finite element and analytical approach to study scattering from different shaped cracks.

Then in 1997, [Zhuang *et al.* \[1997\]](#) suggested a hybrid modelling technique to simulate the reflection of axisymmetric guided waves from cracks in welds. However, there was no experimental validation conducted. Around the same time, [Moser *et al.* \[1999\]](#) noted the use of commercial finite element codes in the simulation of guided wave propagation and dispersion. Within the paper they discuss the merits

of boundary elements and finite element codes and used finite element analysis due to its commercial availability. They first validated the finite element modelling technique against analytical solutions in plates and then went on to model wave propagation around a circular annulus. In the early 2000s, [Zhu \[2002\]](#) used 2D and 3D finite element analysis to investigate the reflection of longitudinal guided waves from idealised corrosion flaws of different shapes in pipes and [Sanderson \[2003\]](#) presented a 3D parametric study of the reflection coefficient of the L(0,2) wave mode from notch-like flaws of various shapes and sizes and at a range of frequencies using the commercial finite element analysis code ABAQUS Explicit [[ABAQUS, 2010](#)]. Around the same time, [Hayashi & Rose \[2003\]](#) used a semi-analytical finite element analysis technique to simulate guided wave behaviour in a plate and a pipe. They used this to examine focusing in straight pipe and mode conversion around a pipe bend.

A simple transmission line model for predicting the reflections from volumetric flaws in pipes was proposed by [Choi *et al.* \[2004\]](#) but only qualitative agreement was achieved when compared with experiment. [Bartoli *et al.* \[2005\]](#) also used ABAQUS Explicit to simulate wave propagation and reflections from flaws in railway rails and [Rudd *et al.* \[2007\]](#) discussed the merits of using an explicit (or finite) integration technique to simulate guided wave propagation. They also used this to simulate guided wave propagation in pipe networks with a number of bends. [Ratassepp & Klauson \[2006\]](#) used an analytical theory to study axisymmetric longitudinal wave propagation in pipes of different diameters and wall thicknesses. [Kwun & Kim \[2007\]](#) used a one-dimensional analytical modelling approach to simulate reflection from flaws. They used this to predict the reflection coefficients from notches of varying lengths with respect to wavelength and achieved relatively good agreement but concluded that the model was limited to simple flaw shapes.

[Velichko & Wilcox \[2009a\]](#) investigated the relationship between solutions for wave propagation in plates and pipes and showed that it was possible to use plate solutions to obtain reflection coefficients for through-thickness circumferential cracks in pipes. [Zhou *et al.* \[2009\]](#) used a hybrid wave finite element and finite element technique to simulate scattering from elliptical flaws of different lengths and depths in pipes at a range of frequencies.

In summary, a number of modelling techniques have been investigated by various researchers. These range from full 3D finite element analysis to hybrid approaches and approximations. Full finite element analyses require differential equation solvers to be written or purchased and have relatively long computation times whereas the currently available hybrid techniques also require differential equation

solvers and are limited to simplified scenarios. Neither are therefore suitable for practical use with field equipment. The work presented in this thesis and work recently published [Sanderson & Catton, 2011b] addresses this need by presenting a hybrid modelling technique that provides computationally fast results for the generalised simulation of excitation arrays. Additionally, similar hybrid modelling techniques have also been developed for dealing with complex situations such as multiple flaws and pipe bends.

3.6 Flaw sizing and characterisation using guided waves

Fuller [1981] studied the transmission of flexural wave modes through discontinuities in pipes. The method presented was analytical and was limited to thin walled shells and therefore to low frequencies where the through thickness variation of the wave mode is linear. Ditri [1994] developed formulae based on the crack opening displacement and the stress field of the scattered mode for the simulation of guided wave interaction with circumferential cracks in pipes. Bai *et al.* [2001] also studied the reflections of guided waves from cracks in pipes. They used a quasi-one-dimensional modelling technique similar to SAFEM to quantify the reflection and transmission coefficients of the L(0,2) wave mode from a range of crack circumferential extents and depths.

Alleyne & Lowe [1998] used finite element analysis with a combination of axisymmetric and shell elements to study the reflection characteristics of the L(0,2) wave mode from notch-like flaws in pipes. Lowe *et al.* [1998a] expanded on the study to examine the mode conversions caused by the interaction of the L(0,2) with the flaws.

Cawley *et al.* [2002] and Sanderson [2003] used finite element analysis to calculate the reflection coefficients of L(0,2) from notch-like flaws in pipes of different axial, through wall and circumferential extent. Demma *et al.* [2003] carried out a similar study for the T(0,1) wave mode. The results yielded some clear trends with the variation of each individual parameter of flaw dimension but it was still not possible to use this data in an inverse way to distinguish the dimensions of the flaw from the received signals. Then, Demma *et al.* [2004] brought this work together and put forward approximate formulae for extrapolation to other pipe sizes and suggested a possible method for determining the circumferential and through wall extent of flaws based on the ratio of the flexural to axisymmetric wave mode reflections from flaws.

An alternative method for flaw sizing using focusing was investigated a num-

ber of authors such as Mudge & Catton [2007], Mu *et al.* [2007], Sanderson [2007], Catton *et al.* [2008a] and Catton *et al.* [2008b].

Then, the idea of using the ratio between the flexural reflections and the axisymmetric reflections from a flaw was developed further and investigated theoretically and experimentally by Catton [2009] and Sanderson & Catton [2011a]. Experimental measurements of the through wall and circumferential extent of flaws were carried out for a 168.3mm outer diameter, 7.11mm wall thickness pipe.

The reflections from flaws of complex profiles were investigated in a series of studies [Carandente *et al.*, 2010; Carandente & Cawley, 2011, 2012]. It was observed that the cyclic relationship between the wavelength and axial extent of a flaw shifted with the through wall extent of the flaw and the use of this to determine the through wall extent of the flaw was investigated. However, this technique is limited to flaws within a certain range of axial extents.

Some recent work has been carried out by Cobb *et al.* [2012] into determining the size of large patches of corrosion. The variation of the attenuation of the guided waves as a function of both frequency and temperature was investigated experimentally with a view to using the trends to determine the severity of the corrosion.

A number of techniques have been investigated to advance guided wave inspection to the point where quantitative rather than qualitative information about the severity of corrosion can be found. However, none of these are yet suitable for practical use in the field. This is an important issue to resolve as merely showing the existence of corrosion is not enough information to allow pipeline operators to make decisions. The work presented in this thesis takes forward the technique of using the ratio between flexural and axisymmetric wave modes. A practical procedure is suggested. This procedure has been successfully validated using a combination of finite element analysis and experiments for a range of different pipes sizes and flaw shapes and sizes. Additionally, a refinement to the method for characterising smaller flaws is suggested and tested for a large diameter pipe example.

3.7 Interactions between multiple flaws

Corrosion type flaws are often not found in an isolated region but are more likely to exist as a cluster of flaws. Therefore, the signals from a given flaw are likely to have passed through other features such as flaws or welds before being received. It is therefore important to understand and quantify the interaction between multiple features. If the guided wave inspection technique is being used solely as a screening procedure, the effect of this is likely to be negligible in most cases. However, if refined

signal processing procedures to give more information about the flaws detected are to be used, intelligibility of the signal becomes more important.

As seen in the previous sections, there has been a great deal of work done on the reflections from a single flaw. However, relatively little research has been done on the interactions of multiple flaws in pipes. Work has been done in the past by Domany *et al.* [1984] and Schafbuch *et al.* [1993], to numerically simulate the elastic scattering from two embedded flaws. However, this did not deal with the multimode nature of guided waves in pipes.

Nishiguchi *et al.* [2008] developed a simple analytical model for the prediction of the reflection of T(0,1) from fully circumferential flaws in pipes. The model was compared to finite element solutions and experiments and relatively good agreement was obtained. However, this work concentrated on the T(0,1) wave mode only and did not consider mode conversion into flexural wave modes.

Some recent work has been done to look at the effects of multiple flaws on guided wave signals [Løvstad & Cawley, 2011b,a, 2012]. A number of through wall circular flaws at various locations in an 88.9mm diameter, 5.5mm wall thickness pipe were studied using finite element analysis combined with experimental validation. The research concentrated on relatively small flaws (approximately 2.5% CSA loss, 7° circumferential extent) and the effects of the interaction between flaws were found to be negligible.

The work presented in this thesis quantifies the effects of multiple features on guided wave signals for larger flaws where the interaction becomes significant. A methodology is also proposed which enables the corrupted signals from features beyond others to be corrected.

3.8 Interaction of guided waves with pipe bends

In 1910, Lord Rayleigh published a paper on so-called ‘whispering gallery’ waves [Rayleigh, 1910]. Rayleigh described these waves as creeping around the curved surface. He suggested St Paul’s Cathedral as an accessible example and put forward a mathematical theory to explain the phenomenon. These waves and Rayleigh’s work was discussed over one hundred years later in a recent article by Wright [2012].

In recent years, work has been carried out to understand wave propagation around a curved annulus [Liu & Qu, 1998; Harris, 2002; Wilcox, 1998; Gridin *et al.*, 2003]. It is possible to derive analytical equations for this essentially two-dimensional problem, but this becomes prohibitive when dealing with the three-dimensional problem of a pipe bend, for example [Demma *et al.*, 2005]. Alternative ways of

studying curved structures have therefore been sought.

A number of authors have investigated the use of shell theory to provide approximate solutions for the behaviour of guided waves in pipe bends [Leung & Kwok, 1994; Redekop, 1997; Huang *et al.*, 1997]. Aristegui *et al.* [2000] investigated the use of a shell approximation using finite element analysis. Other authors have also used finite element analysis to investigate guided wave propagation in curved structures [Wang, 2000; Salley & Pan, 2002; Beard, 2002]. Dispersion curves for pipe bends have been calculated [Demma *et al.*, 2002] and the transmission of waves through pipe bends using a combination of finite element analysis and experiments has also been studied by Demma *et al.* [2005]. Some authors have investigated the effects of wave propagation around pipe bends experimentally and have developed a tuning concept to study the sensitivity of guided waves to the detection of a flaw beyond an elbow [Rose & Zhao, 2001; Rose *et al.*, 2005]. Nishino *et al.* [2006] studied the mode conversions that occurred through a small diameter stainless steel pipe (6mm outer diameter) using an interferometer to measure the guided wave signals for different bend angles. Later, Nishino [2010] also studied the effects of pipe bends experimentally and suggested the use of an incremental monitoring procedure in order to detect flaws beyond the bend. However, such a technique would require an array to be permanently attached. Volker & Bloom [2011] extended their work on tomography in straight pipes to pipe bends and presented a model based on wave field extrapolation on an ‘unfolded’ pipe in 2D. Hayashi *et al.* [2005b] put forward a semi-analytical finite element technique for the calculation of guided wave behaviour in pipe bends. This has the advantage of fast computation of the behaviour characteristics of pipe bends but relies on an assumption that the pipe bend has a uniform wall thickness.

An alternative analytical modelling methodology for the prediction of guided wave propagation beyond complex features such as pipe bends is presented. The new method has the advantage of fast computation time and no need for an in-situ finite element solver or a permanently attached array. The method has the potential to be applied to any geometry such as a pipe bend with non-uniform pipe wall thickness. It has also been demonstrated that the method can be used to remove the distortion caused by pipe bends. The technique therefore has the potential to allow more accurate inspection and characterisation of flaws beyond pipe bends.

Chapter 4

Analytical Model for Straight Pipe

4.1 Introduction

In many ways guided wave behaviour is more complex than that of the bulk ultrasonic waves used for conventional ultrasonic testing. Even at the low test frequencies involved (typically 10kHz-100kHz) there are numerous wave modes possible in a given structure and most of these wave modes are dispersive causing distortion of the pulse. The ultimate aim is to detect a feature by examining responses from an unexpected reflector. Therefore, spurious signals from unwanted wave modes and pulse distortion are clearly undesirable. However, inspection systems can be designed to minimise unwanted wave modes, or can be used to focus energy in a particular region of a pipe by optimising the excitation array layout and input waveform [Rose, 2002b]. Modelling potentially offers a fast and cost-effective tool to aid the design of systems for new applications and delivers more information by providing the stress or displacement field with time. However, numerical modelling can be computationally intensive and is not something that can be done in real-time in an industrial situation.

This chapter presents an analytical modelling technique for the simulation of long-range ultrasonic guided wave propagation in structures. The model may be used to predict the displacement field in any prismatic structure arising from any excitation arrangement. This is something that is difficult to assess experimentally due to inherent unknowns such as the coupling efficiency. The model can ultimately be used as a tool to design and optimise inspection systems. To illustrate the technique an example of a pipe is used. The analytical model is computationally

efficient and relatively simple to implement whilst providing a similar accuracy to finite element analysis.

4.2 Guided wave inspection optimisation

The design of an effective inspection technique relies on the careful consideration of a number of key factors. These factors include: transducer selection, array design and the transducer excitation function. The motivation behind the development of this analytical modelling approach is to help optimise the selection of these parameters.

Transducer selection is important since the direction of displacements will determine which wave modes are excited and their relative amplitudes. The sensitivity to different flaws varies from one wave mode to another and so it is important to design inspection equipment that allows efficient excitation and reception of wave modes sensitive to the types of flaws that are desirable to detect. For example, it could be beneficial to use a combination of transducers with excitations in different orientations so that a wider range of wave modes can be excited.

The number of transducers and layout of those transducers will also affect the wave modes generated in the structure. [Drinkwater & Wilcox \[2006\]](#) recently reviewed the subject of array design and highlighted the benefit of modelling for the design of arrays. The example of guided waves in a pipe is now a well understood case [[Alleyne & Cawley, 1996](#); [Alleyne *et al.*, 2001](#); [Mudge, 2001](#)]. Typically, rings of transducer elements are placed around the circumference to generate axisymmetric waves and two or three of these rings are placed along the axis of the pipe with a typical spacing of around 40mm. The aim is to isolate a single axisymmetric wave mode and ensure it propagates in a single axial direction. The two most commonly used wave modes are $T(0,1)$ and $L(0,2)$, as $T(0,1)$ is non-dispersive and frequency ranges exist where $L(0,2)$ has little dispersion. In order to isolate these wave modes from their respective ‘families’ of flexural wave modes, a number of transducer elements around the circumference are required. This number must be greater than the highest possible order of flexural wave mode that exists at the test frequency in the desired family. For example, using 24 transducer elements around the circumference will prevent flexural modes up to $F(23,m)$ from being excited. However, this array could preferentially excite $F(24,m)$ but this wave mode normally only exists above the test frequencies used in practice.

Two transducer rings are required to ensure the output waveform only propagates in one direction along the length of the pipe. This is achieved by transmitting with appropriate phase delays applied between the rings. $T(0,1)$ can be generated

in isolation to other mode families using circumferentially aligned shear transducers. In order to excite the L(0,2) wave mode, shear transducers are aligned axially. However, although the L(0,1) has mostly radial displacements, it is also sensitive to axial displacements and will therefore be generated in addition to the L(0,2) wave mode, albeit to a lesser degree. Therefore, more than two rings of transducers are required to isolate L(0,2) from L(0,1) while still ensuring single direction output. It is worth noting that a similar issue could arise for the T(0,2) wave mode, however, guided wave systems are generally operated at frequencies below the T(0,2) cut-off. Using multiple rings with a suitably high number of transducer elements per ring is the standard array design used in practice, but cases where access to the pipe is restricted it may be possible to redesign the array to accommodate this.

The transducer excitation function can be optimised to enhance inspection. For example, focusing is one technique used to concentrate the energy in a region of the structure where there is a suspected flaw, thereby improving the chances of detection. This technique works by applying an appropriate excitation pattern across the array [Hayashi *et al.*, 2005a].

4.3 Approach

4.3.1 Excitability

For linear elastic scenarios, such as ultrasonic wave propagation in a steel pipe, the net displacement field can be calculated from the superposition of the individual displacement field of each wave mode present. For a given excitation, a number of wave modes will be excited with different amplitudes depending on the sensitivity of the wave mode to factors such as the direction of excitation or relative location of the transducers. Depending on the complexity of the geometry, dispersion curves can be calculated either analytically or numerically. The dispersion curves show the wave modes that exist at a given frequency. However, the amplitudes for a given excitation or ‘excitability’ of each of these wave modes is a key parameter to identify. This does not arise from dispersion curve calculation methods which are modal solutions that simulate no particular excitation. Wilcox *et al.* [2002] discussed the concept of excitability and suggested a method for determining this from knowledge of the mode shape from 2D FE approximations of the natural frequencies and calculation of power flow. This was compared with analytical solutions for plates given by Viktorov [1967]. Other authors such as Hayashi *et al.* [2003a] have also discussed the need of the excitability parameter.

An alternative method for the calculation of excitability is presented here.

The method uses a transient finite element model, which means that it can be readily applied to prismatic structures of any cross section. A broadband excitation is chosen so that the excitability calculation can be carried out for a large range of frequencies in a single operation instead of processing a number of frequency extraction results.

The models were generated, solved and analysed using the commercially available finite element code ABAQUS Explicit.

In order to verify the proposed technique, the results were compared with excitability calculations for a 1mm thick aluminium plate published by [Wilcox *et al.* \[2002\]](#).

The applied excitation was chosen to be a 4-cycle 1MHz Hann-windowed excitation [[Priemer, 1991](#)].

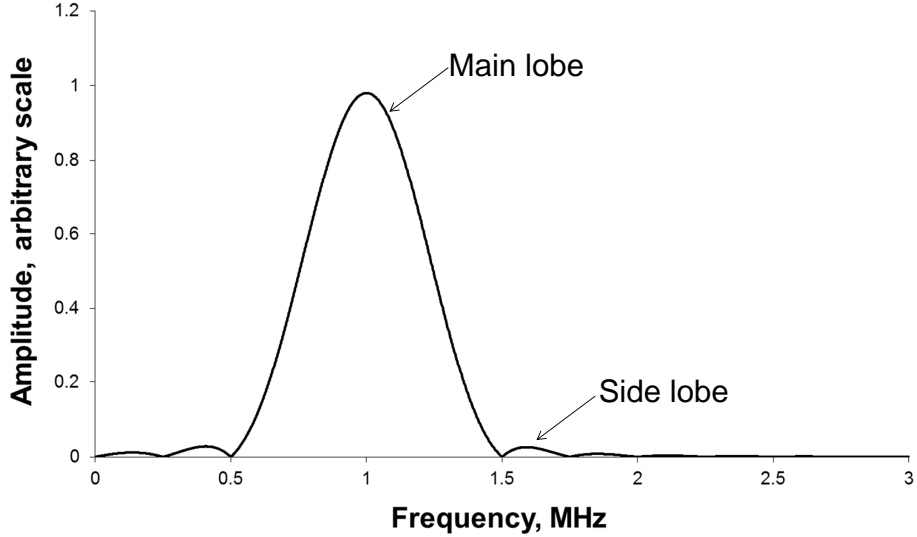


Figure 4.1: Frequency spectrum for 4-cycle 1MHz Hann-windowed excitation

Figure 4.1 shows the frequency spectrum of the signal. There is a main lobe spanning 0.5MHz to 1.5MHz. Then there are a series of side lobes which decrease in amplitude as the frequency moves away from the central frequency of the excitation. This distribution of frequency is typical for Hann-windowed (or similar) excitations.

A 2D plane strain finite element model was used to simulate wave propagation in a 1mm thick aluminium plate. Figure 4.2 shows a schematic of the model. Two separate instances of the model were computed. One with a symmetric excitation to excite the symmetric Lamb wave mode, S0 in isolation and the other with an asymmetric excitation to excite the asymmetric Lamb wave mode, A0 in isolation.

The displacements were applied at two points (one on the top surface and one on the bottom surface) and were normal to the surface in both cases. The model was 2m long with one end constrained in order to simulate symmetry. The excitation was applied at this location so that the simulation was effectively of a 4m long plate with an excitation in the centre.

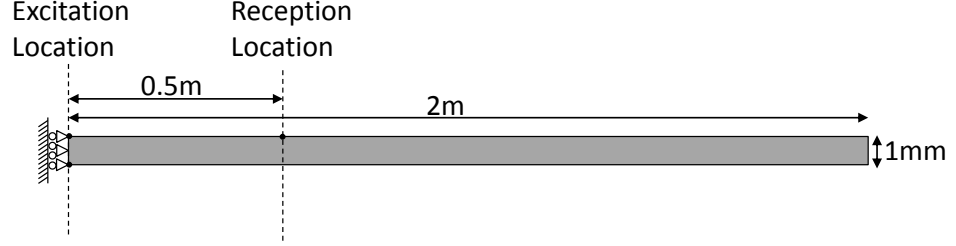


Figure 4.2: Schematic of the 2D model used to calculate excitability in a 1mm thick Aluminium plate.

The displacement history was recorded 0.5m from the excitation at a single point on the surface. The elements were 0.125mm by 0.125mm in size. A suitable level of mesh refinement is where the element length is smaller than one eighth of the smallest wavelength of interest in the system [Alleyne & Lowe, 1998]. The level of mesh refinement used was therefore in excess of the minimum size necessary for accurate results. Plane strain linear elements were used (ABAQUS element type CPE4R) and the time increment was fixed to 5ns. The model was run in two steps. The first step was 4 μ s long (the duration of the excitation) and the second step was 2000 μ s long (sufficient time to allow the pulse to reach and fully pass the reception location).

The material properties used (appropriate for pure aluminium) were as follows:

- Young's Modulus = 70.758GPa
- Poisson's ratio = 0.3375
- Density = 2700kg/m³

In order to calculate the excitability, first, a one-dimensional FFT of the received time domain signal, $F(\omega)$ was calculated:

$$F(\omega) = \int_{-\infty}^{\infty} f(t)e^{-i\omega t} dt, \quad (4.1)$$

where $f(t)$ is the received signal, t is time and ω is the frequency.

A reference FFT, $F_{ref}(\omega)$ was also calculated using the input waveform, $f_{ref}(t)$:

$$F_{ref}(\omega) = \int_{-\infty}^{\infty} f_{ref}(t)e^{-i\omega t}dt \quad (4.2)$$

Then the excitability, $E(\omega)$ was calculated by dividing the amplitude of the FFT of the received signal by the amplitude of the FFT of the reference input waveform signal:

$$E(\omega) = \frac{|F(\omega)|}{|F_{ref}(\omega)|} \quad (4.3)$$

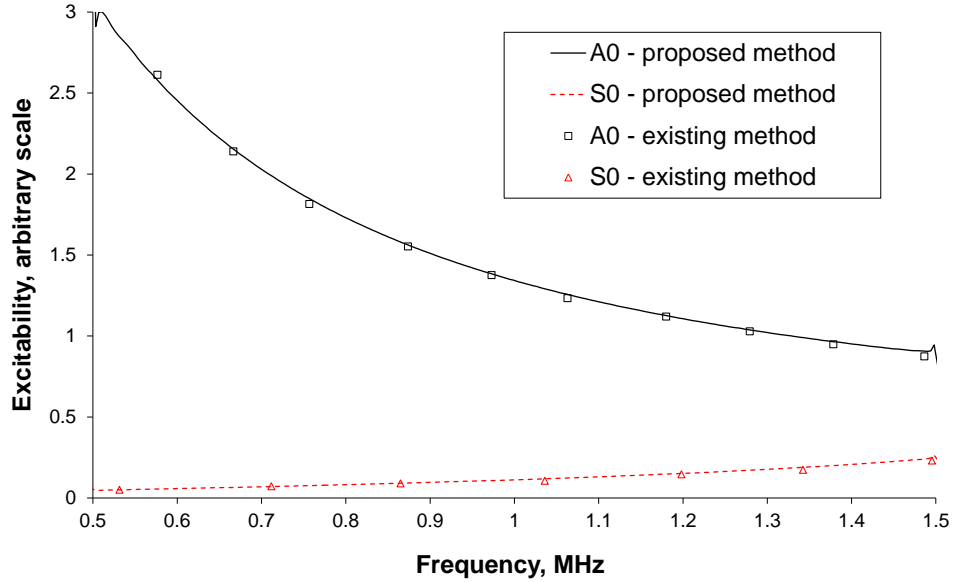


Figure 4.3: Comparison between existing technique (points) and new broadband FFT method (lines) for calculation of excitability in 1mm Aluminium plate for excitation normal to the surface. The perturbations observed at 0.5 and 1.5MHz are due to zero amplitudes on the denominator of Equation 4.3.

The comparison with the natural frequency extraction technique results published by Wilcox *et al.* [2002] is shown in Figure 4.3. Excellent agreement is obtained. There is a slight disturbance observed in the FFT method at 0.5MHz and 1.5MHz. This is caused by values of zero amplitude when the transition in the frequency distribution from the main lobe to the first side lobe occurs. This problem can be solved by altering the bandwidth of the excitation. Note that the natural frequency extraction technique results in a set of discrete points whereas the method presented here has the advantage of being closer to a continuous solution.

In this case it was possible to extract each wave mode individually by applying simple excitation conditions (one symmetric and the other asymmetric). However, at higher frequencies there are several asymmetric/symmetric wave modes. There are a few ways of dealing with this. Either the excitations in the model could be altered in order to excite each wave mode individually using a through-thickness distribution as described by Viktorov [1967]. An alternative could be to use a spatial FFT or two-dimensional FFT approach. This would allow for identification of each wave mode from a single model. The dispersion curves can then be used to translate the data into the frequency domain. However, this method will be sensitive to the accuracy of the dispersion curves which rely on knowledge of the material properties and exact geometry of the component.

4.3.2 Application to pipes

The excitability relationship for wave modes in an 88.9mm outer diameter, 5.49mm wall thickness steel pipe (a standard industrial pipe size) was calculated for an excitation at a central frequency of 56kHz. A Hann-windowed pulse of 14-cycles was used so that the bandwidth of the main lobe was from 48kHz to 64kHz. This frequency and bandwidth were selected so that at least two wave modes in each family existed. In order to achieve mode separation, the models were used to excite each order of wave mode individually from $n=0$ to 9. There was no need to consider other modes as there are no modes possible with order $n=10$ or higher in the frequency range of interest (see Figure 2.6).

In each case the model was 6m long and the excitation was applied over 24 nodes spaced evenly around the circumference at one end. The excitation was in the circumferential direction at each node. This direction is most favourable to the excitation of the $T(0,1)$ family of wave modes (see Chapter 2). As for the previous plate models, the mesh used was sufficiently refined so that there were at least 8 elements per wavelength for the smallest possible wavelength. There were 144 elements around the circumference corresponding to 2mm in length. Four elements were used through the thickness and elements of 2.5mm in length were used along the length of the pipe. As before, the commercially available finite element code ABAQUS was used to generate and solve the models. The elements were 8-noded bricks with reduced integration (ABAQUS element type C3D8R).

In order to isolate each mode order and calculate the respective excitability, the following formula for the amplitude of the excitation with respect to circumferential location was used:

$$A = \cos(n\theta), \quad (4.4)$$

where A is the amplitude, n is the required mode order and θ is the circumferential location.

This formula has the effect of doubling the contribution from order 0 modes (in a similar way to a spatial FFT). The T(0,1) wave mode amplitudes were therefore halved in order to take account of this. In order to obtain a direct comparison, the received signals were extracted in the same circumferential orientation as the excited wave mode ($\theta = 0$).

A symmetry condition was applied to the end so that the simulation was of an excitation applied to the middle of a 12m long pipe.

The material properties (appropriate for ferritic steel) used were as follows:

- Young's Modulus = 207.0 GPa
- Poisson's ratio = 0.3
- Density = 7830 kg/m^3

Figure 4.4 shows the excitability curves calculated using the technique described above at around 56kHz in an 88.9mm outer diameter, 5.49mm wall thickness steel pipe. It was found that the first five modes in the L(0,1) family were not significantly excited and are therefore omitted from the figure for clarity. It can be seen that in most cases the trend with increasing frequency is for the amplitude of excitation to decrease. It is also interesting to note that wave modes of all three families are excited despite the excitation matching the displacement characteristics of the T(0,1) family. The L(0,1) family of wave modes are excited to a greater extent as the order increases until they are no longer in existence in the excited frequency range (the cut-off for F(10,1) is around 63kHz for this pipe size).

4.3.3 Analytical model formulation

An analytical formulation is proposed which combines the excitability data gathered as described above with formulae for the propagation characteristics of waves published by Viktorov [1967]. Since the wave propagation is in the linear elastic regime, the principle of superposition can be applied and the contribution from each wave mode summed to form the solution. To make the formula appropriate for pipes, a term for the variation around the circumference is included. The formula below is for a single family of wave modes:

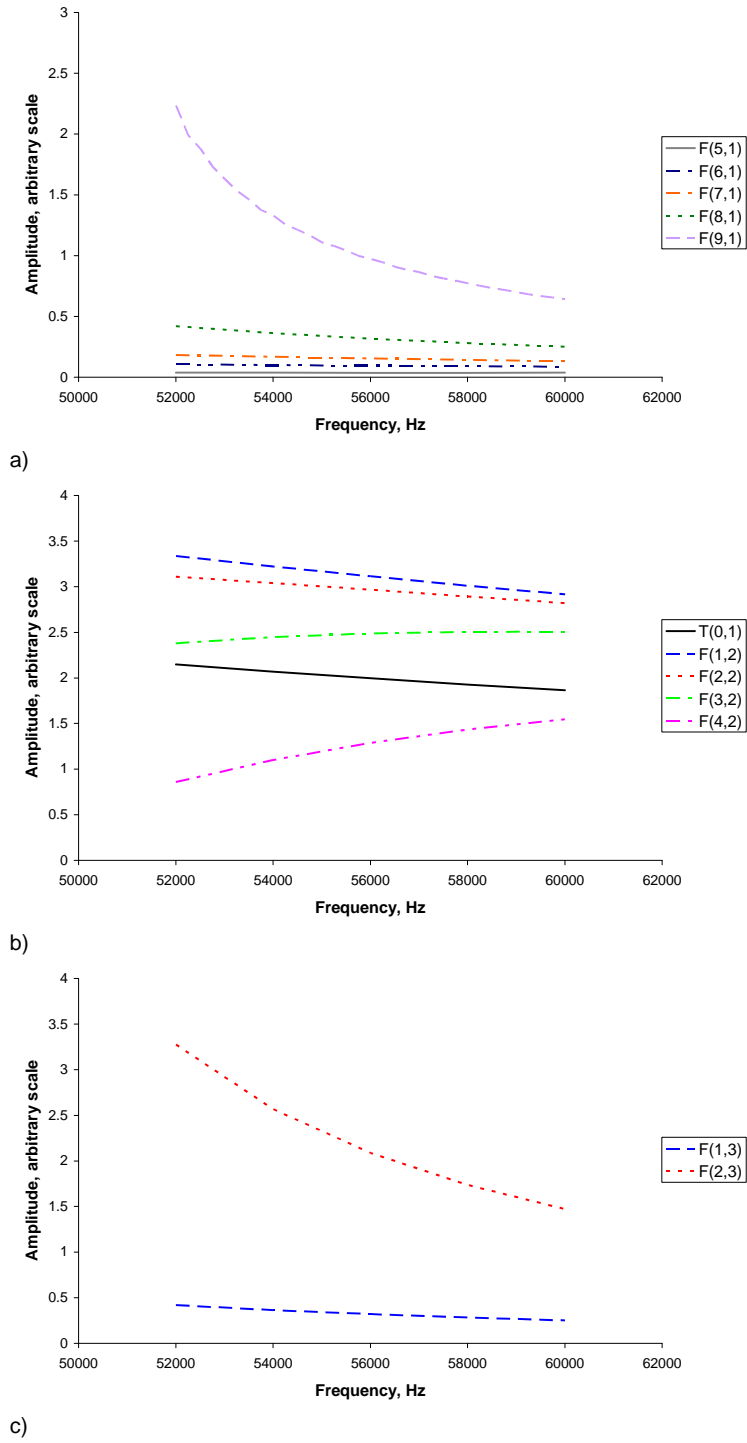


Figure 4.4: Ratio of received amplitude to excited amplitude for a range of excitation frequencies around 56kHz in an 88.9mm outer diameter, 5.49mm wall thickness pipe arising from a single node excitation in the torsional direction. a) L(0,1) family; b) T(0,1) family c) L(0,2) family.

$$u(x, t, \theta) = \sum_{j=0}^M \sum_{i=0}^N -A_i E_{i,j} \cos(2\pi f_i \frac{x}{v_{i,j}} - 2\pi f_i t) \cos(j\theta), \quad (4.5)$$

where u is the particle displacement on the pipe surface, M is the number of wave modes under consideration in a given family of wave modes, N is the length of the vector, A is the amplitude, E is the excitability, f is the frequency, v is the phase velocity, x is the distance travelled and t is time.

Note that this formula must be used separately for each family of wave modes and that the displacement field from each family must be summed to get the final result. The full formulation was programmed into the commercially available MathCAD software. This formula then provides a prediction of the displacement anywhere on the surface of the structure (for a pipe, around the circumference and along the length) at any point in time.

A summary of the overall process is as follows:

- Calculate the relationship between phase velocity, $v_{i,j}$ and frequency (the dispersion curves) for each possible wave mode in the frequency range of interest.
- Calculate the amplitude of each frequency, A_i by taking the magnitude of an FFT of the input signal.
- Calculate the excitability, $E_{i,j}$ for each possible wave mode in the frequency range of interest as described above.
- Combine these parameters in Equation 4.5.

By extracting the excitability relationships, the model is now fully analytical and therefore computationally fast compared to finite element or semi-analytical finite element methods. This technique can be applied to a structure of an arbitrary cross section and any length. In this case, the $\cos(j\theta)$ term corresponds to the wave mode shape on the outside surface of a pipe. In order to adapt the technique to geometries other than pipes, this term should be replaced with the relevant wave mode shape. This could be a through-thickness distribution, therefore allowing the formulation to predict displacements at any point in time and any position in the structure.

4.4 Comparison with finite element modelling results

In order to assess the accuracy of the analytical model, the results were compared with finite element modelling predictions. The finite element model used for the

excitability calculations was altered to simulate a Hann-windowed, 28-cycle 56kHz excitation at a single node in order to restrict the number of modes possible. Firstly, the displacement history results at locations along the length of the pipe (0.5m, 1m, 1.5m, 2m and 2.5m) were compared as shown in Figures 4.5 to 4.9 respectively. The comparison was made at an angle, θ of 0 i.e. in line with the excitation. In each case it is clear that the received waveform is complicated. It is made up of a superposition of all of the possible wave modes and all of these wave modes (with the exception of $T(0,1)$) are dispersive to some degree at this frequency. Therefore the contributions to the signal from the dispersive wave modes such as $F(3,2)$ are likely to be elongated and distorted compared to the input excitation signal. Additionally, the wave modes will constructively and destructively interfere with each other depending on their propagation velocity and hence their position on the time base. This also contributes to the distorted signals observed.

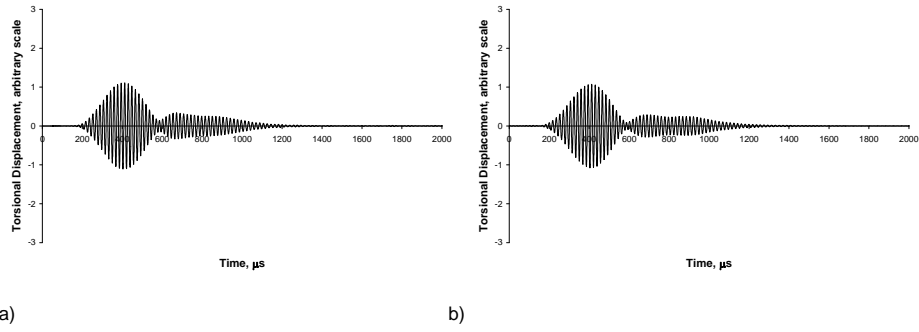


Figure 4.5: Comparison of analytical model and transient finite element result for torsional displacement history 0.5m away from 28-cycle 56kHz excitation: a) Finite element model; b) Analytical model.

It is noticeable in Figure 4.9 that there are some small discrepancies observed in predicted amplitudes for the 2.5m case. This is most likely due to slight differences in the dispersion relationships used in the analytical model and those inherent in the finite element analysis arising from numerical error. As described above, constructive or destructive interference can occur depending on the arrival times of pulses. The result is sensitive to this; a slight change in velocity could result in a change in the pulse shape or amplitude. For example, consider two sine waves, one travelling at 3189m/s and the other travelling 1.1% faster at 3224m/s. The first will take $784\mu s$ to travel 2.5m and the second will take $775\mu s$, a difference in arrival time of $9\mu s$. This is equivalent to half a time period and so the signal will be 180 out of phase (at a frequency of 56kHz). Therefore, a 1.1% shift in velocity can mean

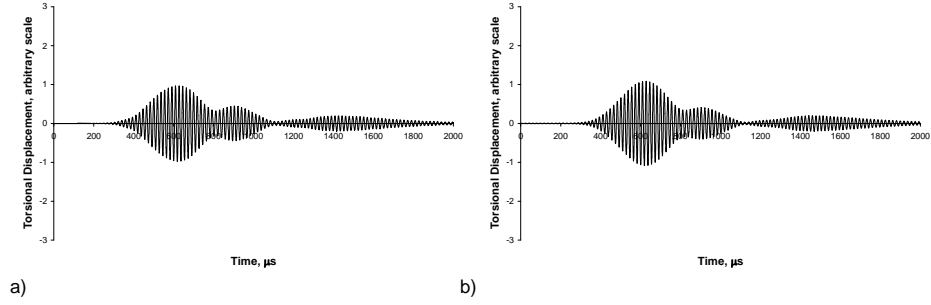


Figure 4.6: Comparison of analytical model and transient finite element result for torsional displacement history 1m away from 28-cycle 56kHz excitation: a) Finite element model; b) Analytical model.

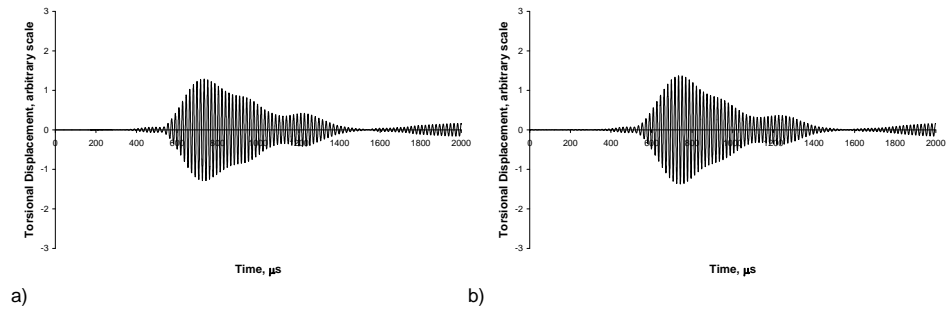


Figure 4.7: Comparison of analytical model and transient finite element result for torsional displacement history 1.5m away from 28-cycle 56kHz excitation: a) Finite element model; b) Analytical model.

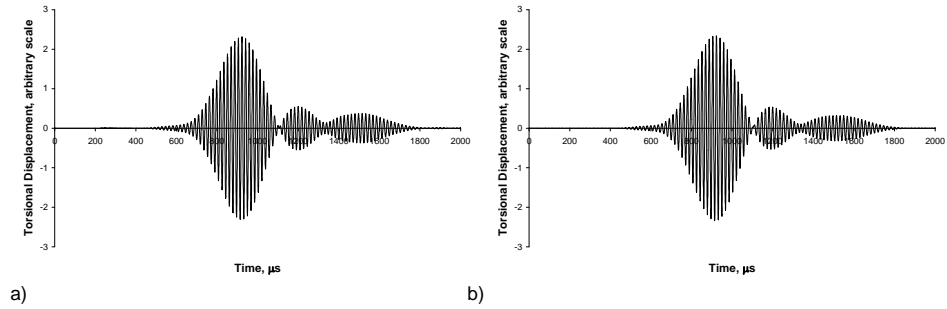


Figure 4.8: Comparison of analytical model and transient finite element result for torsional displacement history 2m away from 28-cycle 56kHz excitation: a) Finite element model; b) Analytical model.

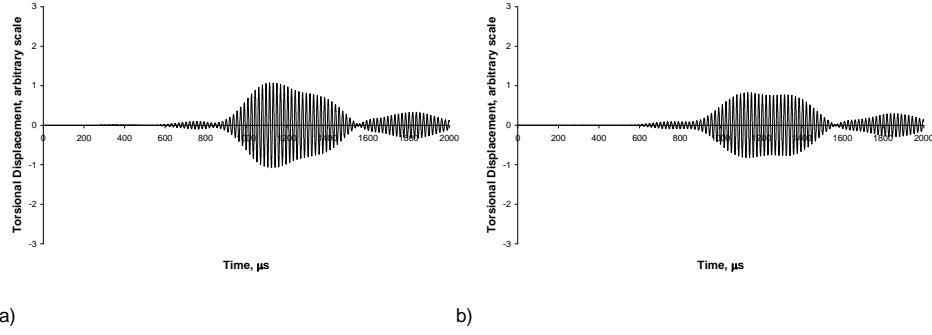


Figure 4.9: Comparison of analytical model and transient finite element result for torsional displacement history 2.5m away from 28-cycle 56kHz excitation: a) Finite element model; b) Analytical model.

the difference between 100% constructive and 100% destructive interference.

The analytical model predictions were then also compared with a spatial plot of displacement along the length of the pipe at $500\mu s$ and $1000\mu s$ as shown in Figures 4.10 and 4.11 respectively. In both cases, good agreement is observed and the two predictions are barely distinguishable.

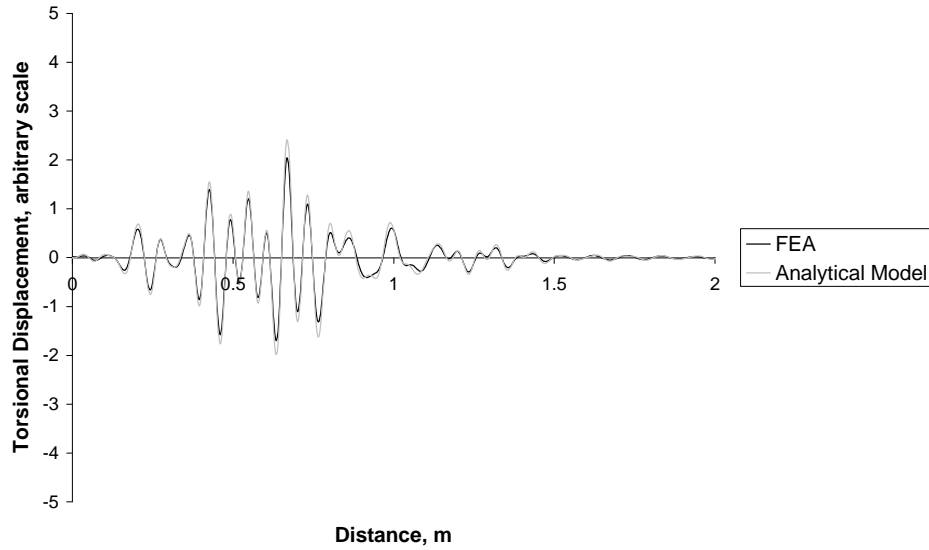


Figure 4.10: Comparison of analytical formulation using MathCAD and transient finite element result for torsional displacement along the length of an 88.9mm outer diameter, 5.49mm wall thickness steel pipe at $500\mu s$.

The analytical model was then used to calculate the distribution of displacements around the circumference at 1.5m from the source. This was carried out from

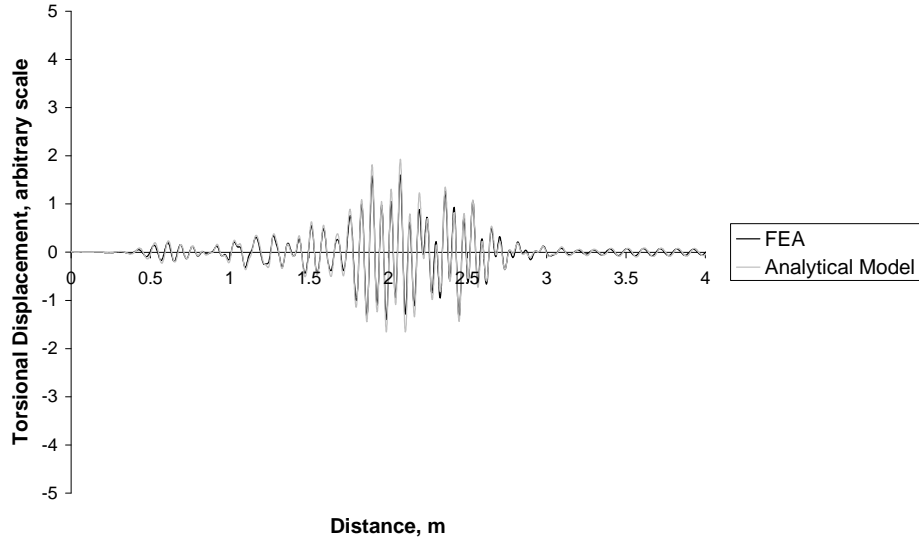


Figure 4.11: Comparison of analytical formulation using MathCAD and transient finite element result for torsional displacement along the length of an 88.9mm outer diameter, 5.49mm wall thickness steel pipe at $1000\mu s$.

694 to $697\mu s$ in increments of $1\mu s$. Figure 4.12 shows how the distribution changes over that short time period.

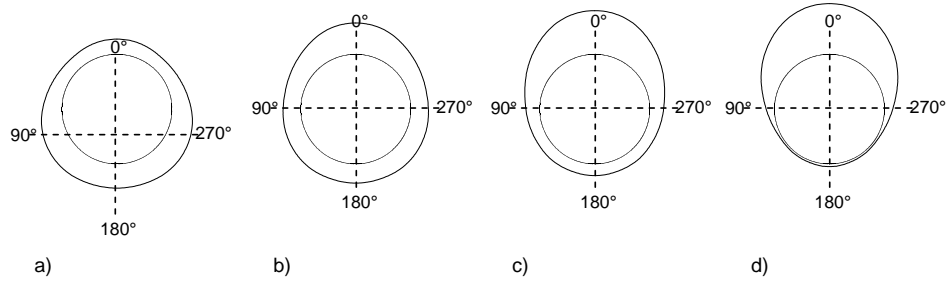


Figure 4.12: Polar plot of analytically predicted displacement distribution around the circumference of the pipe at 1.5m from source. A natural focus is seen to appear at 0 at $697\mu s$: a) $694\mu s$; b) $695\mu s$; c) $696\mu s$; d) $697\mu s$.

The grey line represents a displacement amplitude of zero (i.e. the undeformed pipe). Other authors have investigated the phenomenon of natural focusing [Rose *et al.*, 2005; Li & Rose, 2006]. The analytical model presented here is able to efficiently predict where such natural focus conditions occur. In this case there is a natural focus at 0° at $697\mu s$. There are likely to be many other such cases as the wave modes constructively and destructively interfere with each other whilst

dispersing as they propagate along the pipe.

4.5 Experimental validation

Two transducer arrays were attached to an 11m length of 88.9mm outer diameter, 5.49mm wall thickness ferritic steel pipe, placed in the centre to avoid interference from reflections from the ends of the pipe. The arrays were used in a pitch-catch formation (one was used to transmit and the other to receive). The transmitter array contained just one transducer. The receiver array contained 12 transducers spaced equally around the circumference of the pipe. The transducers were circumferentially aligned in order to produce a predominantly torsional motion on the surface of the pipe. An airline with a pressure regulator was used to ensure uniform transducer contact pressure throughout the experiment. A schematic of the experimental layout is shown in Figure 4.13 and a photograph is shown in Figure 4.14.

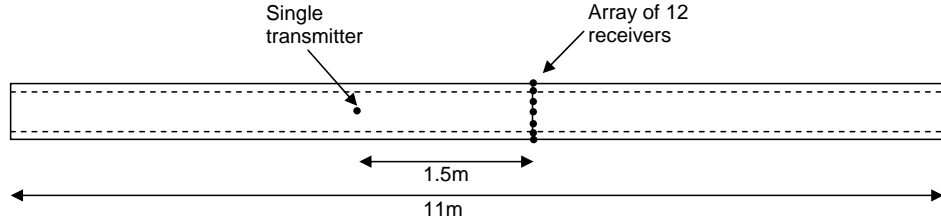


Figure 4.13: Experimental layout.

The transmitter array remained in place for the duration of the experiment with constant coupling conditions. Firstly, the receiver array was placed 1.5m from the transmitter. The excitation was a Hann-windowed 28-cycle 56kHz pulse. Figures 4.15 and 4.16 show the comparison of the recorded displacement history and the analytical model predictions for transducers placed at 0° degrees and 30° from the transmitter. Since the transfer function between the inputs to the FEA and the experimental voltage is an unknown, the FEA results were scaled to the maximum amplitude of the experimental signal. Good agreement is observed between the model and the experiment. The shape of the signal is correctly predicted by the analytical model.

Next the receiver array was shifted in 10mm increments along the length of the pipe so that spatial data could be collected. Figure 4.17 shows the comparison between the analytical model prediction, the finite element prediction and the experimental results. Good agreement is observed between the two models and the experimental data.

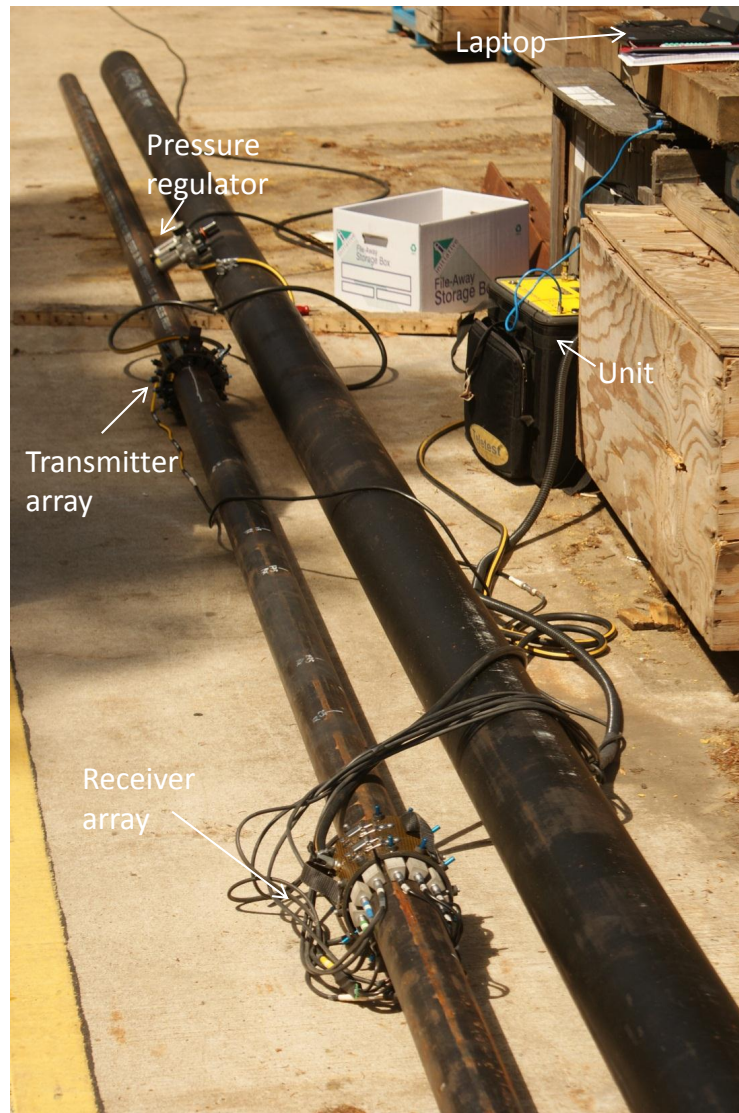


Figure 4.14: Photograph of experimental setup.

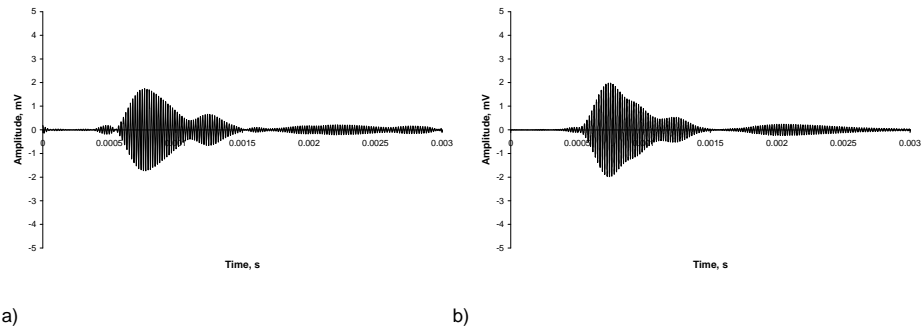


Figure 4.15: Measured amplitude against time 1.5m from excitation, in line with excitation: a) Experimental data; b) Analytical model.

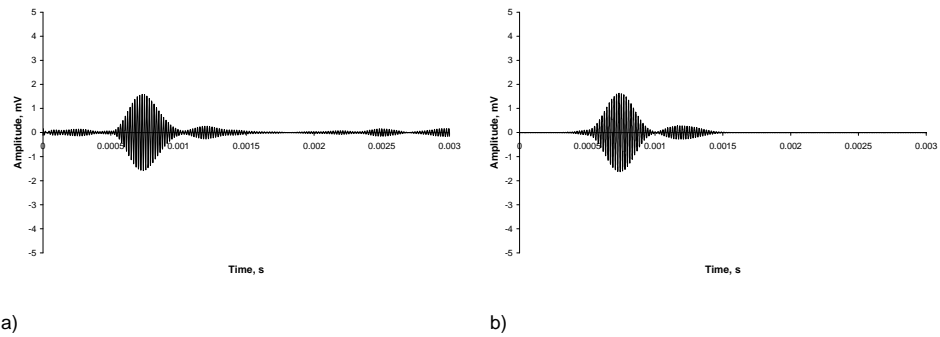


Figure 4.16: Measured amplitude against time 1.5m from excitation, at 30° circumferential location from excitation: a) Experimental data; b) Analytical model.

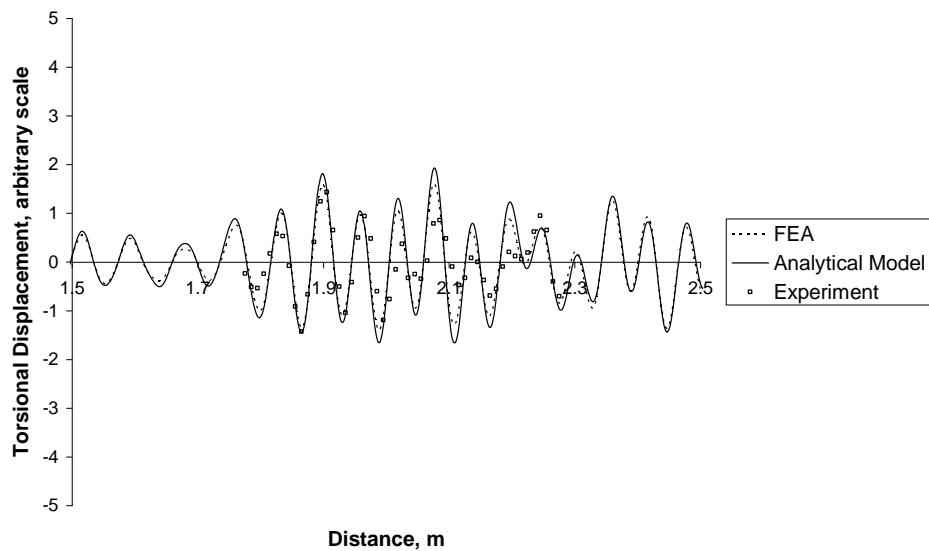


Figure 4.17: Comparison of measured amplitude along the length pipe in line with the excitation.

4.6 Discussion

4.6.1 Potential applications

There are many applications where the techniques described in this chapter can provide an insight and more fundamental understanding into the physical behaviour of structures. The experimental validation and verification against previously validated finite element predictions for wave propagation in pipes give confidence that the analytical modelling method presented here can be used to simulate guided wave inspection.

One potential use could be the development of a part-circumferential array capable of focusing energy anywhere in the pipe. This could be particularly beneficial for situations where access to the pipe is restricted.

Another potential use of the model could be to combine it with other modelling methods in order to develop a hybrid model capable of predicting the propagation of sound in pipe networks. For example, a finite element prediction could be used for the pipe bend and the analytical model for the straight sections of pipe. Similarly, the model could be linked with models of reflections from flaws. Such a hybrid model could be used to improve inspection capability.

The model could also be used to calculate the input parameters in order to focus sound energy at a desired location. If the hybrid approach described above were used, the model would be capable of providing fast solutions to focusing input parameters for pipe networks containing bends.

Once the excitability curves have been obtained over the desired frequency range, any excitation could be simulated using the analytical model. Therefore, the analytical model could be used to investigate the inspection potential of chirp signals, for example.

4.6.2 Potential enhancements

Since a temporal FFT is used for the excitability calculation, mode separation is required in order to apply it effectively. For cases where wave modes of the same order (i.e. the same value of n) have similar velocities, an excessively large model would be required in order to calculate the excitability. In such cases, it may be more computationally efficient to use a spatial FFT instead.

There is likely to be sensitivity to the dispersion curves used in the overall formulation similar to that which was reported regarding the dispersion removal technique developed by Wilcox [2003]. This could cause potential errors in the calculation procedure. Particular sensitivity is likely to occur for dispersive wave modes

as small changes in material parameters will cause large changes in the velocity of the wave mode at a given frequency. One way to mitigate this could be to carry out experimental measurements of the actual material properties. However, dispersive wave modes attenuate and are unlikely to significantly affect the results of long distance inspection. This could mean that the model has some discrepancies close to the excitation location but should be accurate over long distances. Therefore, in this respect it is compatible with long-range inspection. Another potential source of error is that industrial components are made to a certain tolerance and therefore the geometry is likely to vary. This would not be captured by a model based on prismatic geometry such as this one.

The 28-cycle toneburst used in the validation example presented here has a relatively narrow bandwidth when compared with the 5 or 10-cycle tonebursts commonly used in practical guided wave testing. The 28-cycle toneburst restricts the range of velocity dispersion. However, on closer examination of the dispersion curves shown in Figure 4.18, it can be seen that there are a number of highly dispersive wave modes (i.e. those with steep gradients) in the range of the main lobe of the excitation (52-60kHz) such as F(2,3) and F(4,2). Moreover, the excitability curves shown in Figure 4.4 show that these modes significantly contribute to the overall signal. Therefore, the validation results presented here show that the analytical model is capable of predicting dispersive behaviour and so should be suitable for use with shorter tonebursts such as those more commonly used in practical testing.

In the examples presented here just the main lobe in the frequency bandwidth was used in the analytical model. For complete accuracy, all possible frequencies should be considered and a judgement should be made based on the relative amplitude of the frequencies arising from the chosen excitation. In the examples presented here, reasonable accuracy was achieved using the main lobe only. This is roughly equivalent to discarding frequencies with less than $\sim 3\%$ of the amplitude of the central frequency.

The excitability relationship used in the implementation of the analytical modelling method presented here is calculated by assuming the input is a point source with pure excitation in one direction only (torsional). This will not be exactly representative of the real case since piezoelectric transducers have a finite size. The transducers will be in tangential contact with the pipe surface at one circumferential location but will have a short axial distance over which they are active ($\sim 3\text{mm}$). It would be straightforward to simulate this in the finite element model used to calculate the excitability and hence include this affect in the analytical model. Moreover, the model could be used to simulate and study the effects of

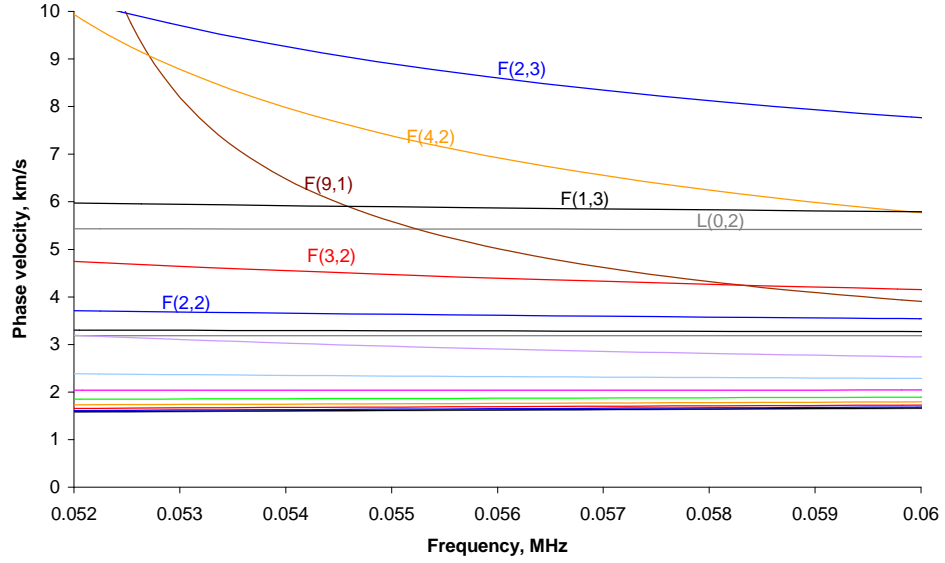


Figure 4.18: Phase velocity dispersion curves for an 88.9mm outer diameter, 5.49mm wall thickness steel pipe over frequency range of main lobe for a 28-cycle 56kHz toneburst excitation.

different transduction techniques on the generation of guided waves.

In the examples presented in this chapter, excitations were applied to the model and extracted from the model in one displacement direction only. In reality, despite being polarised, transducers will have some sensitivity to displacements in other directions (longitudinal, radial). In order to take account of this, the excitability curves used in the analytical model could be scaled accordingly.

4.7 Conclusions

The aim of the work presented here was to develop a fast analytical model for the prediction of guided wave propagation. Finite element models are already used to aid the understanding of guided wave inspection but are computationally intensive and it can take many hours to obtain a solution. The modelling method presented here uses the finite element method to extract key information about the excitation of wave modes (which can be determined relatively quickly) and then uses it in a straightforward analytical formula to provide fast solutions to three dimensional guided wave problems. The method can potentially be applied to any prismatic cross section and could therefore be useful for the development of inspection procedures for structures where guided waves are not currently fully understood.

The proposed analytical modelling method was compared to both transient finite element predictions and experimental data for a pipe example. In order to assess the model, comparisons were made along the length of the pipe and at different circumferential locations. The agreement between the analytical model and the finite element predictions was good in all cases and the two models agreed well with the experimental data.

An article published in IEEE Transactions on Ultrasonics, Ferroelectrics and Frequency Control entitled ‘An analytical model for guided wave inspection optimization for prismatic structures of any cross section’ has arisen from the work presented in this chapter [[Sanderson & Catton, 2011b](#)].

The analytical model addresses the need for a fast simulation of array excitation and wave propagation. However, it does not simulate the reflection and transmission from flaws. The ability to gather quantitative information about flaws would mean that guided wave inspection could be used on a much larger scale. The following chapter deals with the development of a practical flaw sizing technique for guided waves in pipes.

Chapter 5

Flaw Sizing

5.1 Introduction

With any inspection technique, the ability to determine the size and shape of a flaw is important. Current commercial guided wave testing equipment can determine the presence of a flaw but is unable to give detailed enough information to allow the pipeline operator to make a decision based on that alone. Currently, where guided wave inspection identifies an area of concern, further investigation is carried out by a localised inspection method such as conventional ultrasonic testing or radiography.

Research has been conducted into flaw sizing and characterisation using guided waves. This is reviewed in detail in Section 3.6. One potential method involves using the ratio of the axisymmetric reflection to the reflection of the flexural wave modes. The concept of using the ratio between the first order flexural wave mode and the axisymmetric wave mode to find the circumferential extent was suggested by Demma *et al.* [2004]. Then the idea of using a ratio of the axisymmetric wave mode to the sum of the first three flexural wave modes was investigated by the present author and Catton [2009]. The ratio was found to be virtually independent of flaw through wall extent and could therefore be used to find the circumferential extent for any cross-sectional flaw shape. Moreover, the introduction of a number of flexural wave modes was found to result in an increased sensitivity to smaller flaws. A method for then obtaining the through wall extent of the flaw was also suggested and the concept was successfully tested on a range of notch-like flaws in a 168.3mm outer diameter, 7.11mm wall thickness steel pipe [Sanderson & Catton, 2011a].

The first section summarises the theory behind the flaw sizing method and introduces the suggested enhancements to the procedure. Then, the following sections describe the modelling and experimental work carried out to assess the technique for

a range of pipe and flaw geometries. Particular attention is paid to determination of through wall extent of the flaw since this dimension is the most influential on determining whether the pipe is still fit-for-service.

5.2 Acknowledgements

The work presented in this chapter was carried out under a project put together by TWI. The work was sponsored by the Pipeline Research Council International (PRCI), the Electric Power Research Institute (EPRI) and Shell UK. The work was also done in collaboration with ApplusRTD who provided laser profilometry data for a number of real corrosion flaws.

5.3 Flaw sizing procedure

5.3.1 General Method

A technique for determining the through wall and circumferential extent of flaws in pipes from the amplitudes of the reflected wave modes was presented by Catton [2009]. He developed a theoretical formula for the variation of a ratio of individual wave mode amplitudes with circumferential extent. The formula was independent of frequency and pipe geometry. This approach was successfully validated for a range of notch-like flaws in a 168.3mm outer diameter, 7.11mm wall thickness pipe. However, application of the technique to different pipe geometries and test frequencies was not proven. A different approach is presented here which uses finite element analysis to calibrate the equations for a particular pipe size and frequency.

The theoretical derivation for the first three flexural wave modes by Catton [2009] showed that:

$$P = \frac{\phi_f}{\sin(\frac{\phi_f}{2}) + \frac{1}{2} \sin(\phi_f) + \frac{1}{3} \sin(\frac{3\phi_f}{2})}, \quad (5.1)$$

where P is the flaw sizing parameter and ϕ_f is the circumferential extent of the flaw.

The numerator of the equation corresponds to the reflection of the axisymmetric wave mode and the three terms making up the denominator correspond to the reflections of the first three flexural wave modes respectively. Figure 5.1 is from Catton [2009] and shows the comparison of finite element modelling data for flaws of different through wall extent against the theoretical trendline.

However, it is postulated that the frequency and pipe size can cause these to vary. Therefore the addition of scaling factors is suggested as follows:

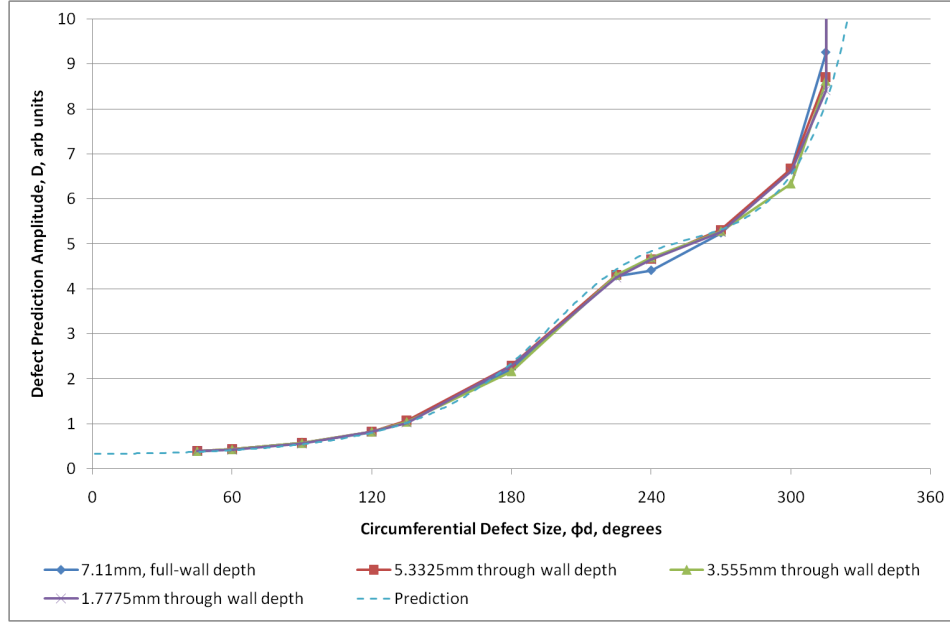


Figure 5.1: Flaw prediction amplitude responses from various flaw through wall extent models over increasing flaw circumferential extent from Catton [2009].

$$P = \frac{A_0 \phi_f}{A_1 \sin(\frac{\phi_f}{2}) + \frac{A_2}{2} \sin(\phi_f) + \frac{A_3}{3} \sin(\frac{3\phi_f}{2})}, \quad (5.2)$$

where A_0 , A_1 , A_2 and A_3 are constants relating to the amplitudes of the axisymmetric wave mode and the first, second and third flexural wave modes respectively. Figure 5.2 illustrates this.

Values of A_1 , A_2 and A_3 can be found for particular pipe sizes and test frequencies by running two finite element models to simulate reflection from a large circumferential flaw. The values required are equal to the maximum possible reflection amplitude of the flexural wave mode. This occurs for flaws with a circumferential extent of 180° for the first order flexural, 90° and 270° for the second order flexural and 60° , 180° and 300° for the third order flexural. Since the reflection of the axisymmetric mode is linear with increasing circumferential extent (for a fixed through wall and axial extent), the value of A_0 can be found from simulation of a flaw of any circumferential extent. Therefore two models, one with a 180° flaw and one with a 270° flaw will be sufficient to determine all of the values required. Section 5.5 describes the finite element modelling method in more detail.

Since it is not possible to make ϕ_f the subject of Equation 5.2, a graph or lookup table must be used to determine the circumferential extent for a given mea-

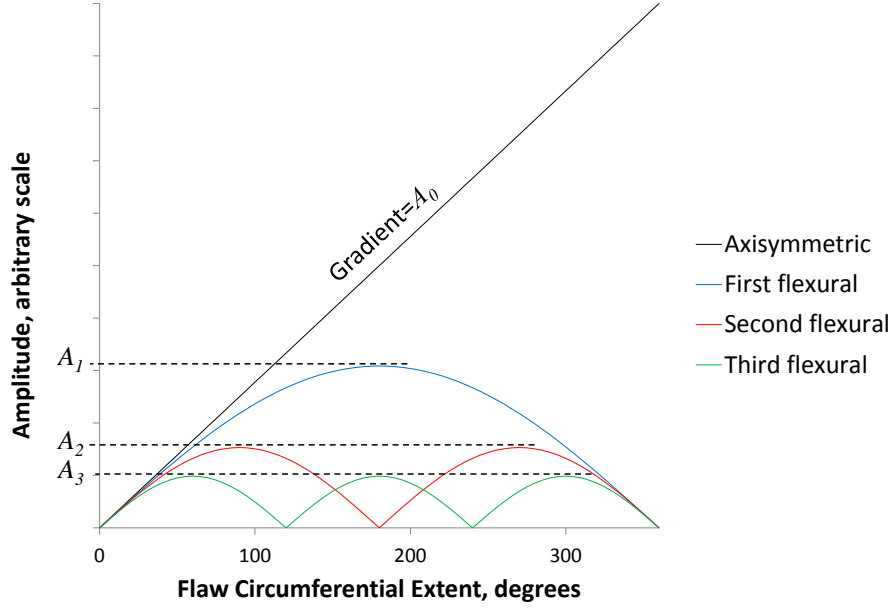


Figure 5.2: Reflection of the first four wave modes with respect to flaw circumferential extent showing how the constants A_0 , A_1 , A_2 and A_3 are defined.

surement. To illustrate this, Figure 5.3 shows Equation 5.1 plotted. The amplitudes of the reflected axisymmetric wave mode divided by the sum of the amplitudes of the first three reflected flexural wave modes gives a measured value of P . Then, the circumferential extent of the flaw can be determined as shown in the Figure. It is noticeable that the gradient of the curve is steep for flaws with a small circumferential extent. Therefore, measurement errors for such flaws are likely to be large.

Once the circumferential extent has been determined, the through wall extent of the flaw can be estimated by linking the estimated cross sectional area loss to an assumed cross sectional flaw shape. For the purposes of this study, a notch-like flaw shape has been assumed. A schematic of this is given in Figure 5.4.

The cross sectional area loss is generally a linear function of the reflection of the axisymmetric wave mode [Alleyne & Lowe, 1998]. The reflection amplitude from a flaw is also dependent on the axial extent particularly for flaws with a large circumferential extent [Sanderson, 2003; Demma *et al.*, 2003]. This can be taken account of in the finite element model calibration by matching the axial extent of the flaw to that of the experiment. However, when the axial extent of the flaw is unknown, the test frequency can be swept to find the frequency at which a maxima occurs. This can then be combined with finite element models of a flaw with an

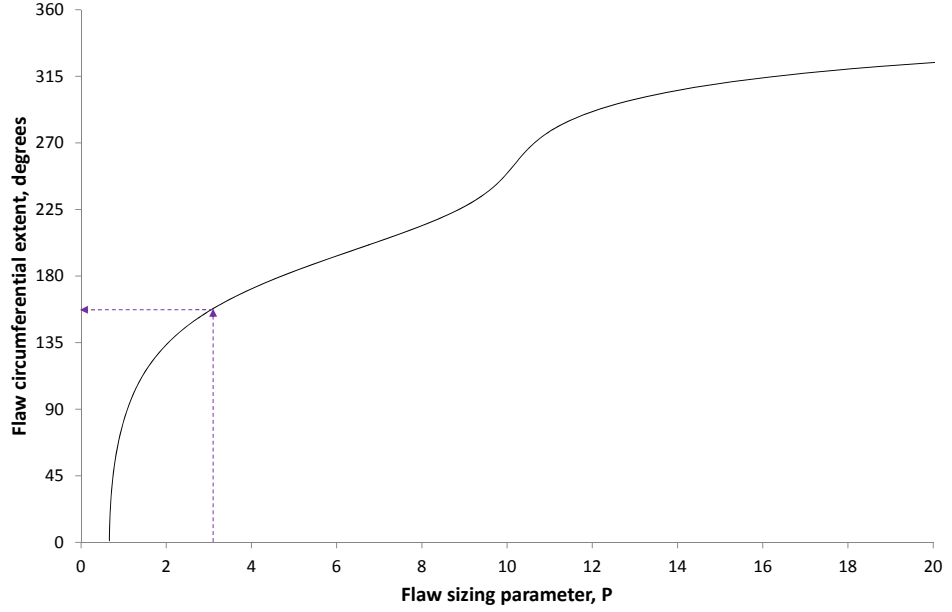


Figure 5.3: Illustration of the procedure for determination of the circumferential extent of a flaw using the ratio of the reflected axisymmetric wave mode to the sum of the reflected flexural wave modes.

axial extent equal to a quarter of the wavelength (i.e. where maximum reflection amplitude will occur).

Assuming a notch-like geometry as shown in Figure 5.4, the relationship between the through wall extent d and the circumferential extent, ϕ_f in radians, and the cross sectional area loss, C as a ratio of the pipe cross sectional area can then be derived to be:

$$d = r_o - \sqrt{r_o^2 - \frac{2C\pi(r_o^2 - r_i^2)}{\phi_f}}, \quad (5.3)$$

where r_o is the outer radius of the pipe and r_i is the inner radius of the pipe.

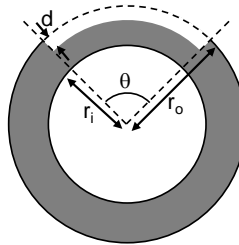


Figure 5.4: Schematic of a notch-like flaw in cross section.

5.3.2 Enhancement and practical application

Catton [2009] also carried out a theoretical study of the inclusion of more than three flexural wave modes in the formulation. This concept is examined further here. As previously mentioned, the gradient becomes steep for flaws with a small circumferential extent. Therefore the gradient of the curve was calculated for a few different flaws for a theoretical formulation where $A_0 = 0.5$ and $A_n=1$ for $n \geq 1$. These values were selected as they were similar to those calculated by finite element analysis for the pipes studied. Figure 5.5 shows the gradient of the curve for three flaws of different circumferential extents. It is confirmed that an increased number of flexural modes reduces the gradient for all three flaws, therefore increasing the accuracy of the measurement of circumferential extent. However, at the frequencies commonly used for guided wave inspection, there are sometimes a limited number of flexural wave modes and the higher order flexural modes are dispersive. This should be taken into consideration when selecting the number of flexural wave modes to use in the equation. In this chapter three flexural wave modes have been used for most cases. In the case of the largest diameter pipe studied (24 inch), an increase to seven flexural wave modes has been tested.

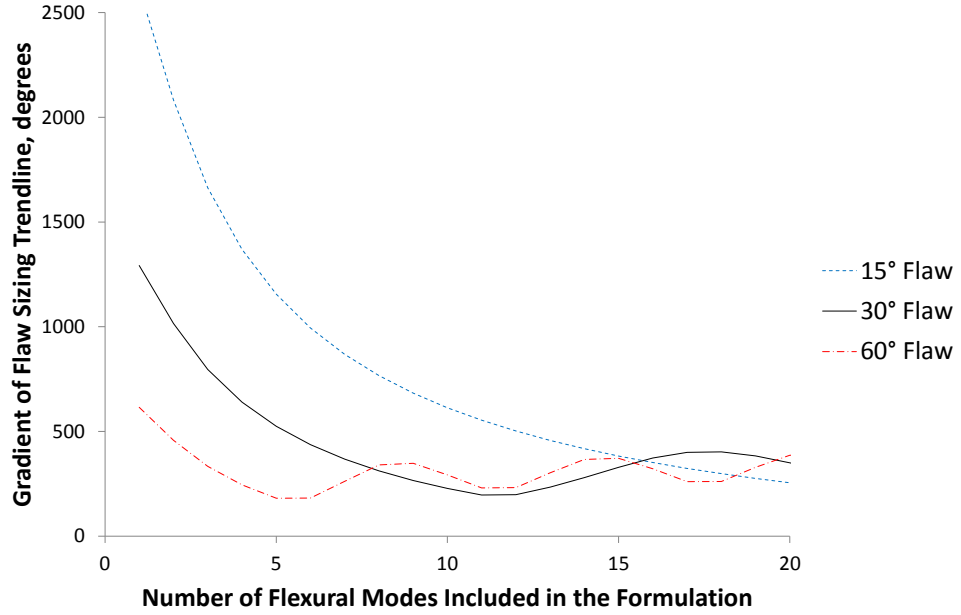


Figure 5.5: Gradient of flaw sizing trendline (extension of Equation 5.2) against number of flexural wave modes included in the equation for three flaw sizes.

A practical addition to the method is suggested which involves classifying a flaw as ‘narrow’ if its circumferential extent is less than or equal to 60°. As ex-

plained, large errors are possible for circumferentially narrow flaws and it is therefore misleading to report their estimated circumferential and through wall extents. At first glance, this rule seems quite restrictive as it means that it would not be possible to determine the size of a large number of flaws. However, this is not the case. Since commercial guided wave inspection is likely to only reliably detect flaws of 9% or bigger, the through wall extent of a narrow flaw is likely to be large. An estimate of the minimum through wall extent can be found by using Equation 5.3. For typical pipe sizes (such as those studied here), the through wall extent is at least 50% of the pipe wall thickness. This is therefore much more likely to be a severe flaw for which repair or replacement would be required. Therefore the flaw sizing method proposed has value as a decision making tool for pipeline operators.

5.4 Characteristics of real corrosion flaws

A total of 41 of the flaws from the ApplusRTD laser profilometry database were analysed. These flaws were from a 508mm outer diameter, 5.5mm wall thickness pipe (NPS 20 inch Schedule 10S¹). The material grade of the pipe was API 5L X52 (52,000 psi or 359MPa minimum yield strength). In many of the cases the images from the database had multiple features. In order to get an idea of the shape of typical corrosion flaws, the overall dimensions of each feature were assessed individually. In cases where there were multiple features, the deepest of the features was used. Table 5.1 gives some basic statistics about these flaws.

	Axial extent,mm	Circumferential extent,degrees	Through wall extent,mm	Cross-sectional area, %
Mean	20.15	3.86	1.75(32% wall loss)	0.25
Standard Dev.	21.51	3.49	0.61(11% wall loss)	0.19
Maximum	130.00	23.20	3.83(70% wall loss)	1.12
Minimum	4.00	1.40	0.88(16% wall loss)	0.07

Table 5.1: Summary of features from ApplusRTD laser profilometry database

All of the flaws in the database are well below the reporting level of commercially available equipment of 9% cross sectional area loss. However, since these flaws are all less than 60° circumferential extent, if they were to be detected, the procedure should class them as ‘narrow’ and therefore they would be flagged for further assessment.

¹NPS stands for Nominal Pipe Size and is a commonly used set of standard sizes for pipes for high or low pressures and temperatures in North America.

Typical aspect ratios of the flaws were examined. The ratio of circumferential extent (in mm) to maximum through wall extent (in mm) was calculated for each flaw. This ranged from 3.7 to 59.8 with an average of 10.3 (i.e. flaws are roughly ten times as wide as they are deep). The ratio of axial extent (in mm) to maximum through wall extent (in mm) was also calculated for each flaw. This ranged from 2.1 to 75.6 with an average of 12.3 (i.e. flaws are roughly twelve times longer than they are deep).

5.5 Finite element analysis

5.5.1 Regular shaped flaws

Modelling work has been carried out to investigate the applicability of the flaw sizing technique for the following pipe sizes and frequencies:

- 60.3mm outer diameter, 3.91mm wall thickness (NPS 2inch Schedule 40¹): 70kHz and 140kHz.
- 168.3mm outer diameter, 7.11mm wall thickness (NPS 6inch Schedule 40¹): 27kHz, 50kHz and 70kHz.
- 323.9mm outer diameter, 10.31mm wall thickness (NPS 12inch Schedule 40¹): 70kHz.
- 609.6mm outer diameter, 17.48mm wall thickness (NPS 24inch Schedule 40¹): 40kHz and 70kHz.
- 914.4mm outer diameter, 9.53mm wall thickness (NPS 36inch Schedule 40S¹): 27kHz, 50kHz and 70kHz.

Finite element models to simulate wave propagation and interaction with flaws were generated using ABAQUS version 6.9. Previously validated rules for mesh density and other modelling parameters were used [Alleyne & Lowe, 1998; Zhu, 2002]. The intention of the study was to assess the flaw sizing procedure rather than validate the finite element technique.

The material was assumed to be ferritic steel with the same material properties as given in Chapter 4 (Young's Modulus=207GPa, Poisson's ratio=0.3 and Density=7830kg/m³).

In order to match with commercially available equipment, the excitation was applied through a ring of nodes around the circumference of the pipe and the applied

loads were in the circumferential direction. This resulted in the $T(0,1)$ wave mode being generated. In all cases a 10-cycle Hann-windowed pulse was used. Other than during the applied excitation, it was assumed that the pipe was free to vibrate (i.e. no boundary conditions were applied).

Each flaw had a constant through wall extent (i.e. notch-like) so that the principle of flaw sizing in a range of diameters could be assessed.

Figure 5.6 shows an example of one of the models used including an image showing the level of mesh refinement.

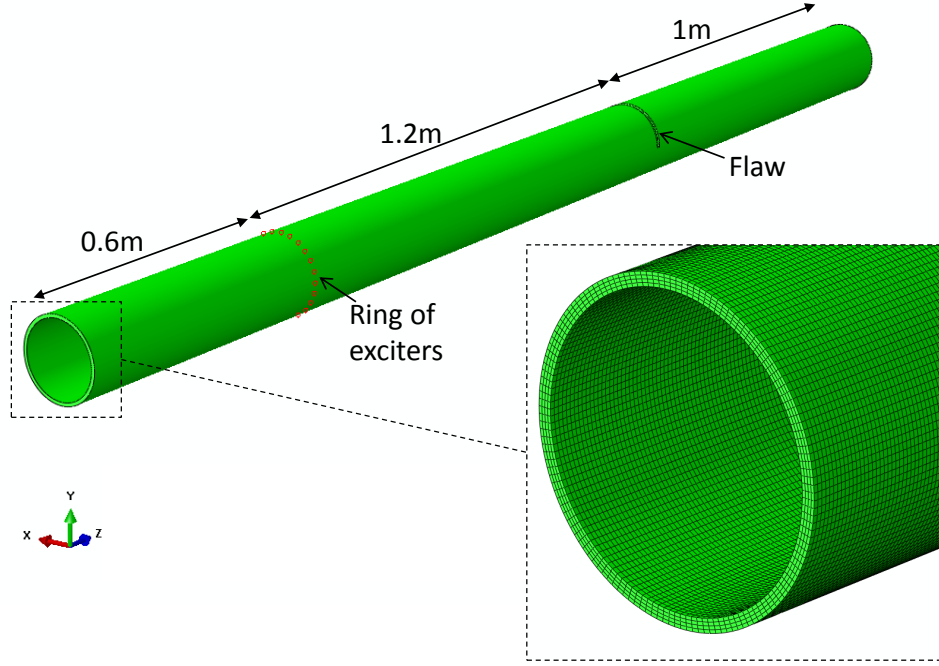


Figure 5.6: Finite element model used to predict reflections from a 180° notch-like flaw in a 168.3mm outer diameter, 7.11mm wall thickness steel pipe.

A total of 78 different notch-like flaw cases were analysed. The through wall extent of these flaws ranged from 25% to 75% wall loss and from 5° to 355° in circumferential extent. The results were processed following the proposed flaw sizing inspection procedure detailed in Section 5.3 so that the waveforms predicted by the FE model were assessed in exactly the same way as experimentally measured waveforms would be.

Out of the total number of flaws 28 were ‘narrow’ ($\leq 60^\circ$ circumferential extent). These were all correctly identified using the technique described in Section 5.3. The remaining 50 flaws were correctly identified as ‘non-narrow’ and the through wall extent was calculated for those cases. Figure 5.7 shows the through wall extent

measurement made using the waveforms from the FE analysis against the actual through wall extent. The dotted line is a one-to-one relationship and therefore flaws that lie on or close to this line are predicted to be accurately measured.

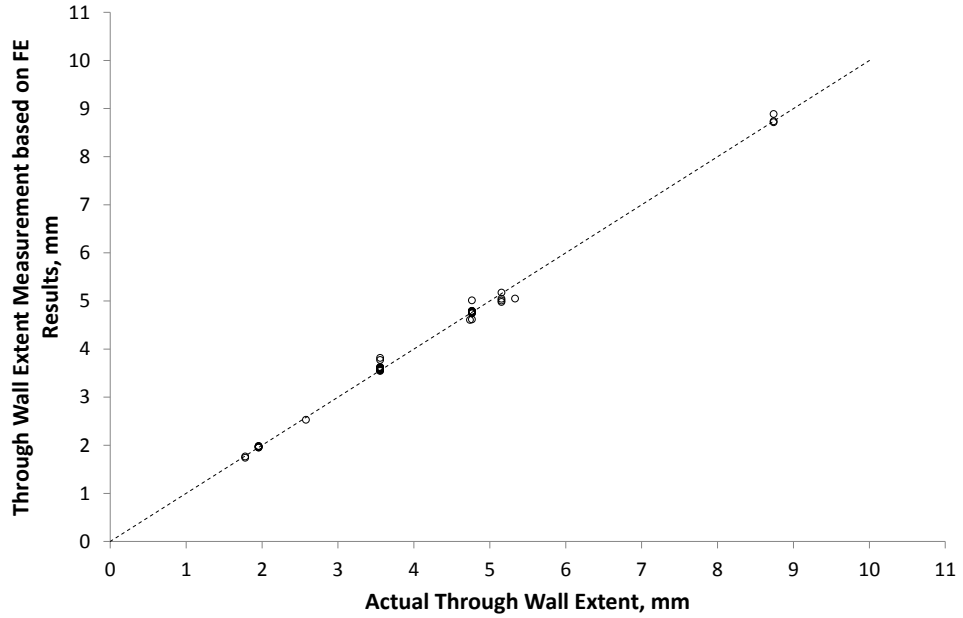


Figure 5.7: Through wall extent measurement from procedure applied to FE predictions against actual through wall extent for a range of flaws, test parameters and pipe dimensions.

All of the points lie close to the line. The largest error in through wall extent measurement was predicted by the finite element model to be 0.3mm and the average error in through wall extent measurement was predicted by the finite element model to be 0.06mm. These results indicate the level of accuracy achievable with the flaw sizing procedure given ideal experimental conditions such as a perfectly balanced transducer array and a corrosion free pipe with an isolated flaw.

5.5.2 Real corrosion flaws

Further modelling was carried out to establish the effect of flaw shape on the flaw sizing procedure. Seven real corrosion cases taken from the ApplusRTD laser profilometry database were simulated. These flaws were all from a 508mm outer diameter, 5.5mm wall thickness pipe (NPS 20inch Schedule 10S¹). Table 5.2 gives details of the flaws that were simulated.

Figure 5.8 shows an example of the flaw from Image 27 after it had been translated to the finite element mesh.

Image ref.	Max.through wall extent,%	Circumferential extent,degrees	Axial length,mm	Description
1	55	6.5	24.0	Irregular shaped pit
50	31	19.0	110.0	Corrosion patch
26	32	14.0	28.0	Corrosion patch
47	70	5.0	26.0	Corrosion pit
4	46	3.6	38.0	Corrosion pit
4	39	10.6	80.0	Two adjacent pits
27	54	11.0	14.0 each	Two separated pits

Table 5.2: Details of the real corrosion flaws that were modelled

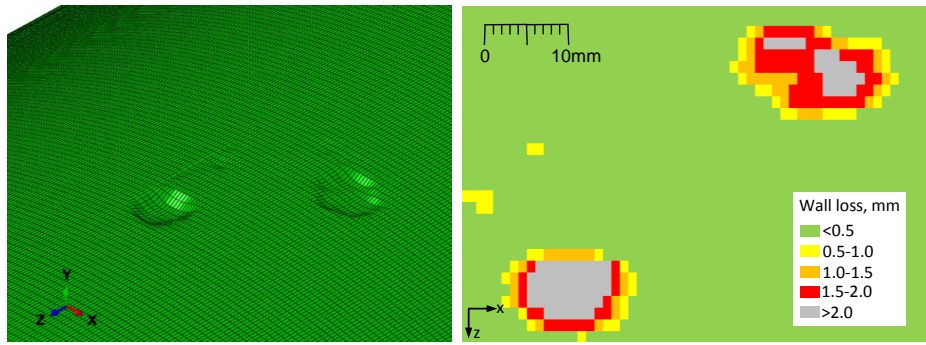


Figure 5.8: Close up isometric image of finite element mesh (left) and plan view of Image 27 from the real corrosion flaw database (right).

The flaws were on the limit of detectability for guided wave inspection. The cross sectional area loss for the seven flaws ranged from 0.4% to 1.1%. They were all also ‘narrow’ flaws with a range of circumferential extent from 4° to 19° . Since the flaws are relatively small, the variation of the reflection amplitudes with axial extent is relatively small. Therefore, a fixed frequency was used for these analyses. The excitation used was a 10-cycle 70kHz Hann windowed pulse.

Figure 5.9 shows an example of one of the predicted time waveforms for the first four reflected wave modes from the real corrosion flaw database. It can be seen that the amplitudes of each of the wave modes are similar. This indicates that the value of the flaw sizing parameter, P will be small and that the flaw is ‘narrow’.

Figure 5.10 shows the actual circumferential extent of the flaw plotted against the flaw sizing parameter, P for each real corrosion flaw modelled. It can be seen that the values are all correctly predicted to be ‘narrow’ (i.e. $\leq 60^\circ$).

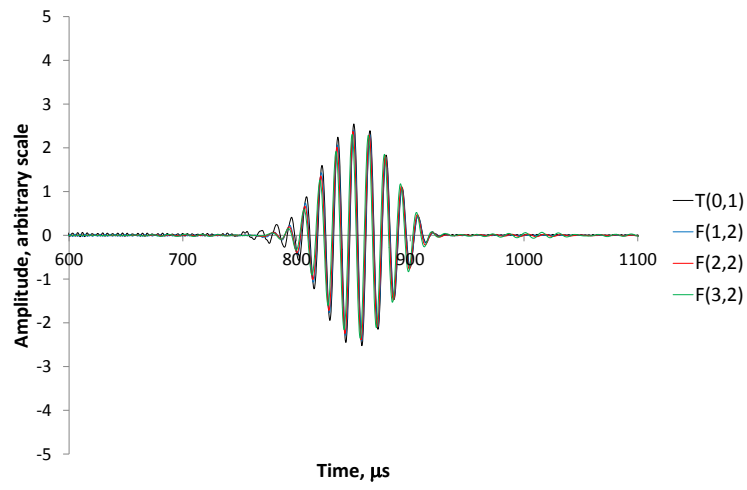


Figure 5.9: Predicted time waveforms for the first four wave modes reflecting from Image 26 from the real corrosion flaw database. The amplitudes of the reflections are similar indicating that the flaw is ‘narrow’.

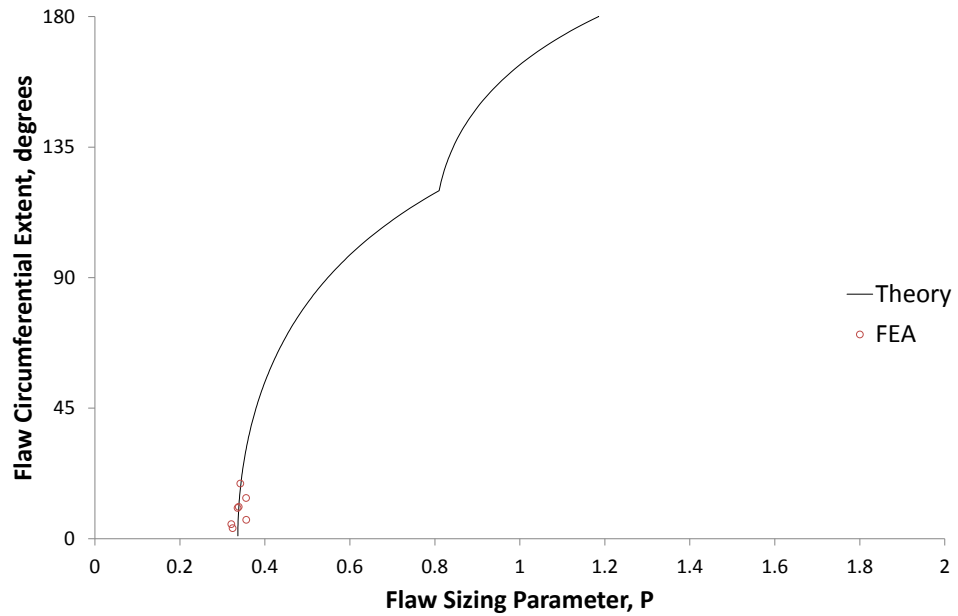


Figure 5.10: Actual flaw circumferential extent against flaw sizing parameter, P for the real corrosion flaws modelled.

5.6 Experimental measurements

5.6.1 Overview

A range of experiments have been conducted to obtain flaw sizing results from a selection of different flaw types and pipe sizes. In addition, the experimental data gathered by Catton [2009] for 168.3mm outer diameter, 7.11mm wall thickness pipe was reanalysed using the proposed technique. The data ranged from laboratory experiments with machined notches to industrial pipes removed from service containing real corrosion flaws, as follows:

- 168.3mm outer diameter, 7.11mm wall thickness pipe (6" pipe) - 8 machined flaws.
- 219.1mm outer diameter, 8.18mm wall thickness pipe (8" pipe) - 3 ground flaws.
- 323.9mm outer diameter, 10.31mm wall thickness (12" pipe) - 10 machined flaws.
- 406.4mm outer diameter, 6mm wall thickness (16" pipe) - one real corrosion flaw.
- 457.2mm outer diameter, 6mm wall thickness (18" pipe) - one real corrosion flaw, two test locations.
- 609.6mm outer diameter, 9.53mm wall thickness (24" pipe) - one ground flaw, two test locations.

The following sections give the details of each of these experiments and the results of the inspection using the suggested flaw sizing procedure.

5.6.2 6" pipe

The experiment carried out by the present author with Catton [2009] involved machining eight flaws into a 168.3mm outer diameter, 7.11mm wall thickness pipe using a milling machine. A schematic of the experiment is shown in Figure 5.11. The layout was designed so that the reflections from the pipe ends would not coincide with the reflections from the flaw. A total of 24 individually addressable transducers around the circumference were used to transmit and receive the guided wave signals. This was done so that the wave modes could be identified individually using a mode filtering technique devised by Catton [2009]. The mode filtering technique

works by multiplying the signals received at points around the circumference by a scaling factor matching that of the circumferential displacement pattern of the desired mode to be filtered. The formula for the scaling factors is as follows:

$$SF = \cos(n(\theta - \alpha)), \quad (5.4)$$

where SF is the scaling factor, n is the order of the mode to be filtered, θ is the circumferential location and α is the circumferential orientation of the wave mode.

The input signal was a 10-cycle 70kHz pulse and the axial extent of the flaws was fixed at 10mm. The details of each flaw and the results after processing using the suggested procedure are summarised in Table 5.3.

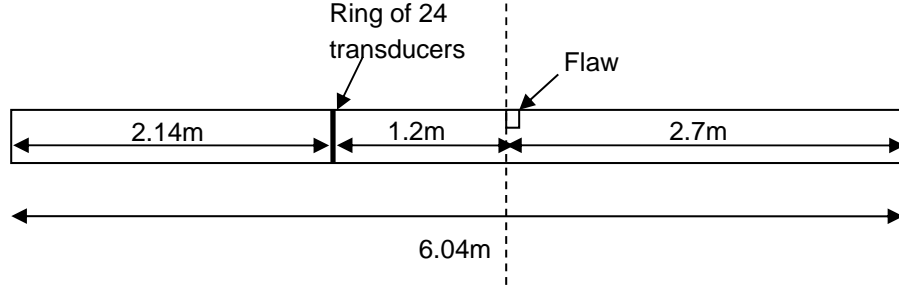


Figure 5.11: Layout of flaw sizing experiments in 6" pipe.

Flaw Index	Actual through wall extent, mm	Actual circ. extent, degrees	Measured circ. extent, degrees	Error in circ. extent, degrees	Measured through wall extent, mm	Error in through wall extent, mm
6-1	1.8	30	'narrow'	n/a	n/a	n/a
6-2	1.8	60	78	18	1.7	-0.1
6-3	1.8	120	117	-3	2.2	0.4
6-4	3.6	120	141	21	3.7	0.1
6-5	3.6	180	199	19	3.9	0.3
6-6	3.6	250	237	-13	4.5	0.9
6-7	4.7	250	259	9	5.1	0.4
6-8	4.7	325	313	-12	4.8	0.1

Table 5.3: Experimental flaw sizing results for 6" pipe.

All flaws (ranging from a cross sectional area loss of 2.1% to 61%) were detected (the amplitude of the reflection from the flaw had a signal to noise ratio of around 6dB or higher).

Figure 5.12 shows the actual flaw circumferential extent against flaw sizing

parameter, P for the measurements made on the flaws. It can be seen that they lay close to the theoretical line and that Flaw 6-1 was correctly determined as ‘narrow’. The other flaws were all correctly determined as ‘non-narrow’ and the through wall and circumferential extent measurements were therefore made. The circumferential extent was determined to within 21° and the depth was determined to within 0.9mm.

Figure 5.13 shows an example of the measured signals for flaw 6-1 which has an approximate cross sectional area loss of 2%.

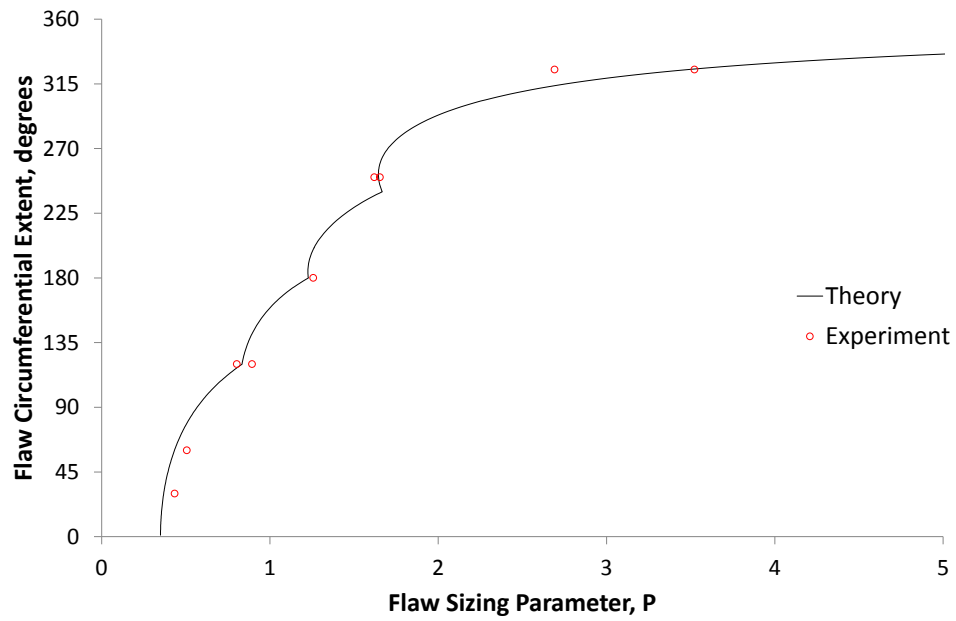


Figure 5.12: Actual flaw circumferential extent against flaw sizing parameter, P for the flaws measured in 6inch pipe. Note that the chosen scale results in the larger signals being cropped.

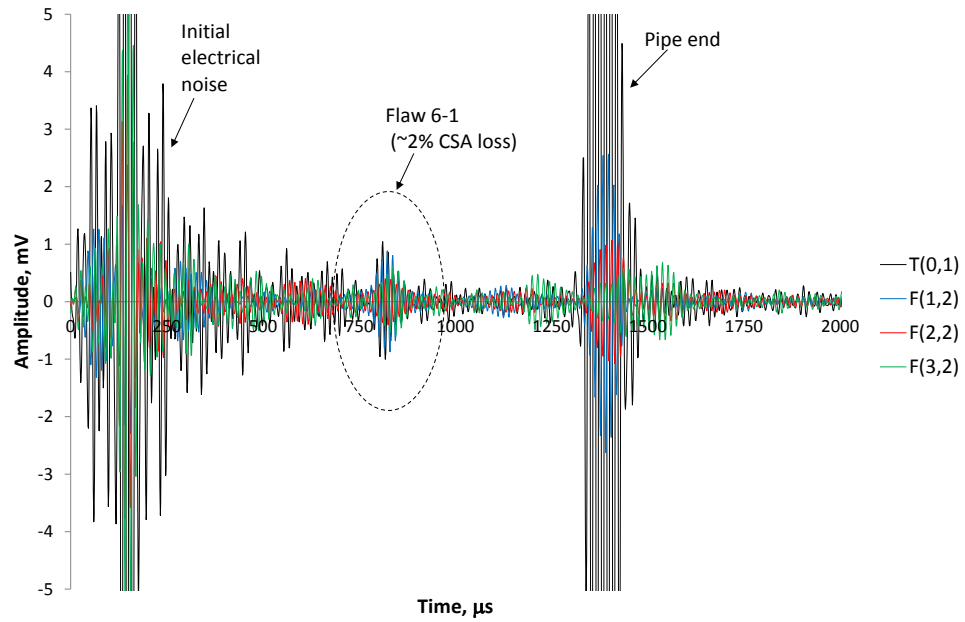


Figure 5.13: Experimentally measured amplitude of T(0,1) family wave modes reflected from flaw 6-1.

5.6.3 8" pipe

Three flaws were introduced into a 219.1mm outer diameter, 8.18mm wall thickness pipe. The flaws were introduced by hand using an angle grinder so that the shape was closer to that of real corrosion. Figure 5.14 shows the layout of the experiment. The flaws ranged from approximately 0.5% to 2% cross sectional area loss. Table 5.4 gives details of the approximate dimensions. The axial extent was roughly 12mm for all three flaws. The input signal was a 10-cycle 60kHz pulse.

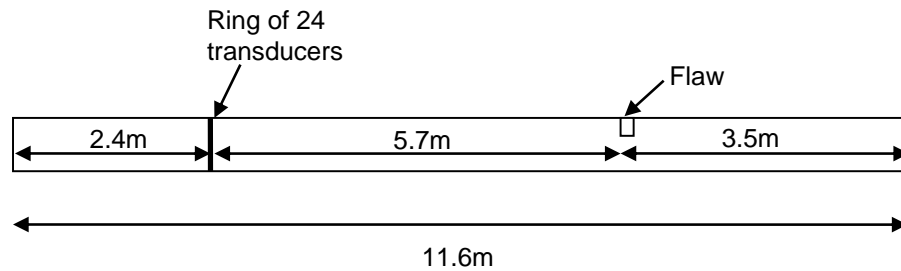


Figure 5.14: Layout of flaw sizing experiments in 8" pipe.

A total of 24 individually addressable transducers around the circumference were used to transmit and receive the guided wave signals. Flaw 8-1 was undetected (the amplitude of the reflection from the flaw had a signal to noise ratio of greater

Flaw Index	Cross sectional area loss, %	Maximum through wall extent, mm	Circumferential extent, mm	Circumferential extent, degrees
8-1	0.5	1.0	29	15
8-2	1	1.5	40	21
8-3	2	2.0	57	30

Table 5.4: Approximate dimensions of flaws in the 8" pipe.

than 6dB). Flaws 8-2 and 8-3 were detected. Figure 5.15 shows the actual flaw circumferential extent against flaw sizing parameter, P for the measurements made on Flaws 8-2 and 8-3. It can be seen that they were correctly identified as ‘narrow’ using the flaw sizing procedure.

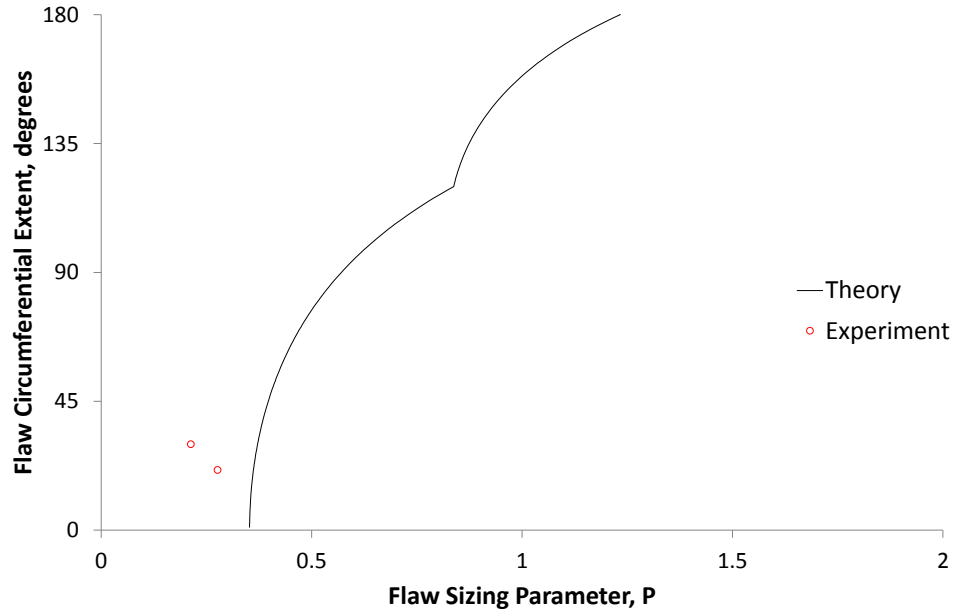


Figure 5.15: Actual flaw circumferential extent against flaw sizing parameter, P for the flaws measured in 8 inch pipe.

5.6.4 12" pipe

An experiment was carried out on a 323.9mm outer diameter, 10.31mm wall thickness pipe. A number of notch-like flaws were machined into the pipe and the guided wave inspections were repeated for each flaw size. The axial extent of the flaw was 8mm and the input signal was a 10-cycle 40kHz pulse.

In this case, there were 32 transducers around the circumference which were split into 16 segments of two transducers. Table 5.5 below gives details of the machined flaw geometries and Figure 5.16 shows the layout of the experiment.

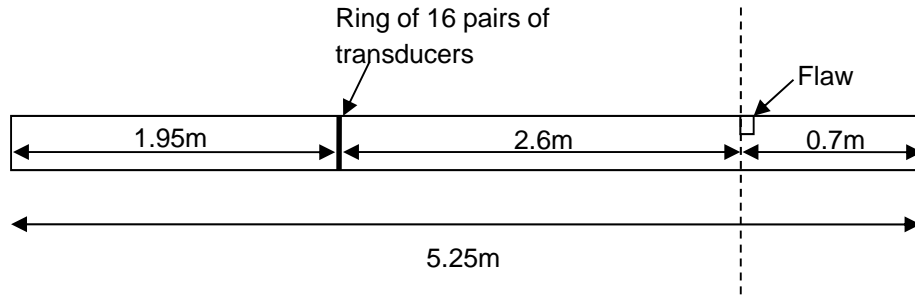


Figure 5.16: Layout of flaw sizing experiments in 12" pipe.

Flaw Index	Through wall extent, mm	Circumferential extent, degrees	Cross sectional area loss, %
12-1	1.3	7.5	0.3
12-2	2.6	7.5	0.5
12-3	2.6	15	1.1
12-4	3.9	15	1.6
12-5	3.9	30	3.2
12-6	3.9	45	4.8
12-7	3.9	60	6.4
12-8	3.9	75	8.0
12-9	3.9	90	9.6
12-10	5.2	90	12.7

Table 5.5: Approximate dimensions of flaws in the 12" pipe.

Flaws 12-1, 12-2 and 12-3 were not detected (the amplitude of the reflection from the flaw had a signal to noise ratio of greater than 6dB). The other flaw (Flaws 12-4 to 12-10) were detected and flaws 12-4 and 12-5 were correctly identified as 'narrow'. Flaw 12-6 was borderline as it was measured to be 60°. The flaw sizing procedure was therefore applied to Flaws 12-6 to 12-10. The measured through wall and circumferential extents are given in Table 5.6. Figure 5.17 shows the actual flaw circumferential extent against flaw sizing parameter, P for the measurements made on Flaws 12-4 to 12-10. The through wall extent was determined correctly to within 1.3mm and the circumferential extent was correct to within 23°.

Flaw Index	Actual circumferential extent, degrees	Actual through wall extent, mm	Measured circumferential extent, degrees	Measured through wall extent, mm
12-6	45	3.9	60	2.6
12-7	60	3.9	88	2.6
12-8	75	3.9	99	2.8
12-9	90	3.9	108	2.9
12-10	90	5.2	113	4.1

Table 5.6: Flaw sizing guided wave measurements for flaws in a 323.8mm outer diameter, 10.31mm wall thickness pipe.

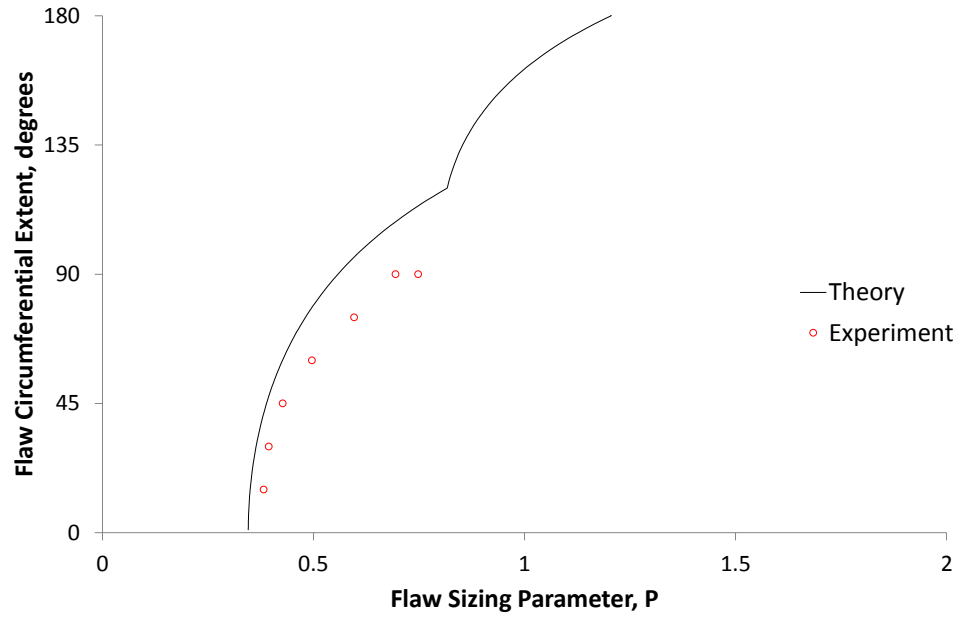


Figure 5.17: Actual flaw circumferential extent against flaw sizing parameter, P for the flaws measured in 12 inch pipe.

5.6.5 16" pipe

Flaw sizing experiments were carried out on a 406.4mm outer diameter, 6mm wall thickness pipe at GDF Suez, Paris. The pipe was previously removed from service and contained an example of real corrosion. The pipe was subsequently wrapped in poly-ethylene (PE) coating. The specimen also contained seam welds. These are both factors that will affect the flaw sizing procedure and were not taken account of. Therefore, this study acts as a basic test of the sensitivity to such effects. The experimental layout is shown in Figure 5.18. The input signal was a 10-cycle 40kHz pulse. This frequency was selected due to the larger pipe size; more modes will exist at a given frequency and therefore the same performance can be achieved at a lower frequency. The commercial 16" collar has forty transducers around the circumference. However, due to the hardware limitations in the maximum number of receiving channels, twenty pairs of transducers were used to excite and receive the signals.

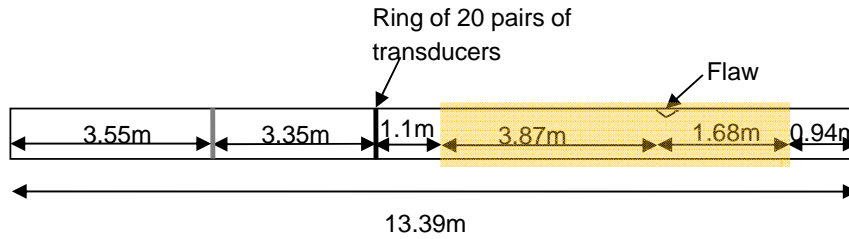


Figure 5.18: Layout of flaw sizing experiments in 16" pipe. Shaded region depicts PE coating.

The maximum through wall extent of the flaw was 1.93mm and the circumferential extent was approximately 10° (or 35mm). The axial extent of the flaw was around 53mm. The cross sectional area loss was therefore less than 0.9%.

The flaw was successfully detected and correctly identified as 'narrow' by the flaw sizing procedure.

5.6.6 18" pipe

Flaw sizing experiments were carried out on a 457.2mm outer diameter, 6mm wall thickness pipe at GDF Suez, Paris. The pipe was previously removed from service and contained real corrosion. The pipe was subsequently wrapped in poly-ethylene (PE) coating. The specimen also contained seam welds. The pipe was inspected from two test locations. The experimental layouts are shown in Figure 5.19. As for the 16" pipe, the input signal was selected to be a 10-cycle 40kHz pulse. The commercial

18" collar has forty-eight transducers around the circumference. However, due to the hardware limitations in the maximum number of receiving channels, twenty-four pairs of transducers were used to excite and receive the signals.

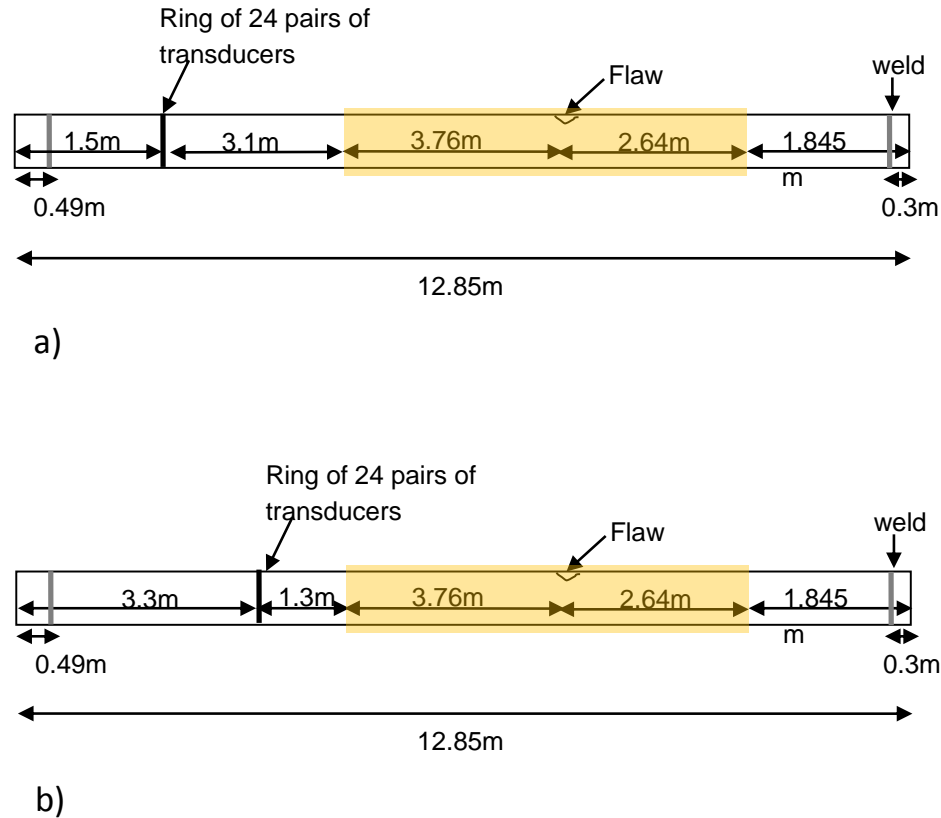


Figure 5.19: Layout of flaw sizing experiments in 18" pipe. Shaded region depicts PE coating; a) Test location 1; b) Test location 2.

The flaw was a single metal loss region with a maximum through wall extent of 2.11mm and circumferential extent of approximately 6° (or 25mm). The axial extent of the flaw was around 25mm. The cross sectional area loss was therefore less than 0.6%.

In the first test location, the flaw was not clearly detected. This is expected as the cross sectional area loss is much less than the accepted reporting level of 9%. In the second test location, the flaw was detected and correctly measured as a 'narrow' flaw. The reason for the non-detection in the first test location compared to the second test location is likely to be the additional dispersion experienced due to the transducer array being further from the flaw or interference from reflections of other features in the pipe such as the welds.

5.6.7 24" pipe

Flaw sizing experiments were carried out on a 24 inch pipe specimen. The largest of the flaws in the specimen was selected for circumferential and through wall sizing measurements. In addition, the data from this flaw was used to test out a refinement to the flaw sizing procedure. The pipe had an outer diameter of 609.6mm and a wall thickness of 9.53mm.



Figure 5.20: The flaw assessed in the 24 inch pipe.

Figure 5.20 shows the flaw in the pipe that was investigated. The flaw had a through wall extent of 5mm, an axial extent of 26mm and a circumferential extent of 29° . The approximate cross sectional area loss of the flaw was 4.3%. Measurements were made in two different locations. One ring of transducers was used with 60 transducers around the circumference grouped in 20 segments of 3. The input signal was a 10-cycle 40kHz pulse. Figure 5.21 shows the layout of the experiment. The flaw was inspected from two locations. The flaw was detected and correctly identified as ‘narrow’ in both tests. Figure 5.22 shows the actual flaw circumferential extent against flaw sizing parameter, P for the two flaws. It can be seen that the flaw was correctly identified as ‘narrow’ from both test locations.

Next, a suggested refinement to the flaw sizing procedure was tested. For large diameter pipes, the number of flexural wave modes is increased. Therefore instead of using a sum of the first three flexural wave modes in the denominator, a

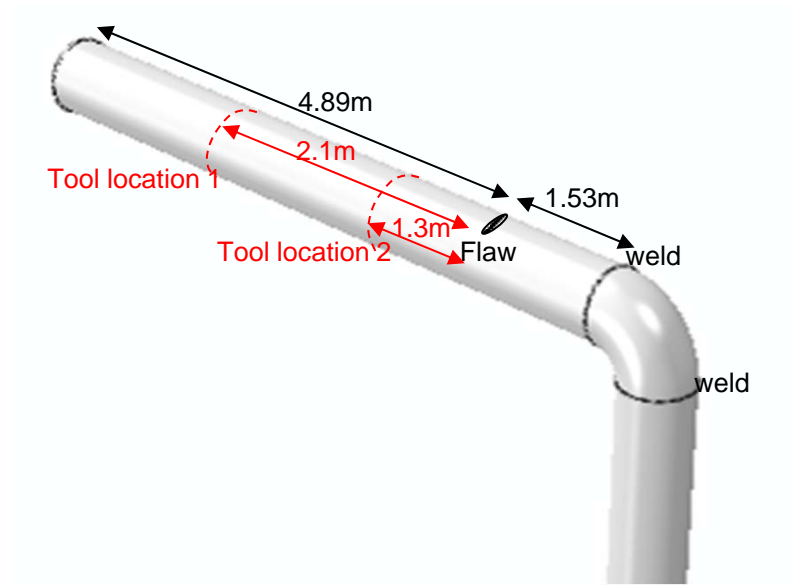


Figure 5.21: Layout of flaw sizing experiments in 24" pipe.

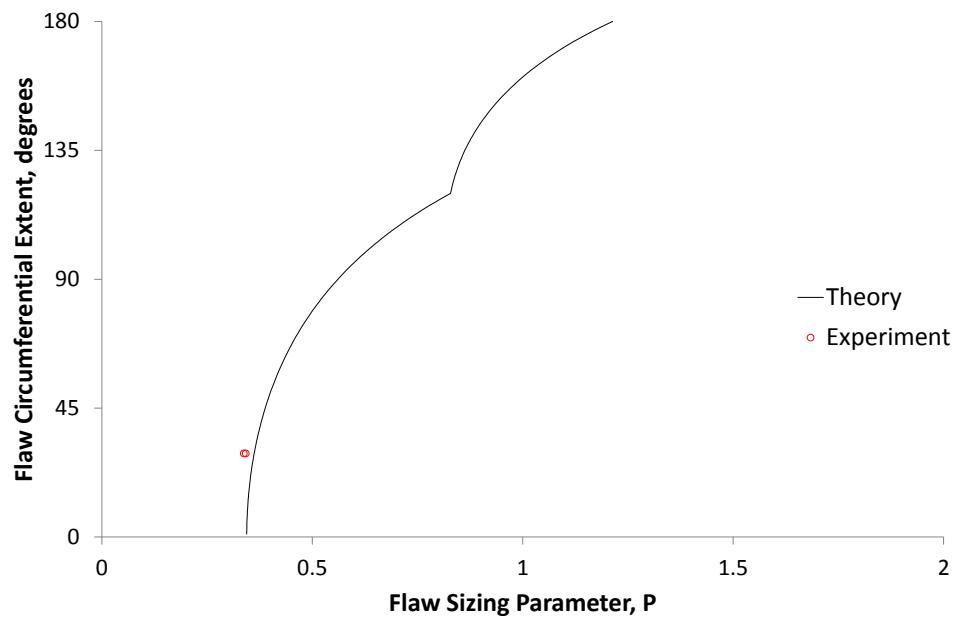


Figure 5.22: Actual flaw circumferential extent against flaw sizing parameter, P for the flaws measured in 24 inch pipe.

sum of the first seven flexural wave modes was tested.

Figure 5.23 shows the actual flaw circumferential extent against the enhanced flaw sizing parameter for the two flaws. Using this refinement, in the first test location the flaw through wall extent was measured to be 3.9mm and in the second test location the flaw through wall extent was measured to be 4.7mm. The actual through wall extent was 5mm. Therefore, the through wall extent was measured to within 1.1mm. This is an initial indication that it will be possible to size ‘narrow’ flaws, at least in larger diameter pipes where a greater number of flexural wave modes exist.

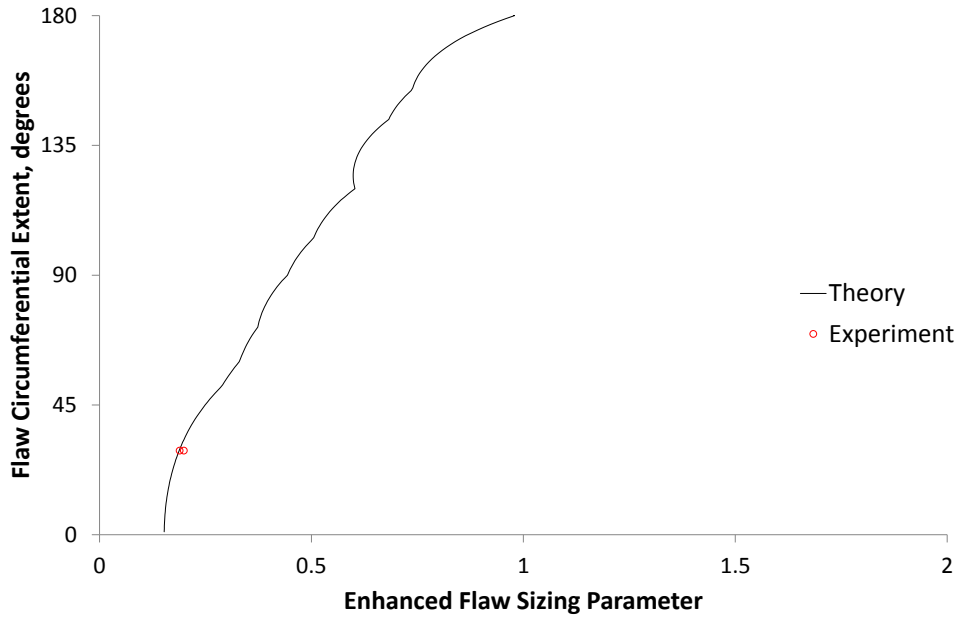


Figure 5.23: Actual flaw circumferential extent against enhanced flaw sizing parameter for the flaws measured in 24 inch pipe.

5.6.8 Assessment of limitations

Figure 5.24 shows the measured through wall extent against the actual through wall extent for all of the experimental data collected for ‘non-narrow’ flaws. The best fit straight line and one-sided 90% prediction interval are also shown on the plot.

The average error is +0.2mm and -0.8mm and the maximum error is -1.3mm. Since this data is a mix of different pipe wall thicknesses, the error as a percentage of wall thickness has also been considered. The average is +7% and -20% of the wall thickness of the pipe and the maximum error is -32% of the wall thickness of the pipe.

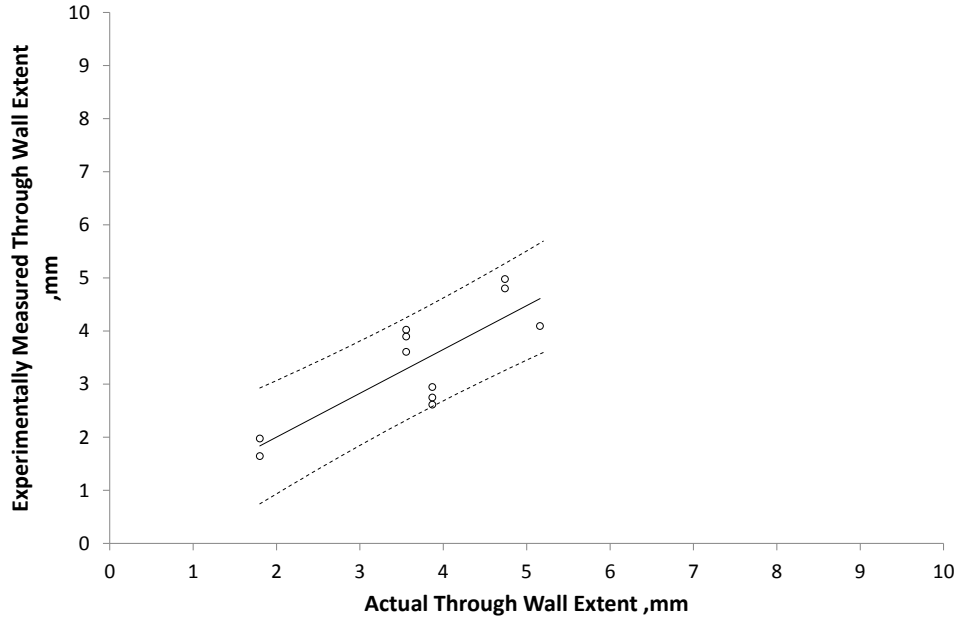


Figure 5.24: Experimentally measured through wall extent measurement against actual through wall extent for a range of flaws, test parameters and pipe dimensions. The best fit (continuous line) and one-sided 90% prediction interval (dotted lines) are shown.

Figure 5.25 shows the measured circumferential extent against the actual circumferential extent for all of the ‘non-narrow’ flaws. The best fit line and one-sided 90% prediction interval are also shown on the plot. The average error is -6° and $+16^\circ$. The maximum error is $+23^\circ$.

The performance of the technique has been assessed for flaws that have been detected but it is also useful to consider the flaws that could remain undetected in the pipe after application of this technique. Moreover, an assessment of the effect this could have on the continued operation of the pipeline is also useful. Flaws with a cross sectional area of around 1% or less were not detected in most cases (i.e. false negative results).

The through wall extent for such a flaw was estimated using Equation 5.3 and flaw circumferential extent to through wall extent aspect ratio of 10.3. This value was derived from the real corrosion data in Section 5.4. Therefore, the likely effect on the revised maximum allowable operating pressure (MAOP) of flaws that could remain undetected in the pipe can be estimated using the equations in Part 4 of ASME B31G. This has been done for two example cases as follows:

- A 609.6mm outer diameter pipe with 9.53mm wall thickness, with a flaw of 1% cross sectional area loss with the typical aspect ratios determined from the

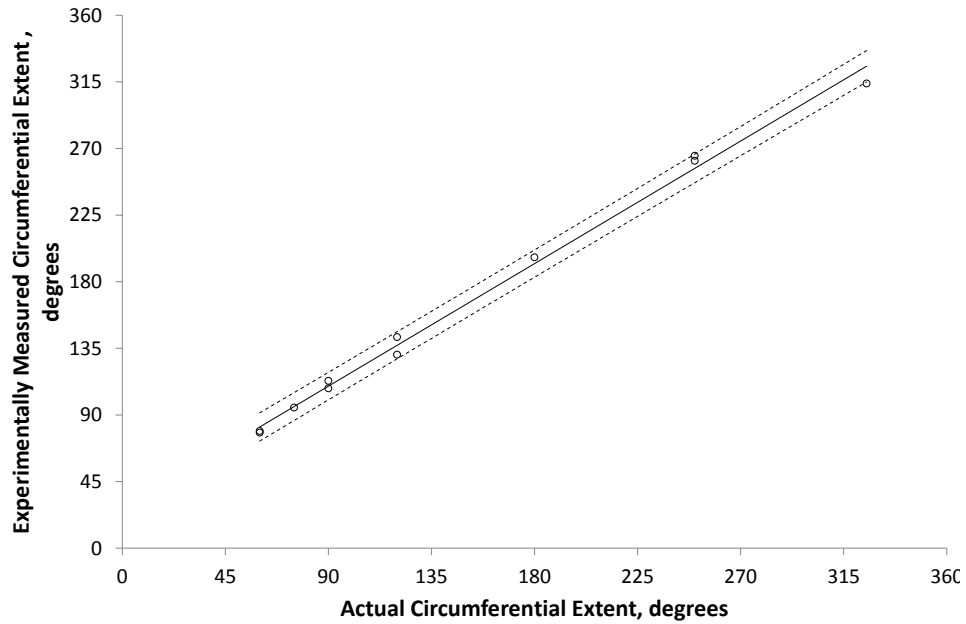


Figure 5.25: Experimentally measured circumferential extent measurement against actual circumferential extent for a range of flaws, test parameters and pipe dimensions. The best fit (continuous line) and one-sided 90% prediction interval (dotted lines) are shown.

ApplusRTD database will have a through wall extent of around 4.2mm (44% of the through wall extent). Using the average ratio from the ApplusRTD database, a typical axial extent of such a flaw will be around 52mm. Such a flaw under ASME B31G could remain in place without the need to revise the MAOP.

- A 168.3mm outer diameter with 7.11mm wall thickness pipe, with a flaw of 1% cross sectional area loss with the typical aspect ratios determined from the ApplusRTD database will have a through wall extent of around 1.9mm (27% of the through wall extent). Using the average ratio from the ApplusRTD database, a typical axial extent of such a flaw will be around 23mm. Such a flaw under ASME B31G could remain in place without the need to revise the MAOP.

The calculation was then repeated for the deepest and the longest individual feature from the set of 41 real corrosion examples from the ApplusRTD database as follows:

- The first had a through wall extent of 3.83mm, an axial extent of 28mm and

an estimated cross sectional area loss of 0.7%. Such a flaw under ASME B31G could remain in place without the need to revise the MAOP.

- The second had a through wall extent of 1.72mm, an axial extent of 130mm and an estimated cross sectional area loss of 1.1%. Such a flaw under ASME B31G could remain in place with a revised MAOP of 95% of the original MAOP.

This basic analysis give some confidence that guided wave inspection could be used as an inspection technique without the need for further inspection with other methods.

5.7 Discussion

The flaw sizing procedure presented here groups detected flaws into two categories: those which are ‘narrow’ and those which are ‘non-narrow’. It is proposed that for flaws which are ‘non-narrow’, the circumferential and through wall extent can be measured relatively accurately. This has been shown to work well in that ‘narrow’ flaws have been correctly identified and a simple calculation has been used to show that these are likely to require repair or replacement and the size of ‘non-narrow’ flaws have been measured relatively accurately. This therefore demonstrates the potential for guided wave inspection to be used to determine the fitness-for-service of pipe.

However, an enhancement to the technique to allow accurate sizing of ‘narrow’ flaws would make it more attractive still. With the current technique, errors in through wall extent measurements can occur for flaws below 60° circumferential extent (hence the proposed classification of ‘narrow’ and further investigation recommended). The relationship between the error in the through wall extent estimate and the circumferential extent of the flaw is illustrated in Figure 5.26 where all of the experimental data are plotted regardless of their classification as ‘narrow’ or not. Testing in regimes where higher order modes exist and can therefore be used in the formulation, has the potential to increase resolution and make the sizing of ‘narrow’ flaws possible. This has been successfully demonstrated for a 29° flaw in 24 inch pipe (see Section 5.6.7). It is possible to apply this using modified current commercial equipment to larger diameter pipes. However, there are fewer higher order modes in existence in smaller diameter pipes at the frequencies that the equipment operates at (up to 80kHz). Modified hardware and tooling could be developed to allow application of the improved flaw sizing technique to smaller diameter pipes

and this should be the subject of future work.

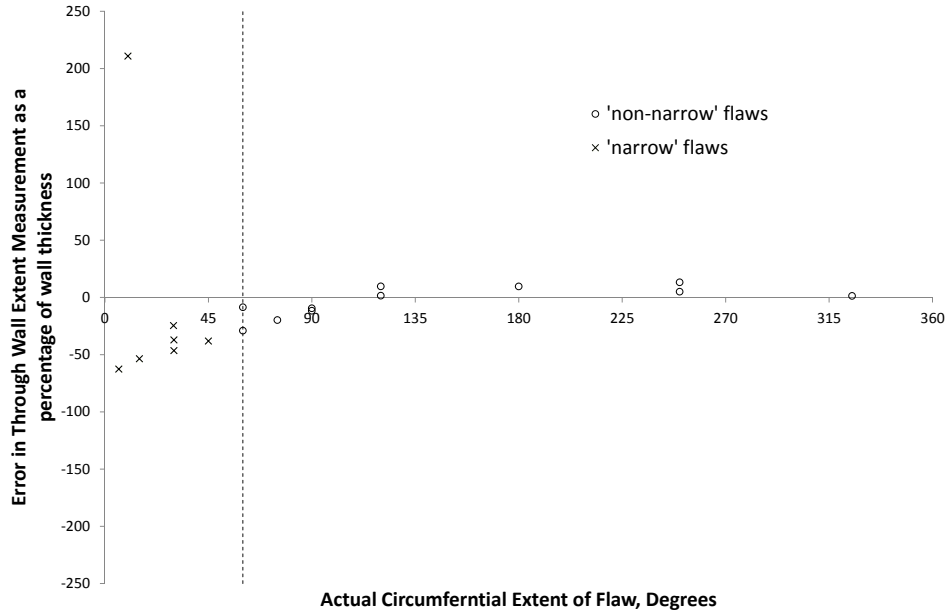


Figure 5.26: Error in through wall extent measurement against circumferential extent of the flaw. Dotted line represents the divide between ‘narrow’ and ‘non-narrow’ flaws at 60°. The error is seen to tend towards zero as circumferential extent increases (22 results plotted).

The axial extent of the flaw is also an important dimension in fitness-for-service assessments. It is possible that frequency sweeps will provide some information about the axial extent but a robust measurement method is needed. This should be the subject of future work.

The flaw sizing technique relies on the relative proportions of wave modes reflected from the flaw. The presence of coatings or material around the pipe could affect this relationship. However, attenuation dispersion curves have been calculated for an 219.1mm outer diameter, 8.18mm wall thickness steel pipe with an epoxy coating [Mu & Rose, 2007]. These curves show that the relative proportions of the wave modes in the torsional family remain relatively constant over the frequency range of standard guided wave inspection. Therefore it is possible that a modification to the flaw sizing algorithm is not necessary to improve accuracy for coated or buried pipes. However this should be the subject of future work and as for all guided wave inspections, the valid test range could be reduced by the presence of a coating.

5.8 Conclusions

Suggested modifications to a flaw sizing procedure have been developed and demonstrated experimentally to work effectively for a range of pipe diameters and flaw sizes and shapes. The circumferential extent of all of the flaws detected were correctly categorised as either ‘narrow’ or ‘non-narrow’. Where it was deemed possible to make measurements (for ‘non-narrow’ flaws), the through wall extent was found to be within 1.3mm of the actual value and the circumferential extent was found to be within 23° of the actual value.

Estimates have been made based on typical flaw shapes taken from laser profilometry data. The deepest flaw that could exist without being detected by the guided wave flaw sizing procedure would result in a reduction in maximum allowable operating pressure of just 5%. This, combined with the accurate flaw size assessment, indicates that the suggested guided wave flaw sizing procedure could be used conservatively as a direct input to a fitness-for-service assessment.

A refinement to the flaw sizing procedure has been tested in a 609.6mm outer diameter, 9.53mm wall thickness pipe. It was shown that it was possible to determine the circumferential extent to within a few degrees and the through wall extent to within 1.1mm for a relatively narrow flaw.

The work presented in this chapter indicates that there is the potential for determining the through wall and circumferential extent of isolated flaws. However, corrosion flaws often occur in clusters. This topic is examined in the next chapter.

Chapter 6

Multiple Flaws

6.1 Introduction

Recent research has advanced the guided wave inspection technique so that it may be possible to characterise individual flaws. Some of these techniques are discussed in more detail in Section 3.6 and one particular technique has been developed and generalised for a range of pipe sizes in the previous chapter of this thesis. However, corrosion often occurs in clusters and therefore the effect of the presence of multiple flaws must be addressed if flaws are to be adequately characterised in the field.

There has been a great deal of work done on the reflections from a single flaw. However, relatively little research has been done on the interactions of multiple flaws in pipes. Work has been done in the past by Domany *et al.* [1984] and Schafbuch *et al.* [1993], on the numerical simulation of the elastic scattering from two embedded flaws. However, this did not deal with the multimode nature of guided waves in pipes. Nishiguchi *et al.* [2008] developed a simple analytical model for the prediction of the reflection of T(0,1) from fully circumferential flaws in pipes. The model was compared to finite element solutions and experiments and relatively good agreement was obtained. However, this work concentrated on the T(0,1) wave mode only and did not consider mode conversions into flexural wave modes.

Some recent work has been done to look at the effects of multiple flaws on guided wave signals in pipes [Løvstad & Cawley, 2011b,a, 2012]. A number of circular flaws at various locations in a pipe were studied using finite element analysis combined with experimental validation. However, the work concentrated on relatively small flaws (approximately 2.5% cross sectional area loss, 7° circumferential extent) where the effects of interaction between the flaws was found to be negligible.

The work presented in this chapter quantifies the effects of multiple flaws on

guided wave signals for larger flaws where the interaction becomes significant. The methodology presented here also enables the signals from features beyond others to be corrected. Finite element analyses simulating the interaction of guided waves with flaws have been first validated against experiments using a single flaw and then used to study the effect of two flaws. Also, with the aim of application to field testing scenarios, where computationally fast solutions are required, an analytical modelling procedure has been developed. The analytical model can be used to simulate the reflection and transmission (the onward propagation from a flaw) of guided waves from multiple flaws. This has been verified by comparison with the finite element simulations.

6.2 Analytical model concept

The development of a generic model to simulate the reflections from a single flaw of any size and shape is not the intention of this work. Well-established numerical techniques such as finite element analysis can be used to calculate this. Instead, a simplified approach has been adopted so that the advantages of shorter computation times and a theoretical understanding of the overall behaviour can be exploited and used in conjunction with analytical models for wave propagation to compute results in an industrial field test scenario.

First, equations have been developed that describe the reflection and transmission characteristics of a single flaw purely as a function of the circumferential extent. It is proposed that this general behaviour can then be scaled depending on other characteristics such as flaw cross sectional shape and pipe geometry. These scaling factors can be determined using finite element analysis of a single flaw case. The reflection and transmission coefficients as a function of circumferential extent of the flaw are then effectively decoupled from other variables. The formulation of the analytical model for multiple flaws is described in more detail in Section 6.4 and later verified against finite element analysis.

6.3 Analytical model for a single flaw

6.3.1 Reflection coefficients for a single flaw

The variation of reflection coefficient with the circumferential extent of a single flaw can be described by considering the flaw to be a set of point sources as shown in Figure 6.1.

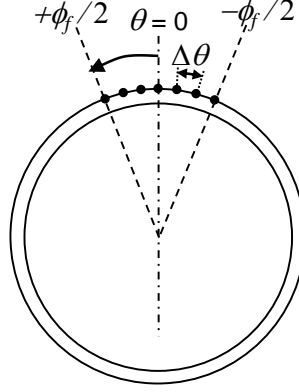


Figure 6.1: Nomenclature for calculation of reflectivity with respect to flaw circumferential extent. The flaw is represented by a series of point sources (indicated by black dots).

For an axisymmetric wave incident on a full thickness flaw, the reflection coefficient, R can be represented by a sum of cosines over the circumferential extent of the flaw as follows:

$$R(\phi_f, n) = \sum_{\frac{-\phi_f}{2}}^{\frac{\phi_f}{2}} \cos(n\theta) \frac{\Delta\theta}{2\pi}, \quad (6.1)$$

where ϕ_f is the circumferential extent of the flaw, n is the order of the reflected wave mode and θ is the angular position around the circumference.

This concept has been confirmed by validation against experimental data [Catton, 2009].

It is proposed that this can be generalised to simulate the reflection of an order n_R mode from a flaw with an incident mode of order n_I and at an angle α as follows:

$$R(\phi_f, n_R, n_I, \alpha) = \sum_{\frac{-\phi_f}{2}}^{\frac{\phi_f}{2}} B \cos(n_R\theta) \cos(n_I(\theta - \alpha)) \frac{\Delta\theta}{2\pi}, \quad (6.2)$$

where B is an integer equal to 2 when $n_I \neq 0$ and 1 otherwise. This is to take account of the effect the wave mode filtering technique (similar to a spatial FFT) has in doubling the contribution from order 0 modes [Catton, 2009].

This formula describes the basic form of the relationship of the reflection coefficient with the circumferential extent of the flaw. There is no analytical solu-

tion available which gives the reflection and transmission coefficients as a function of variables such as frequency, pipe geometry and through wall extent of the flaw. It is therefore necessary to use finite element analysis to derive scaling factors that account for these parameters. It is proposed that a scaling factor, R_f can be introduced to take account of these parameters. The validity of this assumption will be confirmed later by comparison with finite element models of multiple flaws. R_f is defined to be between 0 (no flaw) and 1 (full depth flaw).

As $\Delta\theta$ tends to zero, the reflection coefficient, R can be represented by an integral as follows:

$$R(\phi_f, n_R, n_I, \alpha) = \int_{-\frac{\phi_f}{2}}^{\frac{\phi_f}{2}} B \cos(n_R \theta) \cos(n_I(\theta - \alpha)) \frac{R_f}{2\pi} d\theta, \quad (6.3)$$

which evaluates to:

$$R(\phi_f, n_R, n_I, \alpha) = \frac{B \cos(n_I \alpha) [n_I \sin(\frac{n_I \phi_f}{2}) \cos(\frac{n_R \phi_f}{2}) - n \cos(\frac{n_I \phi_f}{2}) \sin(\frac{n_R \phi_f}{2})] R_f}{\pi(n_I^2 - n_r^2)} \quad (6.4)$$

For cases where $n_R = n_I$ this function is undefined. The cases of $n_R = n_I \neq 0$ and $n_R = n_I = 0$ are considered separately. Firstly, for $n_R = n_I \neq 0$, Equation 6.3 is rearranged using trigonometric identities and values of $B = 2$ and $n = n_R = n_I$ to give the following:

$$R(\phi_f, n, \alpha) = \int_{-\frac{\phi_f}{2}}^{\frac{\phi_f}{2}} 2[\cos(n\theta)^2 \cos(n\alpha) + \cos(n\theta) \sin(n\theta) \sin(n\alpha)] \frac{R_f}{2\pi} d\theta, \quad (6.5)$$

which evaluates to:

$$R(\phi_f, n, \alpha) = \frac{R_f}{2\pi n} \cos(n\alpha) [n\phi_f + \sin(n\phi_f)] \quad (6.6)$$

For the special case where $n_R = n_I = 0$, Equation 6.3 is rearranged and $B = 1$ and $n_R = n_I = 0$ are substituted in to give:

$$R(\phi_f, \alpha) = \int_{-\frac{\phi_f}{2}}^{\frac{\phi_f}{2}} \frac{R_f}{2\pi} d\theta, \quad (6.7)$$

which evaluates to:

$$R(\phi_f) = \frac{\phi_f R_f}{2\pi} \quad (6.8)$$

Figure 6.2 shows the resulting reflection coefficients for the first four wave modes for 100% wall thickness flaws (i.e. $R_f = 1$) calculated using the above formulae. It is worth noting that the shape and amplitudes of the first two curves are the same as those predicted and experimentally measured by Zhou *et al.* [2009] for the longitudinal wave modes L(0,2) and F(1,3). The formulae predict the values of the reflection coefficients to be negative in some cases. If a set of signals are to be summed, it is important to take this into account rather than just using the measured amplitude of each individual signal. This is because it could mean the difference between completely destructive or completely constructive interference.

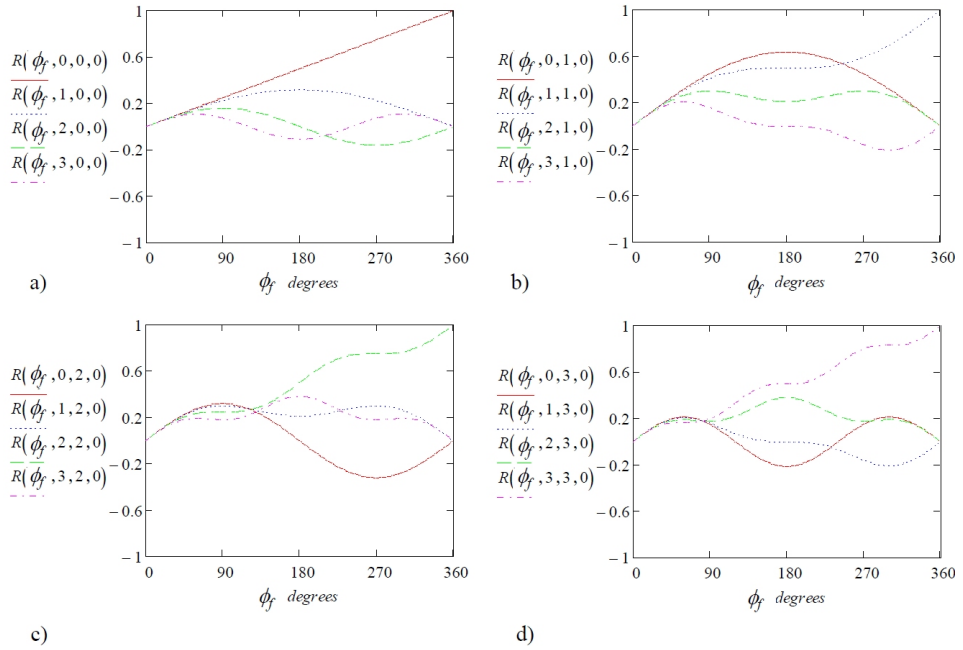


Figure 6.2: Reflection coefficients, $R(\phi_f, n_R, n_I, \alpha)$ against flaw circumferential extent for a 100% wall thickness flaw: a) incident order 0 mode; b) incident order 1 mode; c) incident order 2 mode; d) incident order 3 mode.

Equation 6.4 has a noteworthy solution when $\phi_f = 2\pi$ radians (a fully circumferential flaw). When $n_R \neq n_I$, $R_f = 0$, so no mode conversion will occur. This is a well-known and useful phenomenon, as it is used in commercial guided wave inspection equipment. It allows the distinction between signals from expected features of pipes such as girth welds, and features of more concern such as localised corrosion.

6.3.2 Calculation of R_f

The value of R_f could either be obtained by finite element analysis or experimentally. It is possible to use one finite element model of a single flaw of one size. The procedure for the generation of such a model is described in more detail in Section 5.5. The input could be any wave mode but the simplest model to set up is probably that with an excitation and reception of the T(0,1) wave mode. Once the reflection coefficient has been determined, the value of R_f can be obtained by simple rearrangement of Equations 6.4, 6.6 or 6.8 depending on the incident wave mode selected. In the case of the T(0,1) example, the value of R_f is calculated as follows:

$$R_f = \frac{2\pi R}{\phi_f}, \quad (6.9)$$

where R is the reflection coefficient and ϕ_f is the circumferential extent of the flaw in radians.

The use of a number of finite element models of a range of incident and received wave modes and flaws of different circumferential extents will improve the accuracy of the R_f value determined.

6.3.3 Transmission coefficients for a single flaw

It is postulated that the variation of the transmission coefficient with circumferential extent for a single flaw can be determined by representing the remaining material as a set of point sources. This is illustrated in Figure 6.3.

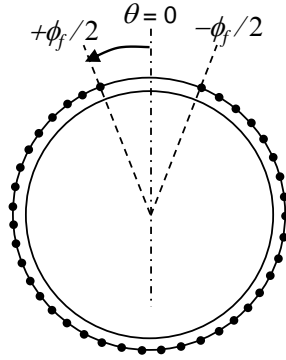


Figure 6.3: Nomenclature for calculation of transmission with respect to flaw circumferential extent. The remaining material is represented by a series of point sources (indicated by black dots).

Instead of deriving the formulae as before, this can be done by replacing ϕ_f

with $2\pi - \phi_f$ in the reflection coefficient equations with $R_f = 1$. The terms that contain ϕ_f are then multiplied by a new scaling factor appropriate for transmission, T_f .

The resulting formulae are as follows:

For $n_R \neq n_I$, Equation 6.4 becomes:

$$T(\phi_f, n_R, n_I, \alpha) = -\frac{B \cos(n_I \alpha) [n_I \sin(\frac{n_I \phi_f}{2}) \cos(\frac{n_R \phi_f}{2}) - n_R \cos(\frac{n_I \phi_f}{2}) \sin(\frac{n_R \phi_f}{2})] T_f}{\pi(n_I^2 - n_R^2)}, \quad (6.10)$$

for $n = n_R = n_I \neq 0$, Equation 6.6 becomes:

$$T(\phi_f, n, \alpha) = [1 - \frac{T_f}{2\pi n} [\phi_f + \sin(n\phi_f)]] \cos(n\alpha), \quad (6.11)$$

and for $n_R = n_I = 0$, Equation 6.8 becomes:

$$T(\phi_f) = 1 - \frac{\phi_f T_f}{2\pi} \quad (6.12)$$

The value of T_f can be calculated in a similar way to R_f , by way of a single finite element model for a given pipe as described in Section 6.3.2. T_f should be between 0 (no flaw) and 1 (full depth flaw). From these equations, it can be seen that when $\phi_f = 2\pi$ radians (a fully circumferential flaw), $T = 0$ for $n_R \neq n_I$ (i.e. no mode conversion will occur as the signal passes through the flaw). Clearly, when the flaw is both fully circumferential and full wall (i.e. a free pipe end), no signal may propagate beyond the flaw (when $T_f = 1$, $T = 0$).

Figure 6.4 shows the transmission coefficients for the first four wave modes for 100% wall thickness flaws calculated using the above formulae with $T_f = 1$.

6.4 Analytical model for multiple flaws

When a wave mode comes into contact with a flaw, mode conversions occur and a number of wave modes are both reflected and transmitted. Since this knowledge is now available for each flaw and each possible incident mode, the cumulative effects of flaws can be summed to calculate the overall reflection characteristics. This is valid since we are considering a linear elastic system. This concept is only valid for separated flaws and cannot be applied to two flaws at the same axial location. Figure 6.5 illustrates the concept using the fundamental torsional wave mode T(0,1) as the incident wave mode and the first flexural wave mode in the T(0,1) family, F(1,2). Only two wave modes have been shown in the diagram for clarity. In the

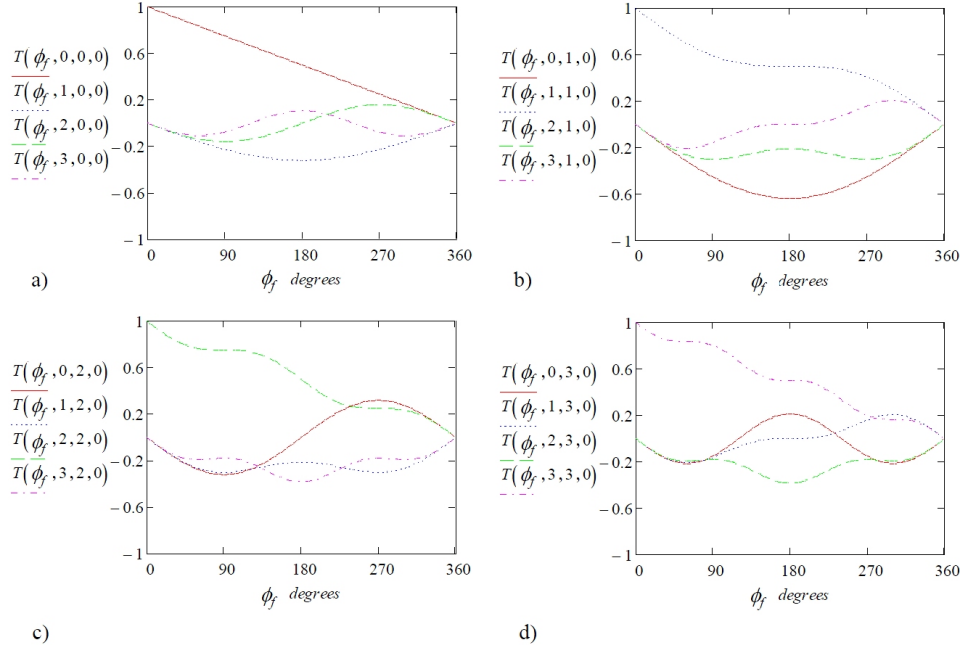


Figure 6.4: Transmission coefficients, $T(\phi_f, n_R, n_I, \alpha)$ against flow circumferential extent for a 100% wall thickness flaw: a) incident order 0 mode; b) incident order 1 mode; c) incident order 2 mode; d) incident order 3 mode.

real scenario many more wave modes will be reflected and transmitted. Similar sequences will exist for other wave mode families. In this example, the $T(0,1)$ reflection from the furthest flaw from the excitation is obtained by the summation of the four different scenarios in which $T(0,1)$ is produced. However, it is not enough to simply sum the amplitudes of reflection and transmission. At a given frequency, each wave mode has a different phase velocity. The summation of different wave modes with different velocities could result in anywhere from complete constructive interference to complete destructive interference. In order to take account of this, the analytical model for straight pipe described in Chapter 4 has been adapted and used to simulate the wave propagation of the signals between flaws.

The distance between flaws travelled by each possible pair of wave mode combinations is taken into account in the modified formula is as follows:

$$u(x, t, n_1, n_2) = \sum_{i=0}^N -A_i \cos\left(2\pi f_i \left(\frac{x}{v_{n_1}} + \frac{x}{v_{n_2}} - t\right)\right) \frac{\Delta f n_c}{2f_c}, \quad (6.13)$$

where, u is the particle displacement, N is the total number of discrete computational points selected, f_c is the central frequency of the excitation, n_c is the number of cycles in the excitation, Δf is the frequency increment, A is the amplitude, n_1

and n_2 are the orders of the mode transmitted from the first flaw and the mode reflected from the second flaw respectively, v_{n_1} and v_{n_2} are the phase velocities of the mode transmitted from the first flaw and the mode reflected from the second flaw respectively, x is the distance between flaws and t is time.

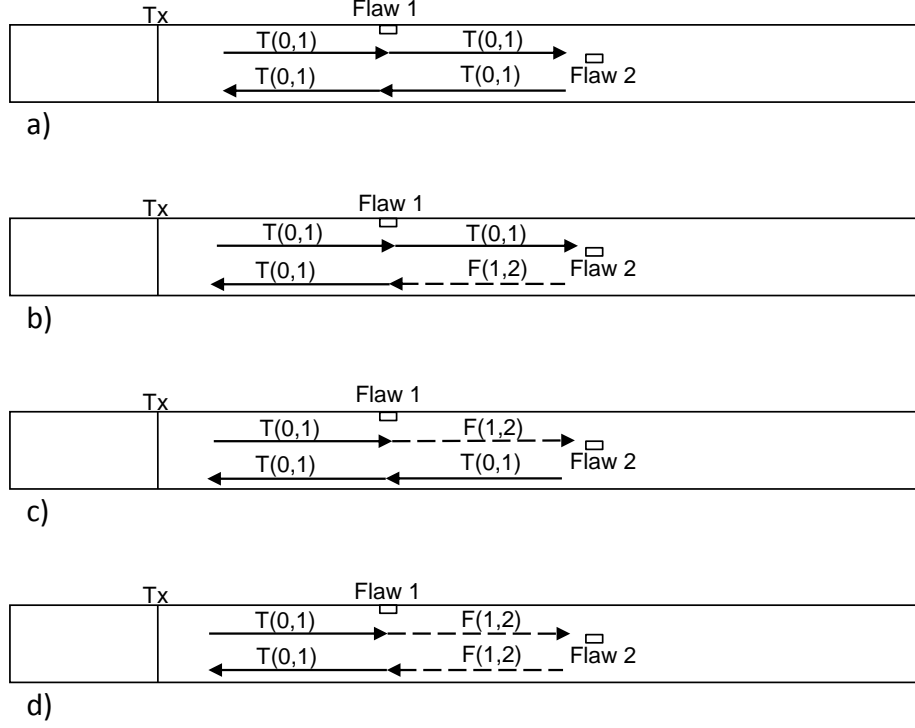


Figure 6.5: Simplified example showing the four different ways in which $T(0,1)$ is received at the excitation location, Tx: a) $T(0,1)$ transmits through flaw 1, reflects from flaw 2 and transmits through flaw 1; b) $T(0,1)$ transmits through flaw 1, $F(1,2)$ is produced when $T(0,1)$ hits flaw 2 and $T(0,1)$ is mode converted when $F(1,2)$ hits flaw 1; c) $F(1,2)$ is produced when $T(0,1)$ hits flaw 1, $T(0,1)$ is produced when $F(1,2)$ reflects from flaw 2 and $T(0,1)$ transmits through flaw 1; d) $F(1,2)$ is produced when $T(0,1)$ hits flaw 1, $F(1,2)$ reflects from flaw 2 and $T(0,1)$ is produced when $F(1,2)$ hits flaw 1. This concept is then applied for all wave modes under consideration.

Equation 6.13 is then summed and adjusted according to the reflection and transmission coefficients for each possible pair of wave mode combinations as follows (as described above and illustrated in Figure 6.5):

$$U(t, n_3) = \sum_{n_1=0}^M \sum_{n_2=0}^M u(x, t, n_1, n_2) T(\phi_{f_1}, n_1, 0, 0) R(\phi_{f_2}, n_2, n_1, \alpha) T(\phi_{f_1}, n_3, n_2, \alpha) \quad (6.14)$$

Here, U is the total displacement on the pipe surface received at the transducer array location, M is the number of wave modes included, x is the distance between flaws, t is time, n_3 is the order of the received mode, T is the transmission coefficient and R is the reflection coefficient as functions of the circumferential extent of flaws 1 and 2, ϕ_{f_1} and ϕ_{f_2} respectively and α is the angle between flaws 1 and 2. Equation 6.14 can then be used to study the effect of one flaw on another at a different axial and/or circumferential location in the pipe.

Moreover, the formulae could be used in conjunction with flaw sizing techniques, such as the one presented in Chapter 5 to determine the size of both flaws. The accuracy of the measurement of the second flaw will of course depend on the accuracy of the measurement of the first flaw.

Equation 6.13 can be logically extended to three flaws by including the additional paths between the three flaws as follows:

$$u(x, y, t, n_1, n_2, n_3, n_4) = \sum_{i=0}^N -A_i \cos(2\pi f_i (\frac{x}{v_{n_1}} + \frac{y}{v_{n_2}} + \frac{x}{v_{n_3}} + \frac{y}{v_{n_4}} - t)) \frac{\Delta f n_c}{2f_c}, \quad (6.15)$$

where x is the distance between the first and second flaws and y is the distance between the second and third flaws. Now there are four possible combinations of wave modes with orders n_1 , n_2 , n_3 and n_4 that result in a given received wave mode at the transducer array. v_{n_1} , v_{n_2} , v_{n_3} and v_{n_4} are the phase velocities of the wave mode transmitted by the first flaw, the wave mode transmitted by the second flaw, the wave mode reflected from the third flaw, and the wave mode transmitted by the second flaw respectively.

Equation 6.14 is then summed and adjusted according to the reflection and transmission coefficients for each possible quartet of wave mode combinations as follows:

$$U(t, n_5) = \sum_{n_4=0}^M \sum_{n_3=0}^M \sum_{n_1=0}^M \sum_{n_2=0}^M [u(x, t, n_1, n_2, n_3, n_4) T(\phi_{f_1}, n_1, 0, 0) T(\phi_{f_2}, n_2, n_1, \alpha) R(\phi_{f_3}, n_3, n_2, \beta) T(\phi_{f_2}, n_4, n_3, \beta) T(\phi_{f_1}, n_5, n_4, \alpha)] \quad (6.16)$$

where n_5 is the order of the received mode, T is the transmission coefficient and R is the reflection coefficient as functions of the circumferential extent of flaws 1, 2

and 3, (ϕ_{f_1} , ϕ_{f_2} and ϕ_{f_3} respectively). The angle of flaw 1 to flaw 2 is α and that of flaw 2 to flaw 3 is β .

The formulae above could be modified to include further flaws in a similar manner. As can be seen, the complexity of the calculation increases rapidly with the number of flaws. However, it may be possible to disregard the contribution from higher order modes since it can be seen from examination of the reflection and transmission coefficients that these have less of an effect on the overall result. The verification of the formulation for more than two flaws is not presented in this thesis.

6.5 Experimental validation

The data gathered from the finite element modelling and experiment on 6 inch pipe described in Sections 5.6.2 and 5.5 respectively, was further examined in order to validate the finite element modelling procedure specifically for this application. Both the finite element and the experimental results were processed using a mode filtering technique suggested by Catton [2009] so that the amplitudes of each individual wave mode reflected from the flaw up to order 4 could be compared. The mode filtering technique works by multiplying the signals received at points around the circumference by a scaling factor matching that of the circumferential displacement pattern of the desired mode to be filtered. The formula for the scaling factors is as follows:

$$SF = \cos(n(\theta - \alpha)), \quad (6.17)$$

where SF is the scaling factor, n is the order of the mode to be filtered, θ is the circumferential location and α is the circumferential orientation of the wave mode.

All of the resulting signals around the circumference are then summed. This has the effect of eliminating all but the target wave mode from the multimode signal. The distance between the flaw and the transducer array was 1.2m in both the experiment and the finite element models.

Figure 6.6 shows the resulting comparison between the finite element model and the experiment. The reflection coefficient was normalised by the through wall extent of the flaw. This allows all of the results to be directly compared and validates the concept that a scaling factor can be used to take account of the through wall extent of the flaw. In each case, both the absolute amplitude and relationship of amplitude with flaw circumferential extent was accurately simulated indicating that the finite element model predicts the interaction of guided waves with flaws adequately.

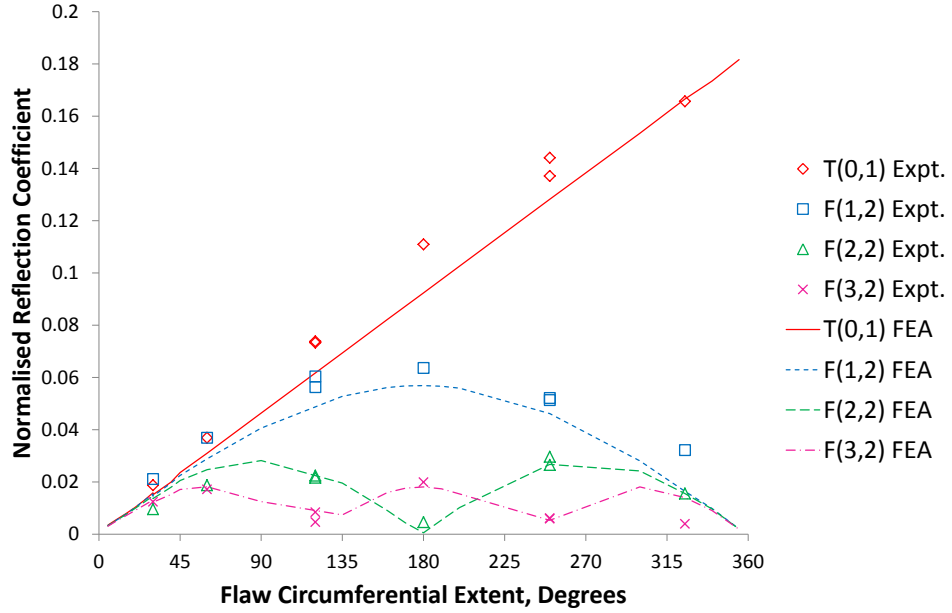


Figure 6.6: Comparison between finite element results (lines) and experiment (points) for a range of flaws normalised by through wall extent.

6.6 Dependence of R_f and T_f

The finite element model was also used to investigate the dependence of the R_f and T_f factors required for the analytical modelling approach.

Firstly, the dependence on frequency was examined. The study was carried out over the frequencies commonly used for guided waves inspection in pipes (30kHz-70kHz) for the selected pipe example (168.3mm outer diameter, 7.11mm wall thickness). Since the axial and through wall extents of the flaw are also known to affect the reflection coefficients [Demma *et al.*, 2003; Sanderson, 2003], the axial extent was kept constant with respect to wavelength so that the length of each flaw was 22% of the wavelength and the through wall extent was kept constant at 50% of the wall thickness. The value of R_f is independent of circumferential extent but for reference, the circumferential extent of the flaws modelled was 180°. Figure 6.7 shows the resulting variation of R_f and T_f with frequency. Both the R_f and T_f values remained relatively constant. It is therefore reasonable to make the simplifying assumption, when using this technique to simulate guided wave inspection scenarios, that the values of R_f and T_f are independent of frequency.

Next, the finite element model was used to study the dependence of R_f on the through wall extent and axial extent of the flaw. A parametric study was carried out for part-wall, partial circumference notch-like flaws. Figure 6.8 shows the resulting

variation with through wall extent for a flaw of a fixed axial extent of 10mm. The circumferential extent of the flaws ranged from 15° to 355° . The trend is linear. Figure 6.9 shows the variation with axial extent for a flaw of a fixed through wall extent of 50% of the pipe wall thickness. For reference, the flaws modelled for this case had a circumferential extent of 30° . The trend observed is sinusoidal.

The study indicates that it would be possible to obtain analytical functions for the variation of R_f and T_f with each key parameter. This would mean that finite element analysis is required for a limited number of cases and it would be relatively straightforward to build a library of R_f and T_f values.

It should be noted that the work carried out concentrated on the T(0,1) family of wave modes. It may be the case that the R_f and T_f values have a non-linear relationship with frequency and flaw through wall extent for other wave mode families, particularly those at higher frequencies.

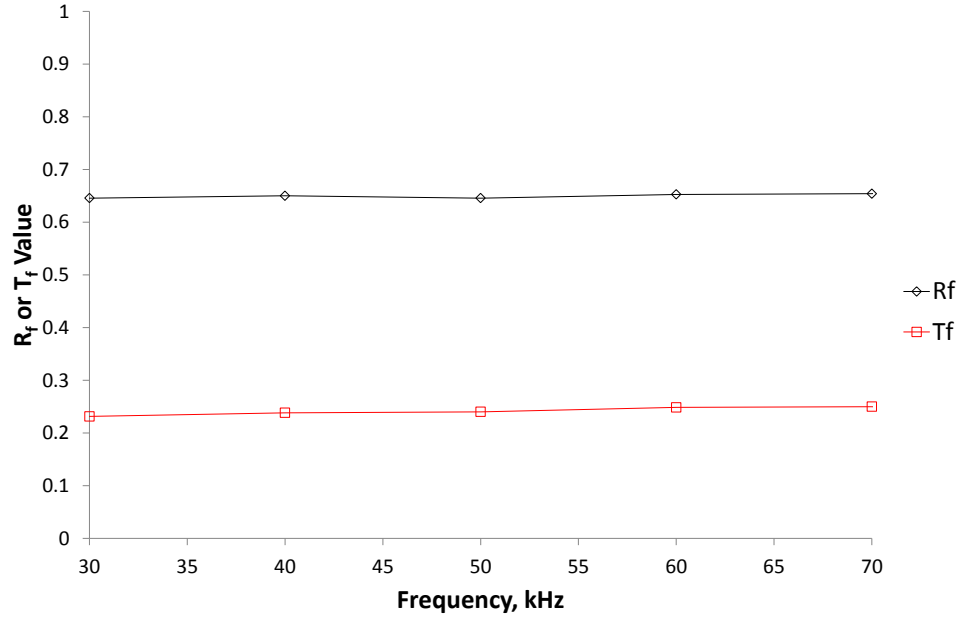


Figure 6.7: Finite element predicted variation of R_f and T_f values with frequency in a 168.3mm outer diameter steel pipe with 7.11mm wall thickness for 50% wall thickness flaws of uniform axial length with respect to wavelength.

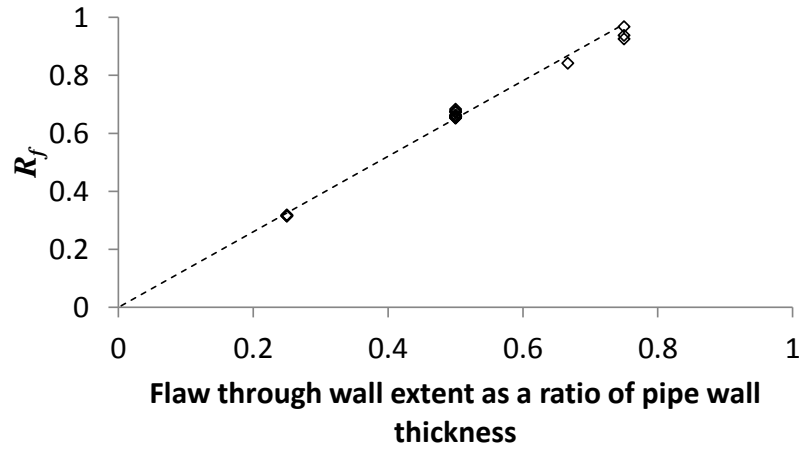


Figure 6.8: Finite element predicted variation of R_f with through wall extent in a 168.3mm outer diameter steel pipe with 7.11mm wall thickness for a flaw with a 10mm axial extent.

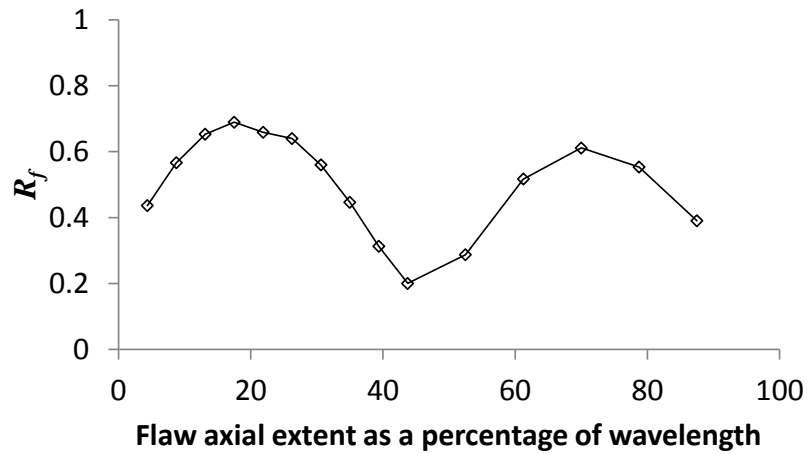


Figure 6.9: Finite element predicted variation of R_f with axial extent in a 168.3mm outer diameter steel pipe with 7.11mm wall thickness for a flaw with a through wall extent equal to 50% of the pipe wall thickness.

6.7 Verification of analytical model for multiple flaws

In order to verify the analytical model for two flaws at different axial locations, the finite element model was extended in length so that a second flaw could be added. Figure 6.10 shows a schematic of the model for one case.

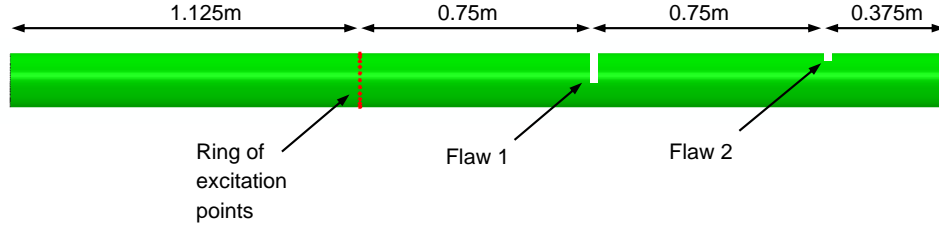


Figure 6.10: Schematic of finite element model used to predict the guided wave response for two flaws at different axial locations.

An example of a first flaw with a through wall extent of 50% wall thickness and 180° circumferential extent was selected. The second flaw was 50% wall thickness. The circumferential extent of the second flaw was varied between angles of 30° to 240° in 30° increments and then from 255° to 330° in 15° increments so that there was a refinement in one region. Both flaws had a constant axial extent of 10mm and the distance between the two flaws was 0.75m. This set of models therefore enabled the calculation of the effect on the reflections from a flaw lying beyond a 180° , 50% wall thickness flaw.

As before, a 10-cycle 70kHz Hann-windowed pulse was excited in the pipe using a ring of 24 points of excitation in the circumferential direction only which resulted in pure $T(0,1)$ being excited in the pipe. The first four modes were used in the analytical model ($M = 4$) and the contribution from modes of order 5 or higher were assumed to be negligible since the reflection coefficient decreases with increasing mode order. To take account of the part wall nature of the flaws being simulated, scaling factors of $R_f = 0.65$ and $T_f = 0.25$ for the reflection and transmission coefficients respectively were used. These were determined by comparison with finite element data for selected flaws of the same through wall extent.

Figure 6.11 shows the comparison between the reflection coefficients from the second flaw with circumferential extent. The reflection coefficients for a 50% wall thickness flaw without the presence of another flaw are also shown on the plots to illustrate the effect that passing through a 180° flaw has on the results. Note that the plot shows the absolute magnitude and does not show the phase relationship since this is difficult to obtain with finite element or experimental data.

The signals were isolated by applying a rectangular gate in the time domain. The pulse reflected from the second flaw should be between $938\mu\text{s}$ and $1081\mu\text{s}$ and the reflection from far end of the pipe should be between $1172\mu\text{s}$ and $1315\mu\text{s}$. Therefore, the gate for the second flaw was between $900\mu\text{s}$ and $1150\mu\text{s}$ and signals outside of this range were set to zero. This process would no longer work if the flaws were so close together that the signals from them overlapped. In this example, this would occur if the distance between the two flaws was less than 0.23m .

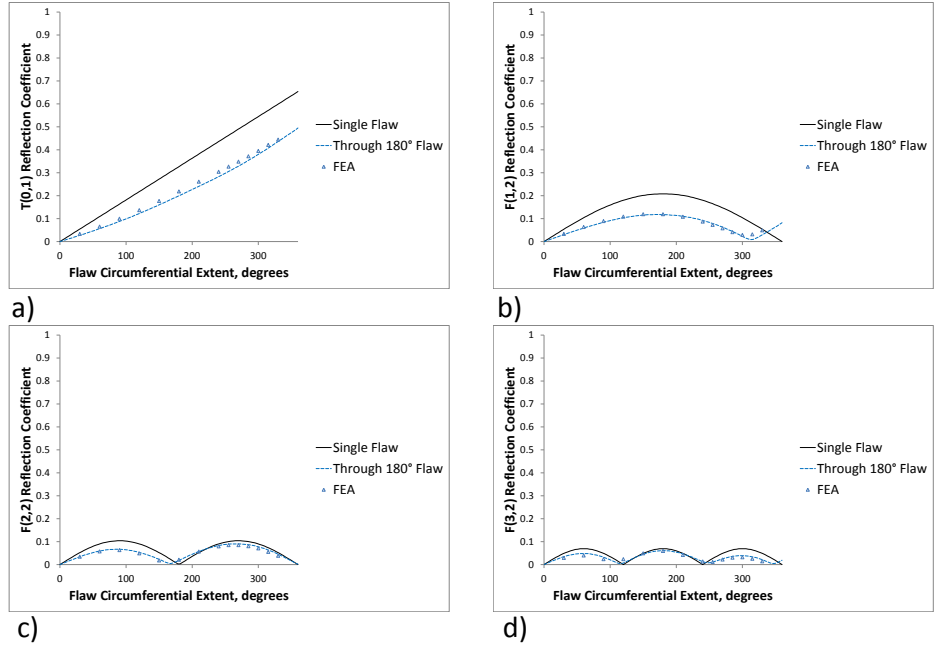


Figure 6.11: Comparison between analytical model (lines) for single flaw analytical model predictions for a 50% wall thickness flaw seen through a 180° , 50% wall thickness flaw and finite element results (points) for the two flaw example: (a) $T(0,1)$ reflection; (b) $F(1,2)$ reflection; (c) $F(2,2)$ reflection; (d) $F(3,2)$ reflection.

The presence of the 180° , 50% wall thickness flaw appears to cause a shift in the location of troughs and peaks which is particularly noticeable in the $F(1,2)$ and $F(2,2)$ cases (Figures 6.11b and 6.11c). The shape is also skewed with the peak amplitude no longer being the same for flaws of certain circumferential extents. For example the $F(2,2)$ amplitude at 90° and 270° is the same for a single flaw but different with a 180° flaw between the flaw and the excitation location (Figure 6.11c). The analytical model appears to predict both of these effects and the overall amplitude well.

The effects of two flaws on guided wave signals have been adequately simu-

lated using the analytical model. This indicates that the formulation is correct and that the assumption of ignoring modes of order 5 or higher is acceptable for this case.

In order to verify the analytical model for two flaws at different angles to one another, the finite element model was used to simulate a second example. This time, the first flaw had a through wall extent of 50% wall thickness and a 30° circumferential extent. The second flaw was at an angle of 45° to the first and had a through wall extent of 50% wall thickness. The circumferential extent was varied between angles of 30° to 330° in 30° increments. The same excitation, flaw axial extent, R_f , T_f and M values as before were used.

Figure 6.12 shows the comparison between the reflection coefficients from the second flaw with circumferential extent. As before, the reflection coefficients for a single flaw are also shown on the plots to illustrate the effect the 30° flaw has on the results. The plot shows the absolute magnitude and does not show the phase relationship since this is difficult to obtain accurately with finite element or experimental data. Again, the shapes and amplitudes are in good agreement. It is worth noting that the reflection coefficient of the F(2,2) wave mode is almost zero. This is because the second flaw is now at an angle of 45° whereas the wave mode filtering procedure was carried out in line with the first flaw. As expected, the reflections from the second flaw were observed to be larger if the wave mode filtering procedure was carried out at an orientation of 45° .

The knowledge gained on the effects of guided waves passing through one flaw allows characterisation methods which rely on the relative amplitudes of the flexural wave modes and the axisymmetric wave mode to be corrected. Notably, the reduction in T(0,1) reflection coefficient after passing through one flaw is up to 50% and the percentage change is larger for smaller flaws. This would result in an underestimate of the cross-sectional area loss by a factor of 2 which is clearly un-conservative and therefore undesirable for non-destructive testing.

6.8 Limitations of analytical model

The analytical modelling method for multiple flaws presented here is likely to be sensitive to the phase velocities used. Wilcox [2003] reported high sensitivity to dispersion curve inaccuracies when working on a dispersion removal technique. The sensitivity is likely to be more pronounced for dispersive wave modes as small changes in material parameters will cause large changes in the velocity of the wave mode at a given frequency. However, dispersive wave modes more readily lose amplitude as

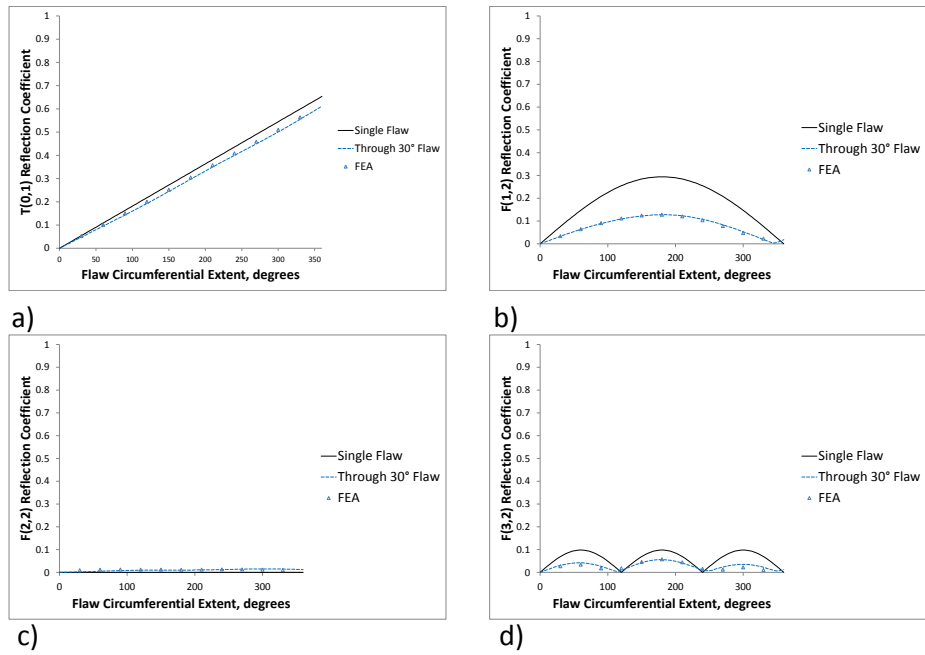


Figure 6.12: Comparison between analytical model and finite element analysis for a 50% wall thickness flaw seen through a 30° flaw 50% wall thickness flaw with the second flaw at an angle of 45°: (a) T(0,1) reflection; (b) F(1,2) reflection; (c) F(2,2) reflection; (d) F(3,2) reflection.

they propagate and will therefore be less likely to affect the results significantly.

In the examples studied, the axial length of the flaw was fixed to 10mm approximately 22% of the wavelength of T(0,1) and the shape was notch-like. This was done to limit the number of variables and therefore make verification of the concept more straightforward. Of course, real corrosion flaws will have variable through wall, circumferential and axial extents and this technique requires the flaw to be approximated to a simple shape so that single values for through wall, circumferential and axial extent can be used. This will have an impact on the accuracy of the result. The effects of reflections from flaws with tapered sides of different angles have been studied by Carandente *et al.* [2010]. Studies such as these could be used to modify the reflection and transmission coefficients presented here to take account of the flaw shape more precisely. A perturbation study to examine how small variations in the flaw shape affect the model would be of particular interest for future work.

In order to implement the model in practice, a technique for determination of flaw shape and size is required so that values of R_f and T_f can be determined for the first flaw. The work presented in Chapter 5 goes some way towards addressing this.

The method presented here deals with the transmitted wave modes from one flaw impinging on a second flaw and then being reflected and transmitted back through the first flaw. By doing this, the main reflection from the two flaws can be calculated. However, there will be smaller reflections arriving at a later time arising from multiple scattering between the two flaws. For simplicity, these have not been considered in the present work.

The work carried out has focussed on typical frequencies used in guided wave inspection of pipes (30kHz to 70kHz) where a limited number of flexural wave modes exist and below the T(0,2) cut off. The model could be extended to mid-range and higher frequencies but the calculation is likely to become cumbersome due to the high number of wave modes to be considered. At this point the solution may no longer be more computationally efficient than finite element analysis.

The modelling method presented here relies on calculation of scaling factors R_f and T_f using finite element analysis. However, once the scaling factors have been determined, the model is capable of simulating an infinite number of scenarios of multiple flaw combinations. The scaling factors required for this can be determined using one finite element model of a single flaw size. For example, consider a parametric study of the effect of two sequential flaws with the second flaw's circumferential extent to be varied 24 times. With the exclusive use of finite element analysis, 24 different models would be required which would take around 20 minutes

each to compute, making a total computation time of 8 hours. Whereas the present procedure would require a single, smaller finite element model, taking approximately 10 minutes to run plus a few seconds for the analytical model to compute the 24 cases.

The analytical model takes into account dispersion of wave modes over the distance between the flaws. However, in order to retain clarity in the formulae presented here, dispersion of wave modes as they travel back to the transducer array has not been taken into account. It would be relatively straightforward to add this to the analytical model using the formulae for straight pipe presented in Chapter 4.

6.9 Conclusions

The ability to use guided waves to detect and characterise corrosion accurately and reliably in pipelines is highly desirable and may become a practical reality in the future. However, corrosion damage rarely results in a single isolated flaw and pipes often have a number of reflectors which each contribute to increased complexity in the received guided wave signals. An analytical model has been established which simulates the reflections from multiple flaws by combining newly developed theoretical approximations to the reflection and transmission coefficients with the analytical wave propagation model presented in Chapter 4.

The analytical model has been successfully verified using validated finite element analysis and can be used to predict and therefore correct for the changes in amplitude of the different wave modes present in the reflected multimode guided wave signal. For an example case of a flaw lying beyond a 180° , 50% wall thickness flaw, the analytical model correctly predicted the changes in shape and amplitudes of reflections from the wave modes in the $T(0,1)$ family. One of the main findings of this work is that the ratio between the modes is not preserved. Since guided waves are likely to have passed through a number of features before being received at the transducer array, it is important to correct for any distortion of the amplitudes if flaw imaging and characterisation techniques are to be used such as the one presented in Chapter 5.

A paper arising from this work was submitted to IEEE Transactions on Ultrasonics, Ferroelectrics and Frequency Control in August 2012.

Techniques have now been developed which deal with multiple flaws in sections of straight pipe. However, pipelines can contain bends and locations with tight bends are often areas where guided waves are an attractive inspection option for op-

erators. The following chapter deals with the signal distortion that occurs when guided waves propagate around pipe bends and presents methods for correcting for it.

Chapter 7

Behaviour of Guided Waves in Pipe Bends

7.1 Introduction

A pipe bend is a common occurrence in pipelines. One example is that of a cased road crossing where it is often not possible to use more conventional inspection techniques such as pigs due to the tight bend radii. Guided wave inspection is a potentially attractive alternative but with the ability that guided waves offer to inspect the whole volume of tens of metres of pipeline, comes complexity. Each feature such as a weld, corrosion flaw, pipe branch or pipe bend will cause a disturbance to the propagation of the waves. Information about the condition of the pipe is contained in the received signals. If it is possible to extract that information, the guided wave inspection technique would be greatly improved.

A more detailed analysis of past research into the topic of pipe bends and curved structures is given in Section 3.8. The most relevant work to this chapter is summarised here. Demma *et al.* [2005] calculated dispersion curves and studied the transmission of waves through pipe bends using a combination of finite element analysis and experiments. They found a dependence on pipe geometry, bend radius and the length of the bend. They also discussed the need for an analytical model to predict the behaviour in pipe bends. The reflections from artificial flaws beyond pipe bends have been investigated experimentally by Nishino *et al.* [2006]; Nishino [2010]. An incremental monitoring technique was suggested where the signal from a specimen without flaws is subtracted from the received signals. However, for practical applications this would require a permanently attached array. Other experimental work has been carried out by Rose & Zhao [2001]; Rose *et al.* [2005]. They used a

tuning concept to study the sensitivity of guided waves to the detection of a flaw beyond an elbow. However, the success of a tuning approach for a wide range of cases has not been proven. Hayashi *et al.* [2005b] put forward a semi-analytical finite element technique for the calculation of guided wave behaviour in pipe bends. This has the advantage of fast computation of the behaviour of pipe bends but relies on an assumption that the pipe bend has a uniform wall thickness.

An alternative analytical modelling methodology for the prediction of guided wave propagation beyond complex features such as pipe bends is presented here. The new method has the advantage of fast computation time and no need for an in-situ finite element solver or a permanently attached array. The method also has flexibility the potential to be applied to any geometry such as a pipe bend with non-uniform pipe wall thickness. Firstly, finite element modelling has been used to quantify the effect of propagation through the bend on a number of key wave modes. This gives an insight into the effect that pipe bends would have on standard inspection procedures. Then, the results from the models have been combined with the suggested analytical modelling procedure which allows fast calculation of the wave propagation around pipe bends and, moreover, correction of the signal distortion caused by pipe bends. Finally, this has been brought together and an inspection procedure has been developed which involves the use of time reversed signals and the analytical model to remove distortion. This has the potential to allow more accurate inspection and characterisation of flaws beyond pipe bends.

7.2 Behaviour in pipe bends

7.2.1 Approach

Finite element modelling has been used to simulate the behaviour of guided waves when they propagate around bends in pipes. An example is taken of an 88.9mm outer diameter, 5.49mm wall thickness ferritic steel pipe with a 90° bend and a 229mm mean bend radius. This pipe size was selected as field experience from using commercially available inspection equipment indicates that guided waves in smaller diameter pipes are more susceptible to the presence of bends. The bend radius was selected as it was the tightest radius that could be made using induction bending (a commonly used technique that involves heating whilst applying force to form a bend). The excitation was a 10-cycle 25kHz Hann-windowed pulse. This was chosen so that some, but not many flexural wave modes were present to limit the number of calculations required whilst the method was established and verified. Figure 7.1 shows the layout of the model and experiment. The excitation was in the

circumferential direction so the $T(0,1)$ family of wave modes will be preferentially excited. For these conditions, three main wave modes are possible: $T(0,1)$, $F(1,2)$ and $F(2,2)$.

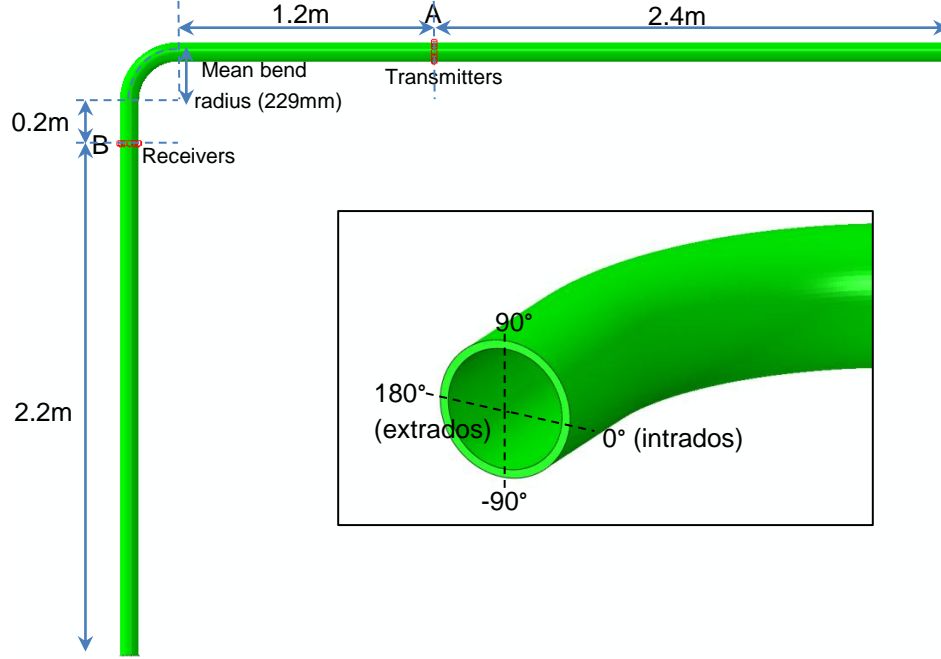


Figure 7.1: Layout of finite element model and pipe bend experiment. The inset shows the convention used for the circumferential position.

The model was generated and processed using the commercially available finite element software, ABAQUS version 6.10. The model was three-dimensional and used linear brick elements (ABAQUS element type C3D8R). Material properties of 207GPa, 0.3 and 7830kg/m³ were used for Young's modulus, Poisson's ratio and density respectively. A regular mesh was used with elements of 2.5mm along the length and approximately 3mm around the circumference. Four elements were used through the thickness. In the bend, the element lengths ranged from around 2mm on the intrados to 3mm on the extrados. This level of mesh refinement was used so that there were enough elements to adequately represent the smallest wavelength of interest in the system [Alleyne & Lowe, 1998; Zhu, 2002].

The excitation was applied using a concentrated force in the circumferential direction at twelve evenly spaced points around the circumference, 1.2m from the bend at point A. The signals were recorded at twelve evenly spaced points around the circumference, 0.2m from the other side of the bend at point B. Twelve points were

used to match the number of transducers around the circumference in commercially available equipment.

In order to quantify the effect of the pipe bend on all three of the possible torsional family wave modes in all possible orientations, the following set of models were generated. Firstly, the T(0,1) mode was excited, then the amplitude of the excitation was varied around the circumference in order to excite the flexural wave modes F(1,2) and F(2,2). The F(1,2) wave mode was excited at six different circumferential orientations from 0° to 150° in 30° increments. The F(2,2) wave mode was excited at three different circumferential orientations from 0° to 60° in 30° increments. Due to symmetry, this set of models was sufficient to represent all of the possible orientations. The formula used to calculate the amplitude of the input pulse was as follows:

$$A = \cos[n(\theta - \alpha)], \quad (7.1)$$

where A is the amplitude, n is the required mode order, θ is the circumferential position and α is the desired circumferential orientation of the wave mode.

The convention adopted for the angles was the intrados as 0°, top dead centre as 90° and the extrados as 180° as illustrated in Figure 7.1.

The output signals were processed using a wave mode filtering technique [Catton, 2009]. This involves reapplying the excitation amplitudes to the signal at each point and then summing all twelve signals. The technique is described in more detail in Section 5.6.2. The filtering technique allowed the individual wave modes to be examined separately.

7.2.2 Finite element modelling results

Figure 7.2 shows the received signals at point B after the bend for an excitation of T(0,1) before the bend at point A. It can be seen that all three wave modes are present in the received signal. The strongest signal is the T(0,1) wave mode with the second strongest being the F(1,2) which is around 5% of the amplitude of the T(0,1) signal. The flexural wave modes are both aligned at 0° (i.e. their maximum displacement is at 0°). This suggests that there may be more sensitivity to flaws aligned with the extrados or intrados of the bend and less sensitivity to flaws at other orientations since the reflection from flaws is greatest when their orientation matches that of the incident flexural wave mode (see Chapter 6). The predicted amplitude of the T(0,1) signal received after propagation through the bend divided by the amplitude of the incident T(0,1) signal was 0.99. The signal loss is minimal

which indicates that there is potential for inspection of pipes containing a number of bends, in this case. However, at higher frequencies the loss of amplitude may be greater [Demma *et al.*, 2005].

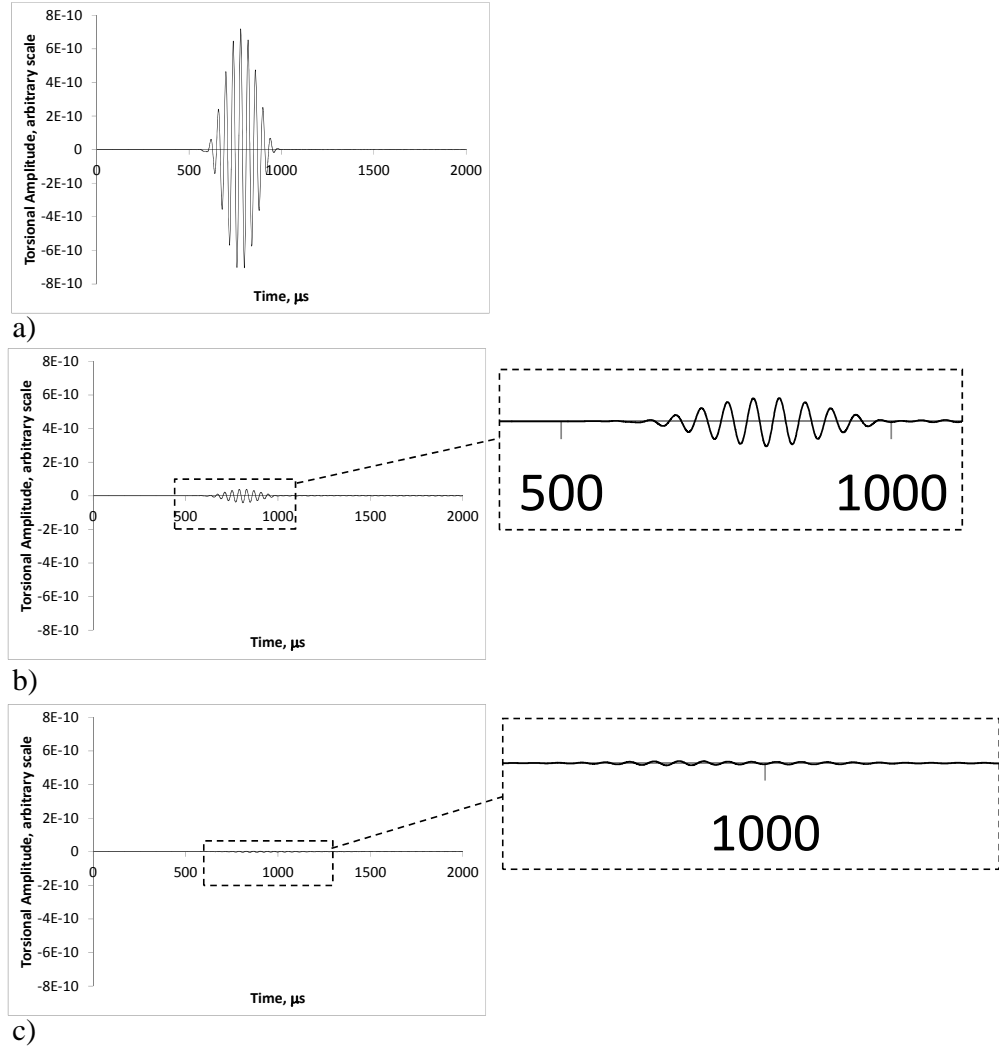


Figure 7.2: Finite element predictions of wave modes after propagation of T(0,1) around a 90° bend with a 229mm mean bend radius in an 88.9mm outer diameter, 5.49mm wall thickness steel pipe: a) T(0,1); b) F(1,2); c) F(2,2).

The effect of the orientation of incident flexural wave modes was studied by varying the orientation around the circumference in 30° intervals (as described in more detail above). It was found that all three wave modes were generated to varying degrees in most cases. Figure 7.3 shows an example of the wave modes received after the bend at point B from excitation of purely the F(1,2) wave mode

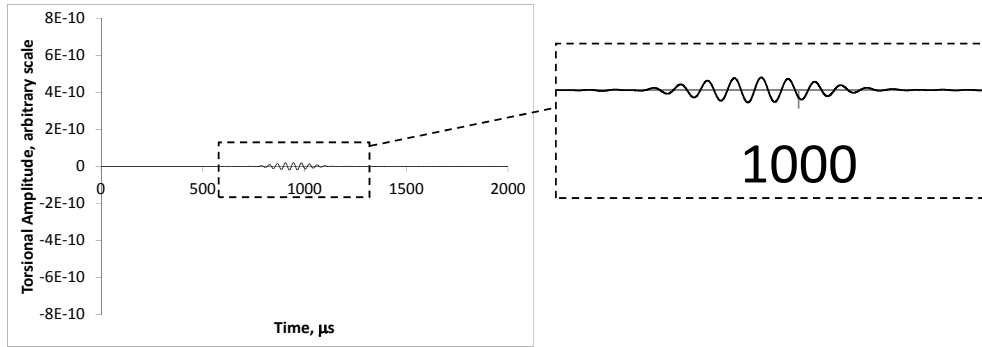
at 60° before the bend at point A. The transmitted wave mode has the largest amplitude and the other two possible wave modes (T(0,1) and F(2,2)) are present in the signal with similar amplitudes to each other. The ratio of the amplitude of the F(1,2) signal received after propagation through the bend to the amplitude of the incident F(1,2) signal was 0.81. It was found that the alignment of the flexural wave modes was not preserved after propagation around the bend. In the example given, the F(1,2) wave mode was aligned at 75° after the bend and the F(2,2) wave modes was aligned at 30° .

The models were also used to study the relationship between the orientation of the flexural wave mode before the bend and the orientation of the transmitted/excited wave modes after the bend. Figure 7.4 shows the results of this analysis for excitation of the F(1,2) wave mode. The F(2,2) wave mode appears to follow a linear trend whereas the F(1,2) wave mode does not. The two wave modes do not necessarily have the same orientation after the bend as each other. This is an important point to note as the orientation of the flexural wave modes can be used to determine the circumferential location of a flaw. Therefore, the presence of a bend in a pipe will distort the results of such an analysis.

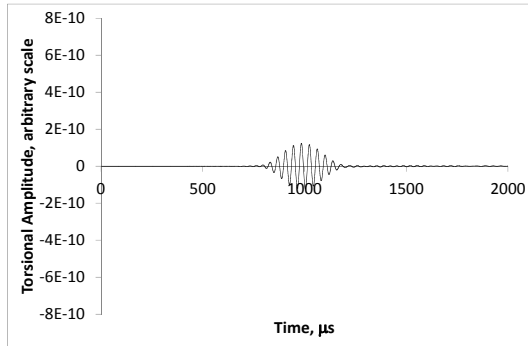
Figure 7.5 shows the amplitude of T(0,1) after excitation of F(1,2) and F(2,2) before the bend at a range of orientations. Both trends appear to be sinusoidal. For an excitation of F(1,2) at 90° there is no generation of T(0,1) whereas F(2,2) always appears to generate some T(0,1) regardless of its orientation.

7.2.3 Effect of wall thickness variation in the bend

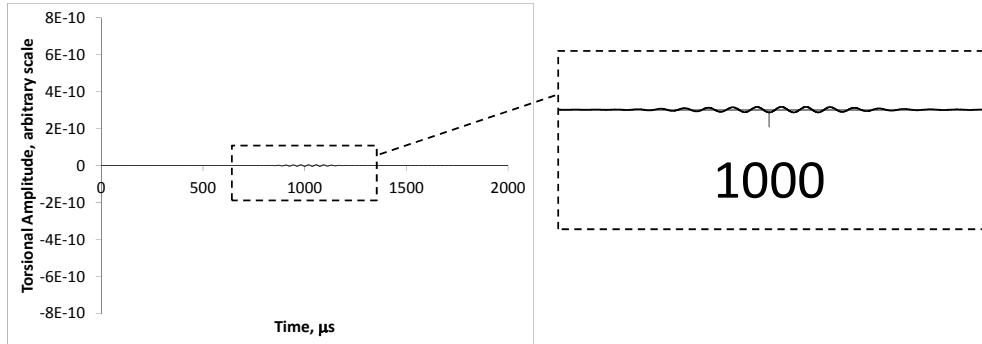
Pipe bends are made either by welding on an elbow section or formed using an induction bending technique. The behaviour of guided wave propagation in the latter is studied here. The induction bending technique uses a combination of locally applied heating and mechanical force to form the bend. This results in a thinning of the pipe wall at the extrados and a thickening of the pipe wall at the intrados. The resulting ovality and change in wall thickness will affect the behaviour of guided waves. In order to study the significance of this for the pipe bend example taken, a manual ultrasonic flaw detector (Sonatest Masterscan 380M) with a 10MHz probe (Panametrics 6.4mm diameter, 0°) was used to take spot measurements at 8 positions around the middle of the bend. An idealised shape of the pipe cross section was estimated from these measurements and put into a finite element model. Figure 7.6 shows the idealised shape assumed. Table 7.1 shows the measurements compared with the resulting thicknesses from the idealised shape in the finite element analysis. The maximum difference was 0.42mm.



a)



b)



c)

Figure 7.3: Finite element predictions of wave modes after propagation of $F(1,2)$ at 60° around a 90° bend with a 229mm mean bend radius in an 88.9mm outer diameter, 5.49mm wall thickness steel pipe: a) $T(0,1)$; b) $F(1,2)$; c) $F(2,2)$.

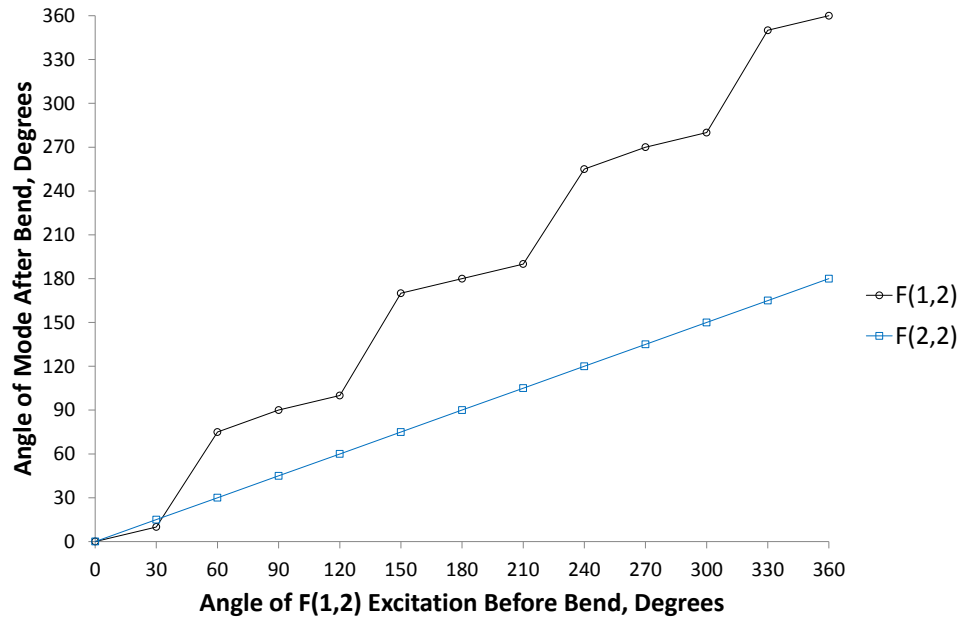


Figure 7.4: Orientation of wave modes received after an excitation of F(1,2) before a 90° bend with a 229mm mean bend radius in an 88.9mm outer diameter, 5.49mm wall thickness steel pipe.

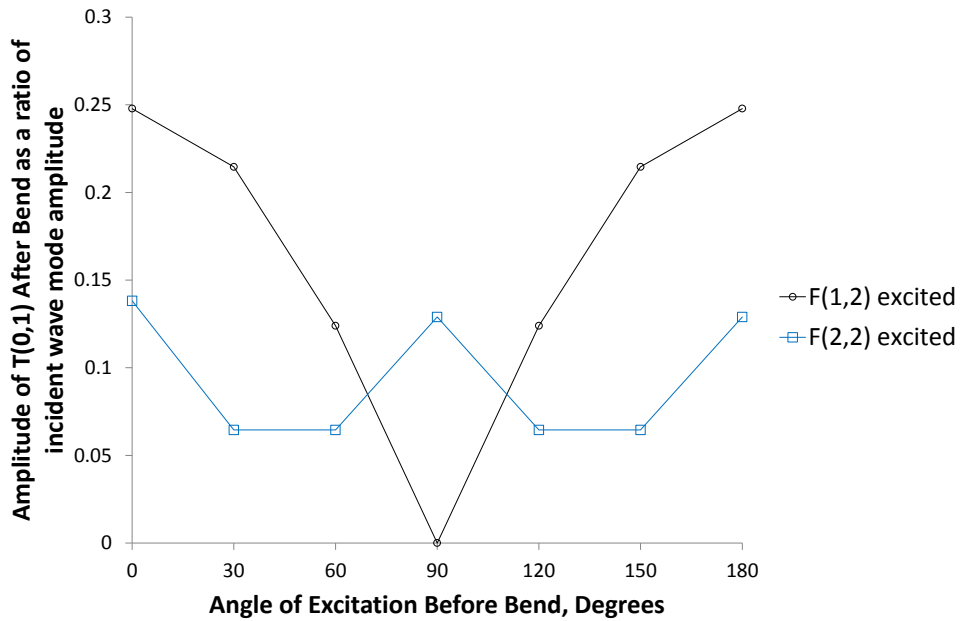


Figure 7.5: Amplitude of T(0,1) after a 229mm mean radius, 90° bend in an 88.9mm outer diameter, 5.49mm wall thickness steel pipe from excitation of flexural waves modes at different orientations before the bend.

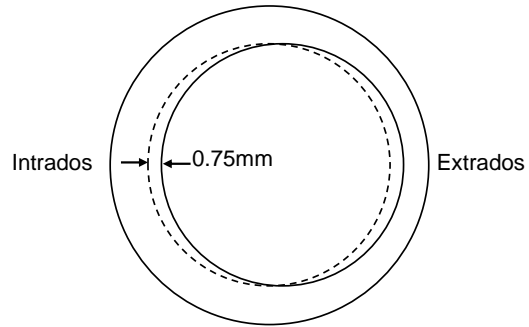


Figure 7.6: Schematic of cross section of centre of pipe bend showing how the wall thickness was varied in the model to approximate the wall thickness changed caused by induction bending.

Location, degrees	Measured value, mm	Wall thickness in finite element analysis, mm
0 (intrados)	6.28	6.24
45	6.25	6.02
90	5.08	5.5
135	4.99	4.96
180 (extrados)	4.93	4.74
225	4.88	4.96
270	5.25	5.5
315	6.2	6.02

Table 7.1: Wall thickness measurements in the middle of the bend

Figure 7.7 shows the finite element predictions for the received signals from a uniform pipe cross section and the measured pipe cross section after excitation of a 10-cycle 25 kHz Hann-windowed pulse of $T(0,1)$ before the bend. When compared with Figure 7.2, it is observed that the amplitude and shape of the $T(0,1)$ signal is virtually unchanged. The amplitude of the $F(1,2)$ signal is slightly reduced by around 7% and the amplitude of the $F(2,2)$ signal is increased by around 78%. However, the amplitude of the $F(2,2)$ is small compared to the other modes and this change is therefore less significant (its amplitude is less than 1% of the $T(0,1)$ amplitude). The potential ovalisation of the pipe has not been studied here and this could cause additional variations in the received signals. Additionally, the bend may not be a perfectly circular arc which also has the potential to change the behaviour of guided waves.

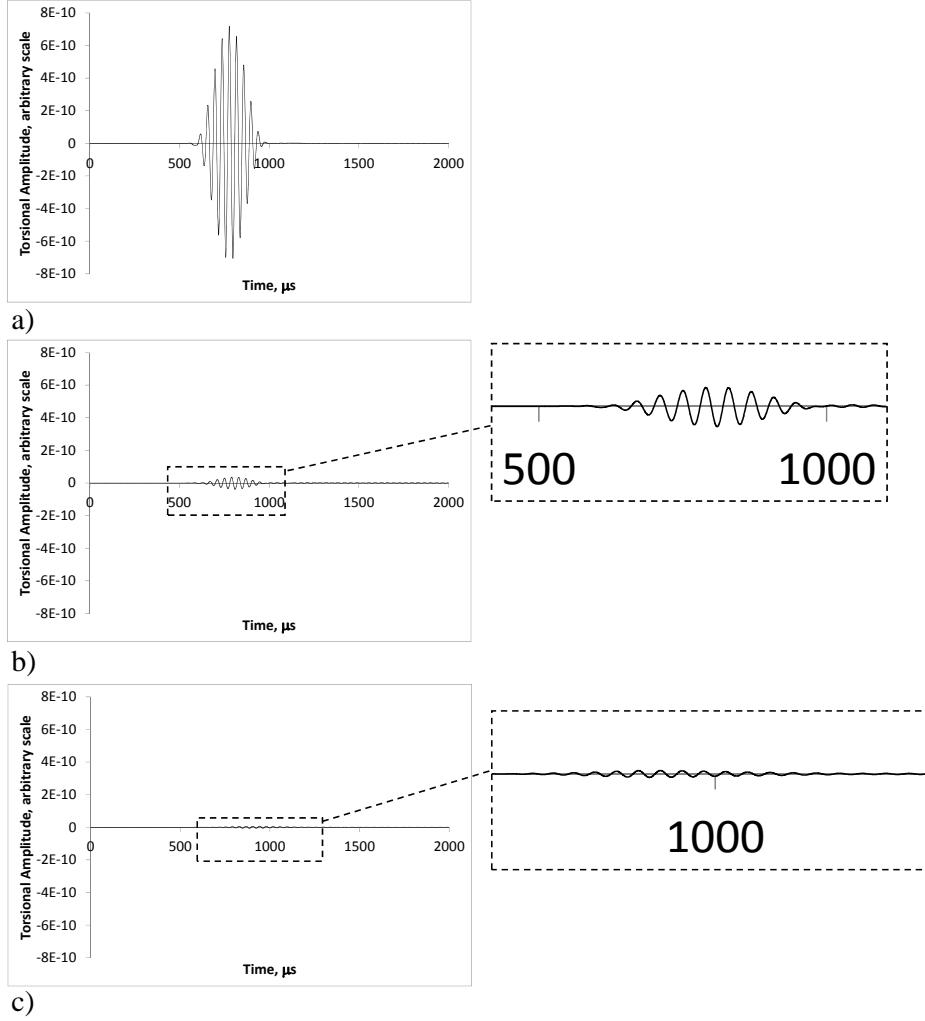


Figure 7.7: Finite element predictions of wave modes after propagation of $T(0,1)$ around a 90° bend with a 229mm mean bend radius in an 88.9mm outer diameter, 5.49mm wall thickness steel pipe with thickness variations in the bend: a) $T(0,1)$; b) $F(1,2)$; c) $F(2,2)$.

7.3 Experimental validation

An 88.9mm outer diameter, 5.49mm wall thickness pipe specimen was made using an induction bending technique to produce a 229mm mean radius, 90° bend.

Two transducer arrays were attached to the specimen using an inflatable bladder and collar arrangement. The arrays were used in a pitch-catch formation (one was used to transmit and the other to receive). The layout matches the finite element model and is shown in Figure 7.1. The transmitting array was placed 1.2m from the bend at point A and the receiving array was placed 0.2m from the other side of the bend at point B. Both arrays contained a single ring of 12 piezoelectric transducers spaced evenly around the circumference of the pipe. The transducers were arranged in order to produce a predominantly torsional motion on the surface of the pipe. An air-line with a pressure regulator was used to ensure uniform transducer contact pressure throughout the experiment.

Firstly, a 10-cycle 25kHz Hann-windowed pulse was applied equally to all twelve transducers in the transmitting array in order to excite T(0,1) before the bend. Figure 7.8 shows the received signals. When compared to the finite element predictions in Figure 7.2, it can be seen that the pulse shapes and arrival times are in close agreement. The ratios between the amplitude of the T(0,1) wave mode and the flexural wave modes are also similar. The ratio of the F(1,2) amplitude to the T(0,1) amplitude was predicted by the FEA to be -25dB whereas the experimental value was -28dB. The amplitude of F(2,2) relative to T(0,1) was predicted to be small (-46dB). In the experiment it was found to be higher (-29dB).

A second case was taken of the excitation of the F(1,2) wave mode at 90° before the bend. In order to excite this wave mode, different amplitudes of excitation were applied to each transducer (the method for this is described in more detail in Chapter 4). Figures 7.9 and 7.10 show the results of the F(1,2) and F(2,2) wave modes received compared with the finite element predictions. The experimentally measured value of the ratio of the F(2,2) amplitude to the F(1,2) amplitude was -22dB compared with a predicted value of -20dB. The finite element model predicted that the T(0,1) wave mode was not generated after the bend for this case. The experimental results measured some T(0,1).

The most likely cause of the differences between the model and the experiment is the coupling conditions around the circumference between the transducers and the pipe or differences in the output of the transducers themselves. Variable output of the transducers will cause excitation of flexural wave modes in addition to the prescribed excitation. Another possible cause is the differences between the

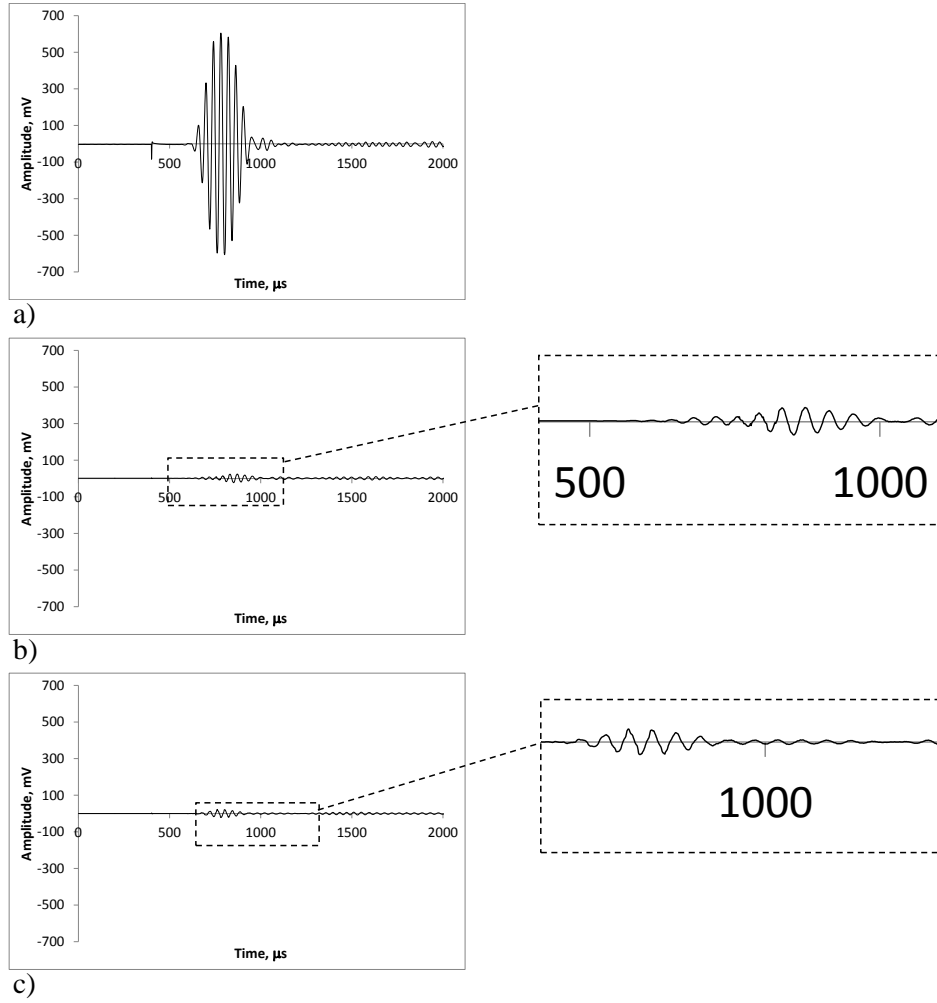


Figure 7.8: Experimentally measured wave modes after propagation of T(0,1) around a 90° bend with a 229mm mean bend radius in an 88.9mm outer diameter, 5.49mm wall thickness steel pipe: a) T(0,1); b) F(1,2); c) F(2,2).

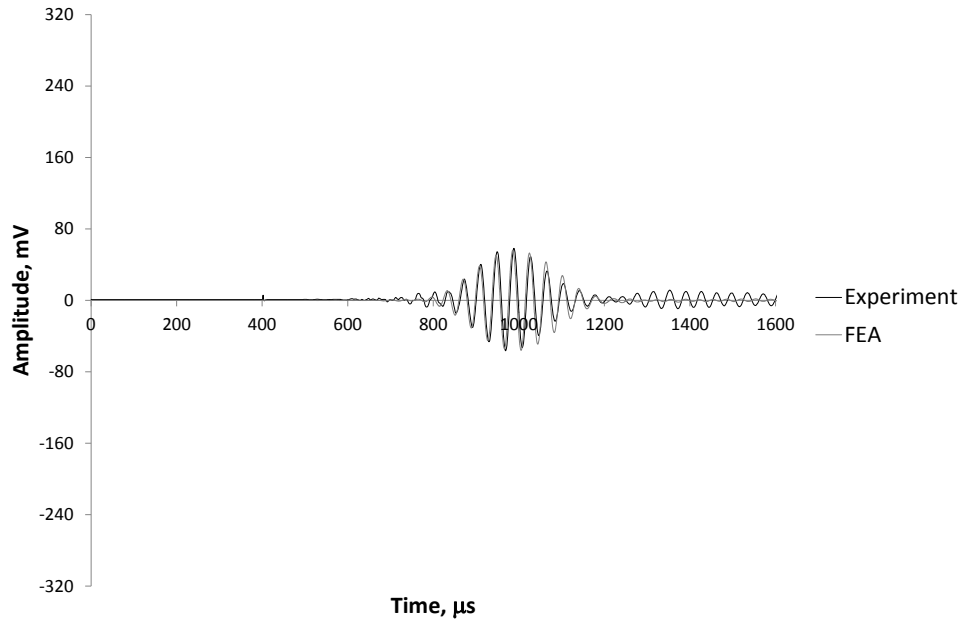


Figure 7.9: Experimentally measured versus finite element predicted F(1,2) wave mode received after propagation of F(1,2) around a 90° bend with a 229mm mean bend radius in an 88.9mm outer diameter, 5.49mm wall thickness steel pipe.

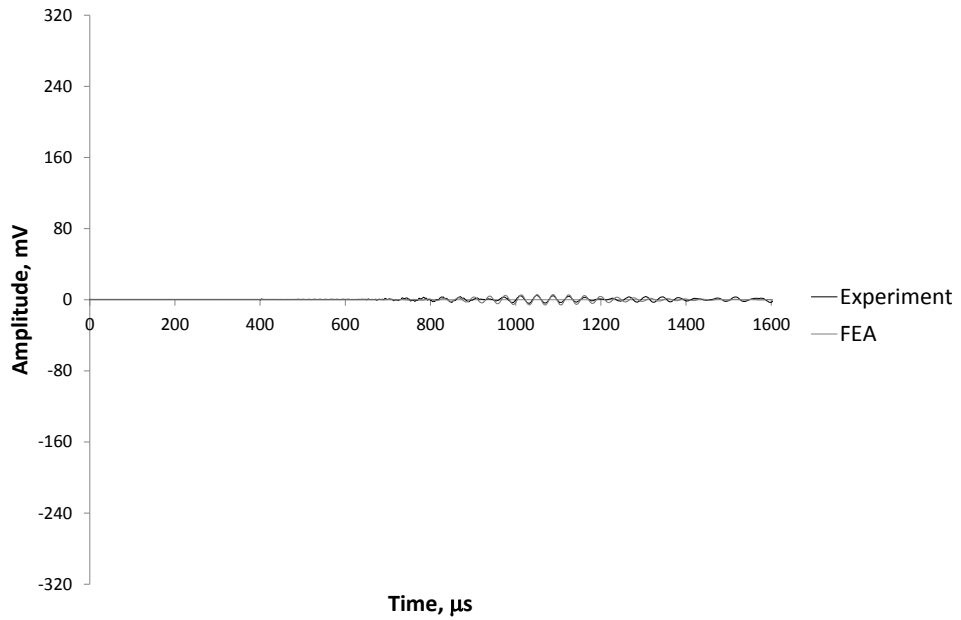


Figure 7.10: Experimentally measured versus finite element predicted F(2,2) wave mode received after propagation of F(1,2) around a 90° bend with a 229mm mean bend radius in an 88.9mm outer diameter, 5.49mm wall thickness steel pipe.

bend geometry. Wall thickness variations have been shown to have a relatively small effect on guided wave behaviour but other factors which have not been studied here such as ovalisation could have a more significant effect and cause differences between the finite element and experimental results.

7.4 Analytical model

7.4.1 Concept

The aim was to develop an analytical model of guided wave propagation through a pipe bend which can be used to predict the transmission behaviour and also correct the signal distortion caused by the bend. Finite element modelling is a useful technique for understanding the behaviour of wave propagation in complex situations such as this. However, the computation time is relatively long and a separate model is required for each desired variation.

Therefore, an alternative analytical modelling methodology for the prediction of guided wave propagation beyond complex features such as pipe bends was developed. The approach uses finite element analysis to first calculate the intrinsic behaviour of the bend. This can be carried out separately and need only be done once for each bend geometry and test frequency. The finite element results are then decomposed into individual mode responses and this can then be combined with an analytical model for straight pipe. After the initial outlay of the finite element analyses, the approach has the advantage of allowing an unlimited number of situations such as different transducer array locations and different flaw sizes and locations beyond the bend. The analytical model has a significantly faster computation time which means that it can be used directly with field equipment.

The approach also allows flexibility in the geometry of the feature being simulated. For example, effects such as the wall thickness in a pipe bend or welds attaching an elbow section can be included in the model. The model can also be used to reverse the effects of the bend on signals which makes inspection beyond the bend more accurate and allows the potential to determine the size of flaws beyond pipe bends using techniques such as those described in Chapters 5 and 6.

7.4.2 Formulation for a pipe bend example

The first step is to use finite element models to calculate the signals after propagation through the bend as described above. A separate model is required for each possible wave mode and each possible orientation of the circumferential distribution

of flexural wave mode. In the example selected (a 10-cycle 25kHz Hann-windowed pulse with torsional excitations in an 88.9mm outer diameter, 5.49mm wall thickness pipe with a mean bend radius of 229mm), there are three main wave modes possible for a torsional excitation: T(0,1), F(1,2) and F(2,2). A circumferential increment appropriate for the order of flexural wave modes possible should be selected. In the example of a pipe bend given here, results at 30° increments around the circumference were calculated. This means that results for twelve different orientations are required. However, symmetry means that six models are required for the F(1,2) wave mode and only three for the F(2,2) wave mode. The torsional wave mode only requires one model. This makes a total of 10 models. The models for this particular example take around 15 minutes each to solve on a dual quad core Xeon X5570 machine with 24Gb of RAM. Therefore, a total solution time of around 2.5 hours is required. This is not prohibitively long and once done, allows calculations to be carried out analytically for any scenario.

Since the specimen under consideration is relatively short, the effect of dispersion has not been explicitly simulated. It would be important to include this effect in the field where longer lengths of pipe are being inspected. This can be done using the methods described in Chapter 4. The aim of this chapter is to introduce the methodology for analytical simulation of the bend. The assessment of the combination of this with models for straight pipes and flaws will be the subject of future work.

Let the signals from the bend be denoted by $T_{i,j}$ where i is the order of the mode incident to the bend and j is the order of the mode transmitted by the bend. In order to take account of excitability, these functions must be normalised by the amplitude of the applied excitation.

The signals are divided by the input signal in the frequency domain to give a multiplier, $F[H_{i,j}]$:

$$F[H_{i,j}] = \frac{F[T_{i,j}]}{F[I]}, \quad (7.2)$$

where F denotes transformation into the frequency domain and I is the input signal (in the example case this is a 10-cycle 25kHz Hann-windowed pulse).

The multiplier is dependent on the orientation of the flexural wave modes and there will therefore be a different multiplier for each orientation. However, as described above, symmetry of the wave modes reduces the number of angles that need to be considered. A second consideration is that every incident wave mode has the potential to generate every other wave mode, so there are multiple permutations.

Since it is a linear elastic problem, the principal of superposition can be used and each permutation can be summed to give the final result as follows:

$$F[T'_j] = \sum_i F[H_{i,j}]F[S_i], \quad (7.3)$$

where S is the signal to apply the effect of the bend to and T' is the resulting signal after the effect of the bend has been applied. The result can then be obtained in the time domain by taking the inverse FFT. The formulae described above were programmed into the computer aided mathematical processing software, MathCAD.

7.4.3 Verification

The analytical model was verified against finite element predictions for the reflections from a flaw passing through the bend. An example was taken of a 150° notch-like flaw beyond the 229mm mean radius 90° bend. The flaw had a through wall extent of 50% of the wall thickness and an axial extent of 20mm. A 10-cycle 25kHz Hann windowed excitation of T(0,1) was impinged on the flaw. Figure 7.11 shows the layout. This was done to test the model for propagation once through the bend. Figures 7.12 to 7.15 show the comparison. The agreement is good and this indicates that the formulation of the analytical model is correct. In some cases (particularly Figures 7.12 and 7.13), the received signals appear to be made up of two pulses. Both the T(0,1) and F(1,2) wave modes will be reflected from the flaw. The first pulse is therefore likely to be the T(0,1) signal reflected by the flaw and transmitted through the bend. The second pulse is then most likely to be a mode conversion from one of these modes to the other caused by the bend. Since the two modes have different speeds, the arrival times are slightly different.

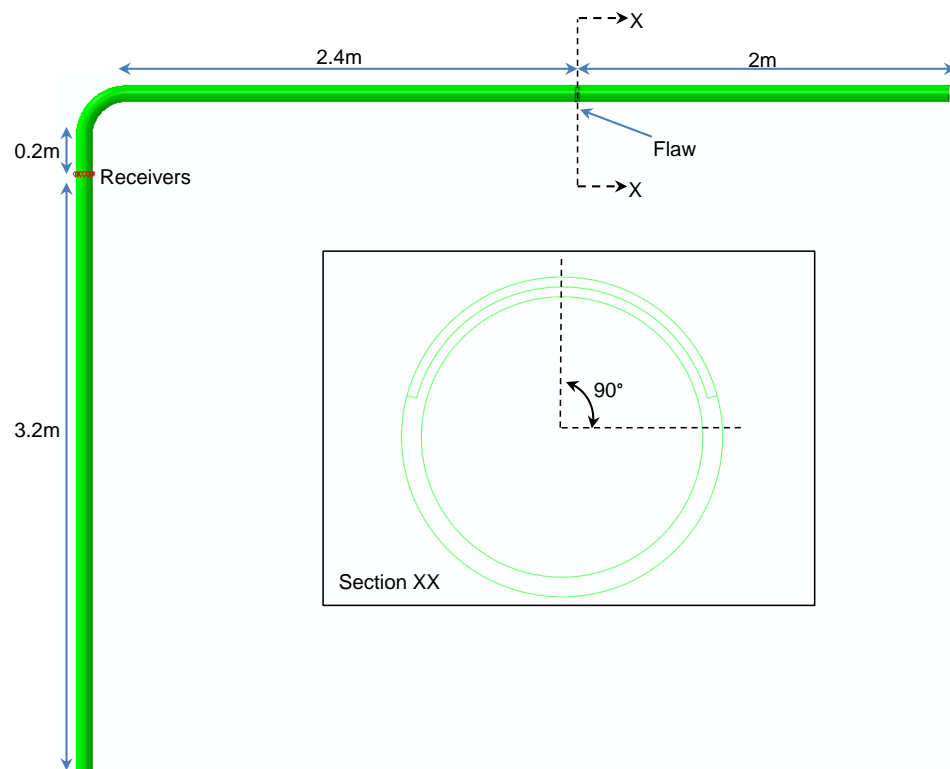
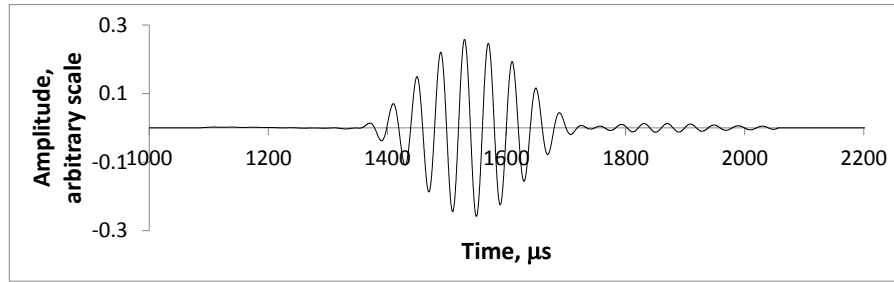
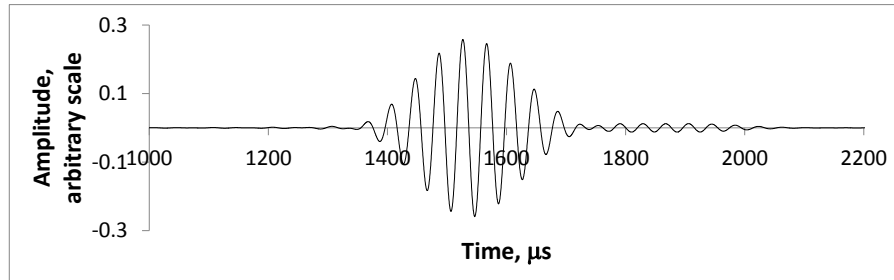


Figure 7.11: Layout of finite element model of an 88.9mm outer diameter, 5.49mm wall thickness steel pipe with a 229mm bend radius used to test the analytical model. A 150° circumferential extent, 50% wall thickness flaw was simulated with different orientations (the flaw is shown oriented at 90° in this case).

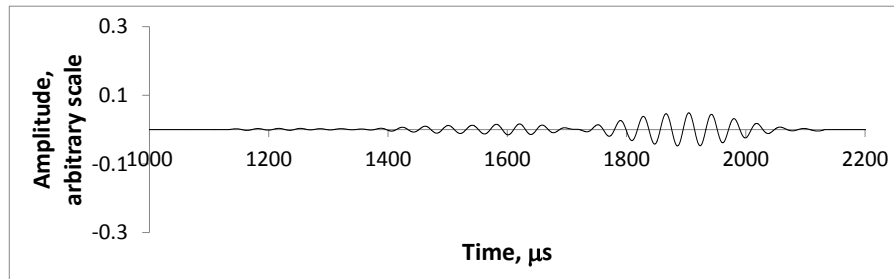


a)

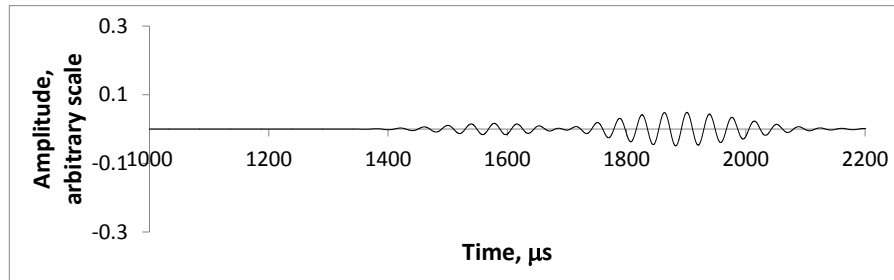


b)

Figure 7.12: Comparison between analytical model and FEA for T(0,1) response from a 150° flaw beyond a 229mm pipe bend in an 88.9mm outer diameter, 5.49mm wall thickness steel pipe for a flaw at 0° : a) FEA; b) Analytical.

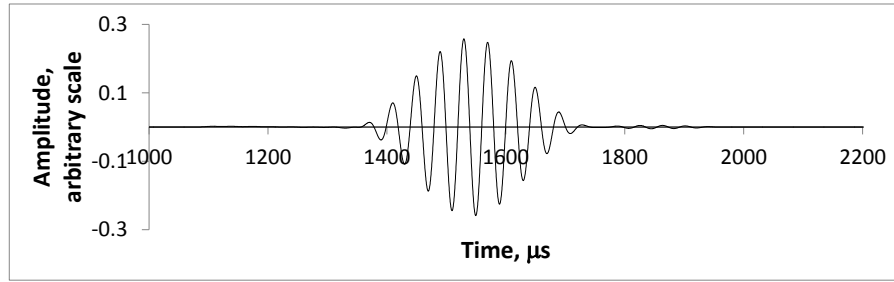


a)

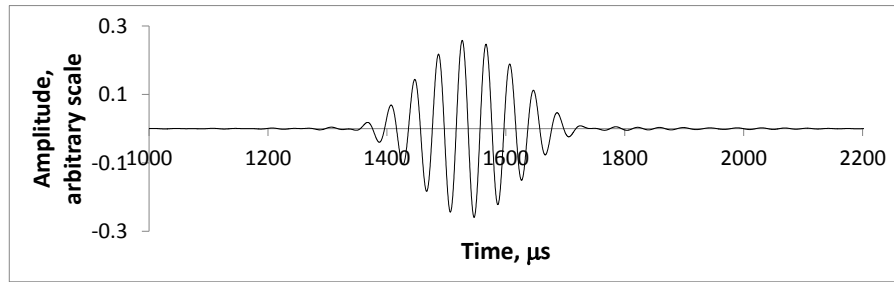


b)

Figure 7.13: Comparison between analytical model and FEA for F(1,2) response from a 150° flaw beyond a 229mm pipe bend in an 88.9mm outer diameter, 5.49mm wall thickness steel pipe for a flaw at 0° : a) FEA; b) Analytical.

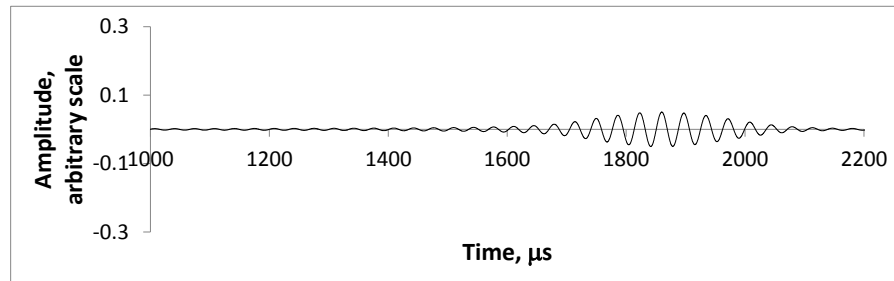


a)

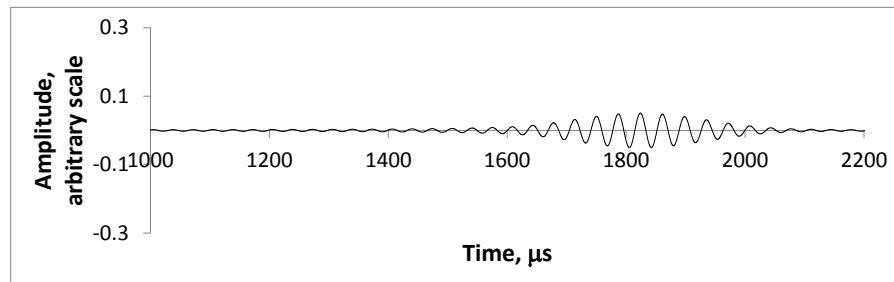


b)

Figure 7.14: Comparison between analytical model and FEA for T(0,1) response from a 150° flaw beyond a 229mm pipe bend in an 88.9mm outer diameter, 5.49mm wall thickness steel pipe for a flaw at 90°:a)FEA; b)Analytical.



a)



b)

Figure 7.15: Comparison between analytical model and FEA for F(1,2) response at 90° from a 150° flaw beyond a 229mm pipe bend in an 88.9mm outer diameter, 5.49mm wall thickness steel pipe for a flaw at 90°:a)FEA; b)Analytical.

7.5 Reconstructing signals from flaws beyond pipe bends

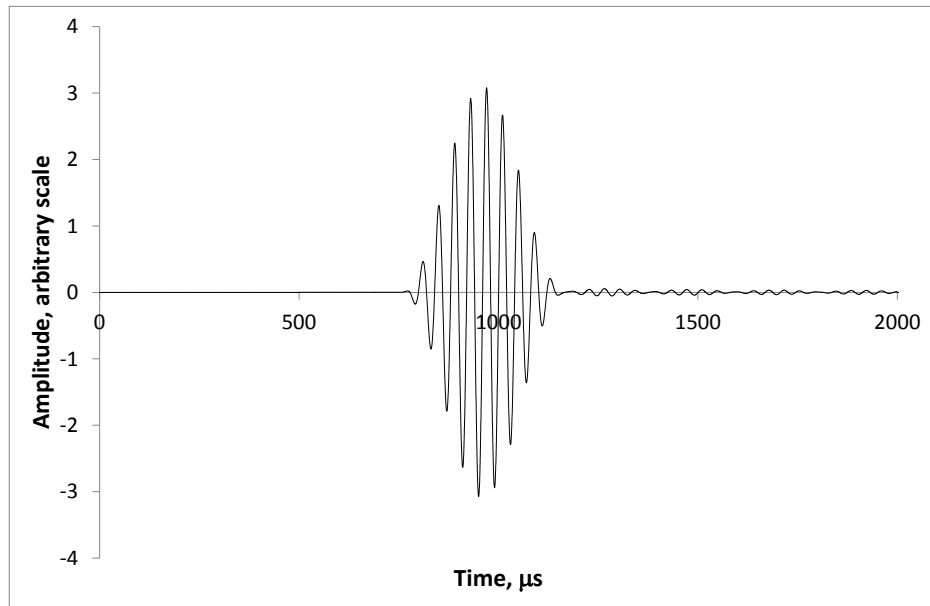
As well as predicting the signals received after a pipe bend from a given arbitrary input signal, the analytical model described above can also be used to ‘undo’ the distortion caused by a pipe bend. Since the analytical model is computationally fast, the correction can be applied real-time in a field test scenario.

The distortion correction is achieved by using time reversed signals as the inputs to the analytical model. An example was taken of a 150° notch-like flaw beyond the 229mm mean radius 90° bend. The flaw had a through wall extent of 50% of the wall thickness and an axial extent of 20mm. A 10-cycle 25kHz Hann windowed excitation of T(0,1) was impinged on the flaw. The layout was the same as that shown in Figure 7.11 except for the alignment of the flaw which was at 60° for this example.

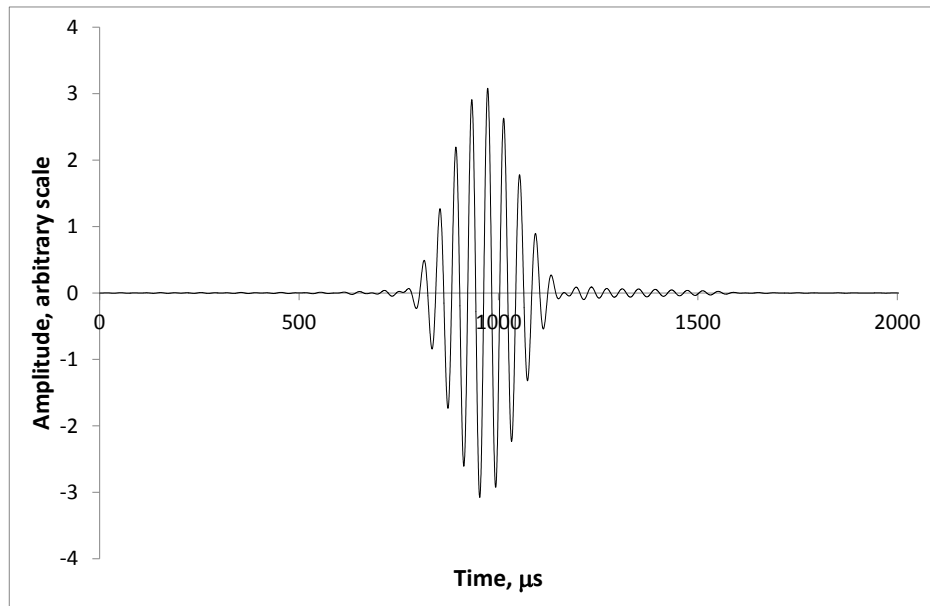
Since the direction of propagation around the bend is significant, the bend multiplier functions were re-arranged for propagation in the opposite direction around the bend. The procedure can be summarised as follows:

- Use finite element analysis to calculate the bend multiplier functions for propagation from the side of the bend without a flaw to the side containing the flaw.
- Gate the signals in the time domain to isolate the reflection from the flaw.
- Time reverse the signals from the flaw (i.e. reverse the order of the amplitude values in the time domain).
- Multiply and sum the signals in the frequency domain as per Equation 7.3 and convert back to the time domain.

Figures 7.16 and 7.17 show the signals after reconstruction compared to finite element predicted signals for the same flaw in a section of straight pipe. The agreement is excellent indicating that it is possible to correct the distortion to the signals caused by the bend using this technique.

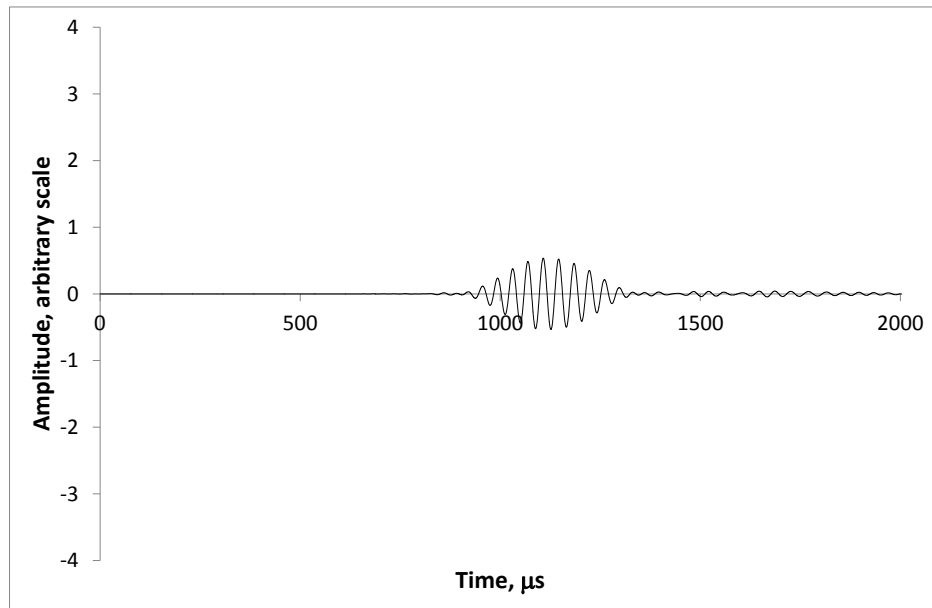


a)

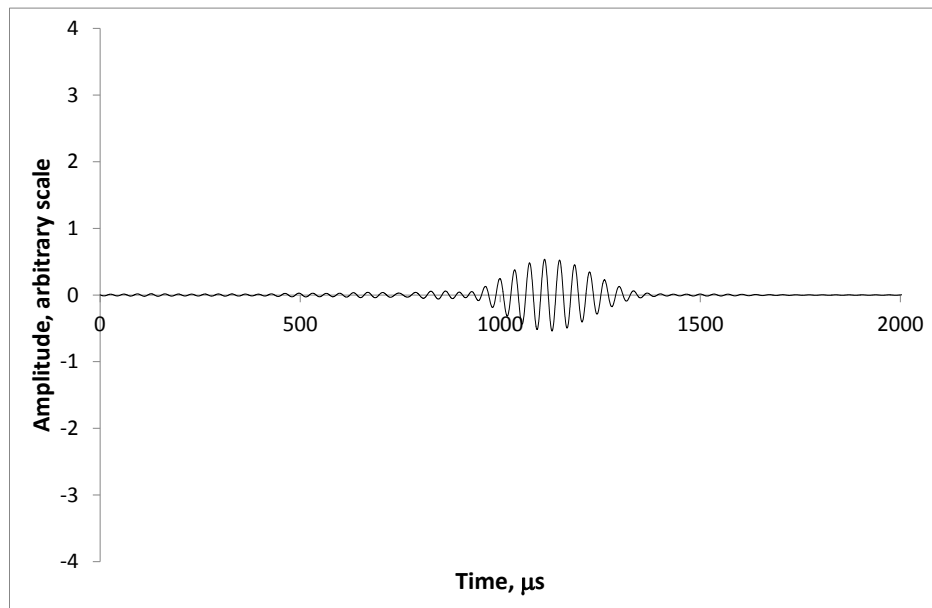


b)

Figure 7.16: Comparison between analytically reconstructed $T(0,1)$ signals from a 150° flaw beyond a pipe bend with finite element for $T(0,1)$ signals from a 150° flaw in straight pipe: a) FEA; b) Analytical.



a)



b)

Figure 7.17: Comparison between analytically reconstructed F(1,2) signals from a 150° flaw beyond a pipe bend with finite element for F(1,2) signals from a 150° flaw in straight pipe:a)FEA; b)Analytical.

7.6 Generation of pure axisymmetric wave modes beyond pipe bends

This example case presented in the previous sections is a deliberately artificial situation to test the concept for propagation once through the bend. It would be far more valuable to be able to ‘undo’ the distortion from the pipe bend from a single test location before the bend. However, if the excitation is allowed to first propagate through a bend, the signals will be distorted before they interact with the flaw and the ability to use flaw sizing or imaging techniques would then be compromised. Therefore, an alternative technique is proposed. Time reversal of the signals can be used to synthetically achieve the excitation of $T(0,1)$ beyond the bend. This was tested by taking the signals from the finite element model where pure $T(0,1)$ was excited one side of the bend, time reversing them and using them as excitations in a second model. Figure 7.18 shows the von-Mises stress field in the model after the pulse has propagated around the bend. It was found that $T(0,1)$ could be excited beyond the bend with a 98.3% purity (the largest amplitude of a flexural wave mode was just 1.67% of the amplitude of $T(0,1)$).

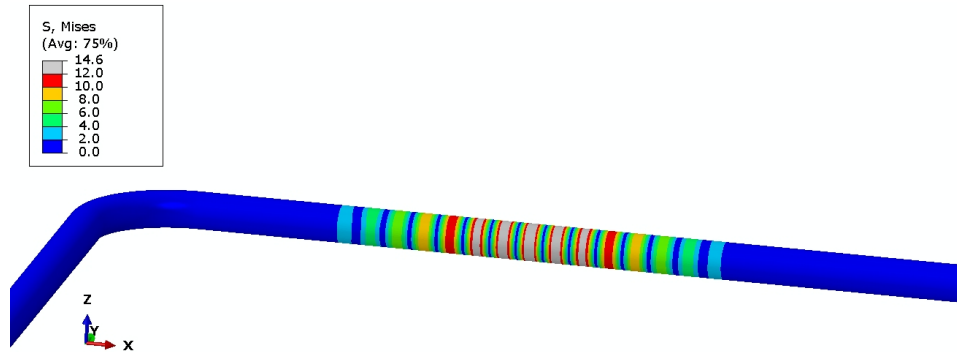


Figure 7.18: Predicted von-Mises stress field just after time reversed pulse has propagated around the bend.

Therefore the overall suggested test procedure for inspection of flaws beyond bends would involve excitation of $T(0,1)$ beyond the bend using this technique followed by removal of the distortion from reflected signals using the analytical model.

7.7 Discussion

The agreement between the finite element analysis and the analytical model is good. This indicates that the analytical model has been implemented correctly and that

the proposed technique is valid. There is also good agreement between finite element modelling and experiment in all cases. The discrepancies observed are most likely due to variations in transducer coupling and the geometry of the pipe bend.

The analytical modelling method presented here requires initial input data. In the example used, finite element analysis has been used to generate the data but it is possible that experimental data could also be used. This would have the advantage of tailoring the analytical calculations to a particular geometry without knowing the dimensions in advance and would potentially enhance the accuracy of the model and its effectiveness in the field.

Although there is an initial outlay involved in gathering the information required for the model, it can be done prior to testing. The successful verification indicates that it could be used for a range of scenarios including reconstructing the signals from around pipe bends. In the example studied, the torsional wave mode was excited beyond the bend which may not be physically possible in practice. However, it has been shown that time reversal techniques can be used to achieve close to the same conditions. The analytical model can also be used to calculate the inputs required for this.

Dispersion has not been included in the analytical model. Some dispersion is included implicitly in the finite element input data used. However, for long sections of straight pipe after the bend, the effect of dispersion will become significant. It is possible to include dispersion in the model using the straight pipe simulation technique presented in Chapter 4. Amongst other features, this would allow the analytical model to be used to calculate inputs for focussing beyond pipe bends. Since the analytical model is significantly faster than finite element analysis, it could be used in the field for this purpose.

Three possible torsional family wave modes exist for the frequency used in the example. At higher frequencies and in larger pipe sizes, more wave modes exist. This would therefore increase the number of finite element models required to create the input data and increase calculation times. However, field experience has shown that the signal distortion from bends is more significant in smaller diameter pipes for which there are limited numbers of wave modes in existence and so the model is well suited to these cases.

The modelling method has been verified using the example of an induction formed pipe bend. However, it is a general procedure that could be applicable to any geometry such as a pipe bend elbow with welds. This is because it uses finite element analysis to calculate the behaviour of the complex geometry and relies on known behaviour of guided waves in straight sections of pipe. Verification of the

procedure for other scenarios will be the subject of future work.

The torsional family has been considered in isolation here since the applied excitations preferentially excite these wave modes. In cases where there are two or more families of wave modes present, the principle of superposition could be applied to include the simulation of the other families. The number of permutations required will increase as will the number of finite element models needed to produce the required input data.

Flaw sizing techniques such as those presented in Chapter 5 have been developed that require precise information about the mode content of the signals. The presence of a pipe bend or other feature will alter this and therefore adversely affect the sizing procedure. It has been shown that it is possible to remove the distortion caused by pipe bends from the signal from a flaw, therefore opening up the possibility of flaw sizing beyond pipe bends.

7.8 Conclusions

An experimentally validated finite element modelling technique has been used to understand the behaviour of torsional family guided waves in pipe bends for a relatively tight bend radius in an 88.9mm outer diameter, 5.49mm wall thickness. The orientation and amplitudes of the wave modes received after the bend were quantified for a range of possible input excitation scenarios. In most cases all of the possible wave modes in the torsional family were excited beyond the bend to some degree. This indicates that standard guided wave inspection would be potentially inaccurate since flexural waves are used to identify the presence of flaws. Additionally, the effect of wall thickness changes arising from the induction bending process (a common method for making bends in pipes) was studied using finite element analysis. The results indicated that changes in wall thickness caused by induction bending did not significantly affect the signals received beyond the pipe bend.

A method has been suggested which can be used to predict the behaviour of guided waves beyond pipe bends. The model was successfully verified against finite element results for the reflections from a flaw propagating through a pipe bend. The analytical method requires the use of finite element data as an input but this is limited and in the example studied a total solution time of 2.5 hours was all that was required. Once this computation has been undertaken for a given geometry, the results may be used for an unlimited number of cases for that scenario.

Moreover, it has been demonstrated that, in conjunction with a time reversal inspection technique, the analytical method can be used to ‘undo’ the distortion of

the signals caused by the pipe bend therefore opening up the possibility of using guided waves to not only detect but characterise flaws beyond pipe bends.

A paper arising from this work was submitted to the Journal of the Acoustical Society of America in May 2012.

Chapter 8

Conclusions and Recommendations for Future Work

8.1 Conclusions

A combination of modelling and experiments has been used to develop quantitative guided wave inspection techniques. Throughout the work, computationally fast methodologies have been sought so that they can be used in conjunction with commercial equipment in the field. Firstly, an analytical model for guided wave excitation and propagation has been developed. This has then been used, in conjunction with newly developed equations for transmission and reflection coefficients from single flaws, to quantify the reflections from multiple flaws. Finally, a method that can be used to correct for signal distortion in complex pipe networks has been established and validated for a pipe bend example. This potentially allows the flaw sizing techniques to be used beyond pipe bends.

A computationally fast analytical model for the prediction of guided wave excitation and propagation has been developed. The method relies on finite element analysis to extract key information about the excitation of wave modes. However, this can be determined relatively quickly. The method can be applied to any prismatic cross section and could therefore be useful for the development of inspection procedures for structures where guided waves are not currently fully understood. It is also useful for more common guided wave inspection scenarios such as pipes in the development of part circumferential arrays for limited access scenarios. The model has the potential to be combined with other models such as those for flaws

and geometric features presented here.

The proposed analytical modelling method was compared to both transient finite element predictions and experimental data for a pipe example. Displacement history comparisons were made for five different positions and a spatial comparison was carried out for a fixed time. The agreement between the analytical model and the finite element predictions was good in all cases and the two models agreed well with the experimental data.

An article published in IEEE Transactions on Ultrasonics, Ferroelectrics and Frequency Control entitled ‘An analytical model for guided wave inspection optimization for prismatic structures of any cross section’ has arisen from the work presented in Chapter 4 [Sanderson & Catton, 2011b].

Suggested modifications to a flaw sizing procedure have been developed and demonstrated experimentally to work effectively for a range of pipe diameters and flaw sizes and shapes. The circumferential extent of all of the flaws detected was correctly categorised as either ‘narrow’ ($\leq 60^\circ$) or ‘non-narrow’. Where it was deemed possible to make measurements (‘non-narrow’ flaws), the through wall extent was found to be within 1.3mm of the actual value and the circumferential extent was found to be within 23° of the actual value.

Estimates have been made based on typical real corrosion shapes taken from laser profilometry data. The deepest flaw that could exist without being detected by the guided wave flaw sizing procedure resulted in a reduction in the maximum allowable operating pressure of just 5%. This, combined with the accurate flaw size assessments, indicates that the suggested guided wave flaw sizing procedure could be used conservatively as a direct input to a fitness-for-service assessment.

The work on flaw sizing goes some way towards allowing guided wave inspection to be used to accurately and reliably detect and characterise corrosion in pipelines. However, corrosion damage rarely results in a single isolated flaw and pipes often have a number of reflectors which each contribute to increased complexity in the received guided wave signals. An analytical model has been established which simulates the reflections from multiple flaws by combining newly developed theoretical approximations to the reflection and transmission coefficients with the analytical wave propagation model presented in Chapter 4.

The analytical model has been successfully verified using validated finite element analysis. It can therefore be used to predict and correct for the changes in amplitude of the different wave modes present in the reflected multimode guided wave signal. One of the main findings of this work is that the ratio between reflected wave modes is not preserved. Since guided waves are likely to have passed through

a number of features before being received at the transducer array, it is important to correct for any distortion of the amplitudes if flaw imaging and sizing techniques (such as the one presented in Chapter 5) are to be used. A paper arising from the work on multiple flaws was submitted to IEEE Transactions on Ultrasonics, Ferroelectrics and Frequency Control in August 2012.

An experimentally validated finite element modelling technique has been used to understand the behaviour of torsional family guided waves in pipe bends for a relatively tight bend radius in a relatively small diameter pipe. The orientation and amplitudes of the wave modes received after the bend were quantified for a range of possible input excitation scenarios. In most cases all of the possible wave modes in the torsional family were excited beyond the bend to some degree. This could cause potential inaccuracy in guided wave inspection results since flexural wave modes are used to indicate the presence of flaws. Additionally, the effect of wall thickness changes arising from the induction bending process (a common method for making bends in pipes) was studied using finite element analysis. The results indicated that changes in wall thickness caused by induction bending did not significantly affect the signals received beyond the pipe bend.

A method has been suggested which can be used to predict the behaviour of guided waves beyond pipe bends. The model was successfully verified against finite element results for the reflections from a flaw propagating through a pipe bend. The analytical method requires the use of finite element data as an input but this is limited and in the example studied a total solution time of a few hours was all that was required. Once this computation has been undertaken for a given geometry, the results may be used for an unlimited number of cases for that scenario.

Moreover, it has been demonstrated that, in conjunction with a time reversal inspection technique, the analytical method can be used to ‘undo’ the distortion of the signals caused by the pipe bend therefore opening up the possibility of using guided waves to not only detect but characterise flaws beyond pipe bends. A paper arising from the work on pipe bends was submitted to the Journal of the Acoustical Society of America in May 2012.

8.2 Recommendations for future work

The advances presented in this thesis all benefit from access to individual transducer elements around the circumference of the pipe. Current hardware is limited in this respect and the experimental work was therefore carried out using bespoke equipment, which would not be practical for field use. Therefore development of

hardware and software in this respect should be considered.

All of the studies carried out here were based on uncoated pipe, surrounded by air. Pipelines are often coated for protection and carry fluids. This will potentially affect the behaviour of guided waves and therefore the quantification techniques presented here. The attenuation can be quantified using programmes such as Disperse[Pavlakovic *et al.*, 1997]. Therefore it should be possible to take account of attenuation due to coatings. The inclusion of attenuation effects into the procedures presented here would be worthwhile and would allow broader use of the methods presented here.

The analytical model was shown to be effective for simulating the excitation of guided waves in pipes. The combination of this model with the techniques suggested for dealing with multiple flaws and pipe bends should be tested experimentally. The capability of such computationally fast models to predict guided wave behaviour in complex pipe networks should be established.

The flaw sizing technique was successfully validated for a range of cases. However, the suggested refinement to the technique involving the use of a greater number of flexural wave modes was only tested for one case. The research indicated that there is likely to be an optimum number of flexural wave modes depending on the pipe size. Further investigation of this using a combination of modelling and experiment would help to establish the optimum for a range of pipes sizes. Moreover, the refinement should be tested to determine whether the size of flaws classed as ‘narrow’ in the current procedure could actually be reliably measured.

The flaw sizing technique was shown to be capable of determining the circumferential extent and through wall extent of flaws. The axial extent of the flaw is also a useful parameter in assessing the fitness-for-service of the pipeline. It was suggested that the cyclic nature of the reflected amplitude could be used to determine the axial extent. However, there are multiple axial extents that would give the same reflected amplitude and so a unique solution using this alone would not be possible. A pattern matching or cross-correlation technique may be one way to establish a unique axial extent measurement.

Further improvements to the accuracy of the flaw sizing technique could be made by tailoring the assumed shape of the cross sectional area to typical corrosion. Data such as the laser profilometry data used could be used to establish a suitable formula for calculating the through wall extent of the flaw from the measured circumferential extent and cross sectional area loss.

The multiple flaws technique was successfully verified against finite element analysis of two flaws. This study should be extended to experimentally validate the

model for two or more flaws. Additionally, other features such as welds are likely to have an effect on the reflected wave modes. The effects of welds could be considered using a procedure similar to that presented for flaws.

The modelling procedure developed for dealing with pipe bends was successfully validated on one pipe size and bend radius. The procedure should be tested for a range of pipe sizes and bend radii. The technique has the potential to be applied to other geometrical features. This should be validated for other common occurrences such as bends with welds, clamps, pipe supports and pipe branches. Additionally, the concept of flaw sizing beyond a bend was developed but was not experimentally validated. An experimental programme to attempt flaw sizing beyond pipe bends should be carried out to establish the limitations of the technique.

The incorporation of the quantitative inspection techniques developed here into commercial equipment and procedures would permit a substantial experimental testing programme to be carried out. This should allow previously unobtainable data on flaws to be gathered and validated (where it is possible to characterise the flaws detected). Validation data would aid industry acceptance of guided wave inspection as a quantitative technique.

References

- ABAQUS. 2010. *ABAQUS Version 6.10 user's manual*. Simulia.
- Alleyne, D N. 1991. *The nondestructive testing of plates using ultrasonic Lamb waves*. Ph.D. thesis, Imperial College.
- Alleyne, D N, & Cawley, P. 1996. The Excitation of Lamb Waves in Pipes Using Dry-Coupled Piezoelectric Transducers. *Journal of Nondestructive Evaluation*, **15**(1).
- Alleyne, D N, & Lowe, M J S. 1998. The reflection of guided waves from circumferential notches in pipes. *ASME J Appl Mech*, **65**, 635 – 641.
- Alleyne, D N, Pavlakovic, B, Lowe, M J S, & Cawley, P. 2001. Rapid, long range inspection of chemical plant pipework using guided waves. *Insight*, **43**(2), 93–96.
- Aristegui, C, Cawley, P, & Lowe, M. 2000. Reflection and mode conversion of guided waves at bends in pipes. *In: Review of Progress in Quantitative Nondestructive Evaluation*.
- Bai, H, Shah, A H, N, Popplewell, & Datta, S K. 2001. Scattering of guided waves by circumferential cracks in steel pipes. *Journal of Applied Mechanics*, **68**, 619–631.
- Barshinger, J, Rose, J, & Avioli, M. 2002. Guided wave resonance tuning for pipe inspection. *Journal of Pressure Vessel Technology*, **124**, 302–310.
- Bartoli, I, Lanza di Scalea, F, Fateh, M, & Viola, E. 2005. Modeling guided wave propagation with application to the long-range defect detection in railroad tracks. *NDT&E International*, **38**, 325–334.
- Beard, M D. 2002. *Guided wave inspection of embedded cylindrical structures*. Ph.D. thesis, Imperial College.

- Böttger, W, Schneider, H, & Weingarten, W. 1987. Prototype EMAT system for tube inspection with guided ultrasonic waves. *Nuclear Engineering and Design*, **102**(102), 369–376.
- Carandente, R, & Cawley, P. 2011. The effect of complex defect profiles on the reflection of guided waves in pipes. *In: Review of Progress in Quantitative Non-destructive Evaluation, Volume 30*.
- Carandente, R, & Cawley, P. 2012. The effect of complex defect profiles on the reflection of the fundamental torsional mode in pipes. *NDT&E International*, **46**, 4147.
- Carandente, R, Ma, J, & Cawley, P. 2010. The scattering of the fundamental torsional mode from axi-symmetric defects with varying depth profile in pipes. *J. Acoust. Soc. Am.*, **127** (6), 34403448.
- Catton, P. 2009. *Long Range Ultrasonic Guided Waves for the Quantitative Inspection of Pipelines*. Ph.D. thesis, Brunel University.
- Catton, P, Mudge, P, & Balachandran, W. 2008a. Advances in Defect characterisation using Long Range Ultrasonic Testing of Pipes. *Insight*, **50**(9).
- Catton, P, Mudge, P, D’Zhurko, D, & Rose, J. 2008b. Improved Methodology For Guided Wave Inspections Of Pipelines. *Pipeline and Gas Journal*, June, 36–44.
- Cawley, P, Lowe, M J S, & Simonetti, F. 2002. The reflection coefficient of extensional guided waves in pipes as a function of defect size and frequency. *J. Mech. Eng. Sci.*, **26**, 1131–1143.
- Cheeke, J D N. 2002. *Fundamentals and Applications of Ultrasonic Waves*. CRC Press.
- Choi, M-S, Kim, S-Y, Kwun, H, & Light, G M. 2004. Transmission Line Model for Simulation of Guided-Wave Defect Signals in Piping. *IEEE Trans Ultra Ferr Freq Control*, **51**(5), 640–643.
- Cobb, A C, Kwuna, H, Caseres, L, & Janega, G. 2012. Torsional guided wave attenuation in piping from coating, temperature, and large-area corrosion. *NDT&E International*, **47**, 163170.
- Croft, A, Davison, R, & Hargreaves, M. 1992. *Engineering Mathematics*. Addison-Wesley.

- Davies, J, & Cawley, P. 2009. The Application of Synthetic Focusing for Imaging Crack-Like Defects in Pipelines Using Guided Waves. *IEEE Trans Ultra Ferr Freq Control*, **56**(4), 759–771.
- Demma, A, Cawley, P, & Lowe, M J S. 2002. Guided waves in curved pipes. *In: Review of Progress in Quantitative Nondestructive Evaluation, Volume 21*.
- Demma, A, Cawley, P, Lowe, M, & Roosenbrand, A. 2003. The reflection of the fundamental torsional mode from cracks and notches in pipes. *J. Acoust. Soc. Am.*, 611 – 625.
- Demma, A, Cawley, P, Lowe, M, Roosenbrand, A, & Pavlakovic, B. 2004. The reflection of guided waves from notches in pipes: a guide for interpreting corrosion measurements. *NDT&E International*, **37**(3), 167–180.
- Demma, A, Cawley, P, & Lowe, M. 2005. The effect of bends on the propagation of guided waves in pipes. *Transactions of the ASME*, **127**.
- Ditri, J. 1994. Utilization of guided elastic waves for the characterization of circumferential cracks in hollow cylinders. *J. Acoust. Soc. Am.*, **96**(6), 3769–3775.
- Ditri, J, & Rose, J. 1992. Excitation of guided elastic wave modes in hollow cylinders by applied surface tractions. *J. Appl. Phys.*, **72**(7), 2589–2597.
- Domany, E, EntinWohlman, O, & Mizrachi, L. 1984. Multiple scattering formalism: Application to scattering by two spheres. *J. Appl. Phys.*, **56** (132), 132–136.
- Drinkwater, B, Dwyer-Joyce, R, & Cawley, P. 1997. A study of the transmission of ultrasound across solidrubber interfaces. *J. Acoust. Soc. Am.*, **101** (2), 970–981.
- Drinkwater, B W, & Wilcox, P D. 2006. Ultrasonic arrays for non-destructive evaluation: A review. *NDT&E International*, **39**, 525–541.
- Fitch, A H. 1963. Observation of elastic pulse propagation in axially symmetric and nonaxially symmetric longitudinal modes of hollow cylinders. *J. Acoust. Soc. Am.*, **35**(5), 706–707.
- Fromme, P, Wilcox, P D, Lowe, M J S, & Cawley, P. 2006. On the Development and Testing of a Guided Ultrasonic Wave Array for Structural Integrity Monitoring. *IEEE Trans Ultra Ferr Freq Control*, **53**(4).
- Fuller, C R. 1981. The effects of wall discontinuities on the propagation of flexural waves in cylindrical shells. *Journal of Sound and Vibration*, **75**(2), 207–228.

- Gavric, L. 1995. Computation of Propagative Waves in Free Rail Using Finite element Technique. *Journal of Sound and Vibration*, **185**, 531–543.
- Gazis, D. 1959. Three-dimensional investigation of the propagation of waves in hollow circular cylinders. I. Analytical foundation and II. Numerical results. *Acoustical society of America*, **31**(5), 568–573.
- Ghosh, J. 1923. Longitudinal Vibrations of a Hollow Cylinder. *Bulletin of the Calcutta Mathematical Society*, **14**(1), 31–40.
- Gridin, D, Craster, R V, Fong, J, Lowe, M J S, & Beard, M. 2003. The high-frequency asymptotic analysis of guided waves in a circular elastic annulus. *Wave Motion*, **38**, 6790.
- Harris, J G. 2002. Rayleigh wave propagation in curved waveguides. *Wave Motion*, **36**, 425–441.
- Hayashi, T, & Murase, M. 2005. Defect imaging with guided waves in a pipe. *J. Acoust. Soc. Am.*, **117**, 2134–2140.
- Hayashi, T, & Rose, J L. 2003. Guided wave simulation and visualization by a semianalytical finite element method. *Materials Evaluation*, 75–79.
- Hayashi, T, Kawashima, K, Sun, Z, & Rose, J. 2003a. Analysis of flexural mode focusing by semianalytical finite element method. *J. Acoust. Soc. Am.*, **113**(3), 1241–1248.
- Hayashi, T, Song, W, & Rose, J. 2003b. Guided wave dispersion curves for a bar with an arbitrary cross-section, a rod and rail example. *Ultrasonics*, **41**, 175–183.
- Hayashi, T, Kawashima, K, Sun, Z, & Rose, J. 2005a. Guided wave focusing mechanics in pipe. *Journal of Pressure Vessel Technology*, **127**, 317–321.
- Hayashi, T, Kawashima, K, Sun, Z, & Rose, J L. 2005b. Guided Wave Propagation Mechanics Across a Pipe Elbow. *Journal of Pressure Vessel Technology*, **127**, 322–327.
- Hayashi, T, Miyazaki, Y, Kataoka, K, & Takikawa, M. 2007. Long-Range Defect Detection with Guided Waves for Bottom Edges of Rails. *Pages 169–176 of: Thomson, D. O., & Chimenti, D. E. (eds), Review of Progress in Quantitative Nondestructive Evaluation*, vol. 975. Golden, CO: AIP Conference Proceedings.

- Herrmann, G, & Mirsky, I. 1956. Three-dimensional and shell theory analysis of axially-symmetric motions of cylinders. *J. Appl. Mech.*, **23**(4), 563-568.
- Huang, D, Redekop, D, & Xu, B. 1997. Natural frequencies and mode shapes of curved pipes. *Computers & Structures*, **63**(3), 46-73.
- Hutchins, D A, Palmer, S B, & Sturrock, W R. 1991. Rayleigh to shear wave mode conversion at surface defects. *Nondestructive Testing and Evaluation*, **6**.
- Koshiha, M, Karakida, S, & Suzuki, M. 1984. Finite-Element Analysis of Lamb Wave Scattering in an Elastic Plate Waveguide. *IEEE Trans Sonics Ultrason*, **31**(1), 18-25.
- Kwun, H, & Bartels, K A. 1996. Experimental observation of elastic-wave dispersion in bounded solids of various configurations. *J. Acoust. Soc. Am.*, **99** (2), 962-968.
- Kwun, H, & Holt, A E. 1995. Feasibility of under-lagging corrosion detection in steel pipe using the magnetostrictive sensor technique. *NDT&E International*, **28**(4), 211-214.
- Kwun, H, & Kim, S. 2007. Guided-Wave Defect Signal Simulation Based on Transmission Line Model. *Pages 163-169 of: Thomson, D. O., & Chimenti, D. E. (eds), Review of Progress in Quantitative Nondestructive Evaluation*, vol. 975. Golden, CO: AIP Conference Proceedings.
- Kwun, H, Kim, S, & Light, G. 2001. Long-Range Guided Wave Inspection of Structures Using the Magnetostrictive Sensor. *Journal of the Korean Society of NDT*, **21**, 383 - 390.
- Kwun, H, Kim, S Y, Choi, M S, & Walker, S M. 2004. Torsional guided-wave attenuation in coal-tar-enamel-coated, buried piping. *NDT&E International*, **37**, 663-665.
- Lamb, H. 1910. *The Dynamical Theory of Sound*. New York: E. Arnold.
- Leonard, K, & Hinders, M. 2003. Guided wave helical ultrasonic tomography of pipes. *J. Acoust. Soc. Am.*, **114**(2), 767-774.
- Leonard, K R, & Hinders, M K. 2005. Lamb wave tomography of pipe-like structures. *Ultrasonics*, **43**, 574-583.
- Leung, A Y T, & Kwok, N T C. 1994. Free Vibration Analysis of a Toroidal Shell. *Thin-Walled Structures*, **18**, 317-332.

- Leutenegger, T, & Dual, J. 2004. Non-destructive testing of tubes using a time reverse numerical simulation (TRNS) method. *Ultrasonics*, **41**, 811822.
- Li, J, & Rose, J. 2001a. Excitation and propagation of non-axisymmetric guided waves in a hollow cylinder. *Acoustical society of America*, **109**(2), 457–464.
- Li, J, & Rose, J. 2001b. Implementing guided wave mode control by use of a phased transducer array. *IEEE Trans Ultra Ferr Freq Control*, **48**(3), 761–768.
- Li, J, & Rose, J L. 2002. Angular-Profile Tuning of Guided Waves in Hollow Cylinders Using a Circumferential Phased Array. *IEEE Trans Ultra Ferr Freq Control*, **49**(12), 1720–1729.
- Li, J, & Rose, J L. 2006. Natural beam focusing of non-axisymmetric guided waves in large-diameter pipes. *Ultrasonics*, **44**, 3545.
- Liu, G, & Qu, J. 1998. Transient wave propagation in a circular annulus subjected to transient excitation on its outer surface. *J. Acoust. Soc. Am.*, **104** (3), 1210–1220.
- Liu, Z, He, C, Wu, B, Wang, X, & Yang, S. 2006. Circumferential and longitudinal defect detection using T(0,1) mode excited by thickness shear mode piezoelectric elements. *Ultrasonics*, **44**, 11351138.
- Long, R, Lowe, M, & Cawley, P. 2003. Attenuation characteristics of the fundamental modes that propagate in buried iron water pipes. *Ultrasonics*, **41**, 509519.
- Love, A E H. 1911. *Some problems of geodynamics*. Cambridge University Press.
- Løvstad, A, & Cawley, P. 2011a. The reflection of the fundamental torsional guided wave from multiple circular holes in pipes. *NDT&E International*, **44**, 553–562.
- Løvstad, A, & Cawley, P. 2011b. The reflection of the fundamental torsional mode from multiple small defects in pipes. *In: Review of Progress in Quantitative Nondestructive Evaluation, Volume 30*.
- Løvstad, A, & Cawley, P. 2012. The reflection of the fundamental torsional mode from pit clusters in pipes. *NDT&E International*, **46**, 83–93.
- Lowe, M, Alleyne, D, & Cawley, P. 1998a. The Mode Conversion of a Guided Wave by a Part-Circumferential Notch in a pipe. *Journal of Applied Mechanics*, **65**, 649–656.
- Lowe, M J S, Alleyne, D N, & Cawley, P. 1998b. Defect detection in pipes using guided waves. *Ultrasonics*, **36**, 147–154.

- Luo, W, & Rose, J L. 2007. Phased array focusing with guided waves in a viscoelastic coated hollow cylinder. *J. Acoust. Soc. Am.*, **121**(4), 1945–1955.
- Mace, B R, Duhamel, D, Brennan, M J, & Hinke, L. 2005. Finite element prediction of wave motion in structural waveguides. *J. Acoust. Soc. Am.*, **117** (5), 2835–2843.
- Mallett, R, Mudge, P J, Gan, T-H, & Balachandran, W. 2007. Analysis of cross-correlation and wavelet de-noising for the reduction of the effects of dispersion in long-range ultrasonic testing. *Insight*, **49**(6).
- Mead, D J. 1973. A general theory of harmonic wave propagation in linear periodic systems with multiple coupling. *Journal of Sound and Vibration*, **27**(2), 235–260.
- Meeker, T R, & Meitzler, A H. 1964. Guided Wave propagation in Elongated Cylinders and Plates. *Physical acoustics*, **1A**, 111–167.
- Meggert, E. 2008. Situation Report for Prudhoe Bay. *Alaska Department of Environmental Conservation*.
- Meitzler, A. 1961. Mode Coupling Occurring in the Propagation of Elastic Pulses in Wires. *J. Acoust. Soc. Am.*, **33**(4), 435–445.
- Mirsky, I, & Herrmann, G. 1958. Axially symmetric motions of thick cylindrical shells. *J. Appl. Mech.*, **80**, 97–102.
- Mohr, & Holler. 1976. On Inspection of Thin-Walled Tubes for Transverse and Longitudinal Flaws by Guided Ultrasonic Waves. *IEEE Trans Sonics Ultrason*, **23**(5), 369–374.
- Morgan, E, & Crosse, P. 1978. The Acoustic Ranger, a new instrument for tube and pipe inspection. *NDT International*, **11**(4), 179–183.
- Moser, F, Jacobs, L J, & Qu, J. 1999. Modeling elastic wave propagation in waveguides with the finite element method. *NDT&E International*, **32**, 225234.
- Mu, J, & Rose, J L. 2007. Guided wave normal modes in hollow cylinders with viscoelastic coatings. In: *Review of Progress in Quantitative Nondestructive Evaluation*.
- Mu, J, Zhang, L, & Rose, J L. 2007. Defect circumferential sizing by using long range ultrasonic guided wave focusing techniques in pipe. *Nondestructive Testing and Evaluation*, **22**(4), 239253.

- Mudge, P. 2001. Field application of the Teletest long-range ultrasonic testing equipment. *Insight*, **43(2)**, 74–77.
- Mudge, P, & Catton, P. 2007. Quantification of Defect Size from Long Range Guided Wave Ultrasonic Tests on Pipes. *Pages 147–154 of: Thomson, D. O., & Chimenti, D. E. (eds), Review of Progress in Quantitative Nondestructive Evaluation*, vol. 975. Golden, CO: AIP Conference Proceedings.
- Mudge, P J, Lank, A M, & Alleyne, D N. 1996. A long range method of detection of corrosion under insulation in process pipe work. *In: 5th European Union Hydrocarbons Symposium, Edinburgh, 26-28 November.*
- Nishiguchi, I, Sakata, F, & Hamada, S. 2008. Theoretical and experimental investigation of pipe wall thinning detection using guided waves. *In: Proceedings of PVP2008.*
- Nishino, H. 2010. A Feasibility Study on Pipe Inspection Using Ultrasonic Guided Waves for Maintenance of Nuclear Power Plants. *In: International Symposium on the Ageing Management & Maintenance of Nuclear Power Plants.*
- Nishino, H, Yoshida, K, Cho, H, & Takemoto, M. 2006. Propagation phenomena of wideband guided waves in a bended pipe. *Ultrasonics*, **44**, 11391143.
- Pao, Y, & Mindlin, R. 1960. Dispersion of flexural waves in an elastic circular cylinder. *J appl Meteorol*, **27**, 513 – 520.
- Pavlakovic, B, Lowe, M, Alleyne, D, & Cawley, P. 1997. *Disperse: a general purpose program for creating dispersion curves.* Imperial College London.
- Pei, J, Yousuf, M I, Degertekin, F L, Honein, B V, & Khuri-Yakub, B T. 1996. Lamb Wave Tomography and Its Application in Pipe Erosion/Corrosion Monitoring. *Res Nondestr Eval (1996) 8:*, **8**, 189197.
- PHMSA. 2012. *Distribution, Transmission, and Liquid Accident and Incident Data.* Tech. rept. PHMSA.
- Priemer, Roland. 1991. *Introductory Signal Processing.* World Scientific.
- Ratassepp, M, & Klauson, A. 2006. Curvature effects on wave propagation in an infinite pipe. *Ultrasonics*, **2(59)**, 19–25.
- Rayleigh, Lord. 1885. On waves propagated along the plane surface of an elastic solid. *Proc. Lond. Math. Soc.*, **17(4)**.

- Rayleigh, Lord. 1910. The Problem of the Whispering Gallery. *Proc London Math Soc*, **20**, 1001–1004.
- Redekop, D. 1997. Dynamic response of curved pipes. *Int. J. Press. Ves. & Piping*, **70**, 167–172.
- Rose, J. 1999. *Ultrasonic Waves in Solid Media*. Cambridge: Cambridge University Press.
- Rose, J. 2002a. A baseline and vision of ultrasonic guided wave inspection potential. *Journal of Pressure Vessel Technology*, 273–282.
- Rose, J. 2002b. Standing on the shoulders of giants - An example of guided wave inspection. *Materials Evaluation*, **59**, 1234 – 1238.
- Rose, J, Rajana, K, & Carr, F. 1994a. Ultrasonic guided wave inspection concepts for steam generator tubing. *Materials Evaluation*, 307–311.
- Rose, J, Avioli, M, & Song, W. 2002. Application and potential of guided wave rail inspection. *Insight*, **44(6)**, 353–358.
- Rose, J, Zongqi, Sun, Mudge, P, & Avioli, M. 2003. Guided Wave Flexural Mode Tuning and Focusing for Pipe Testing. *Materials Evaluation*, 162 – 167.
- Rose, J, Zhang, L, Avioli, M, & Mudge, P. 2005. A natural focusing low frequency guided wave experiment for the detection of defects beyond elbows. *In: Transactions of the ASME*, vol. 127.
- Rose, J, Mu, J, & Velsor, J. K. Van. 2007. New directions in guided wave pipe testing. *Materials Evaluation*, **375-378**, 621–624.
- Rose, J L. 2000. Guided Wave Nuances for Ultrasonic Nondestructive Evaluation. *IEEE Trans Ultra Ferr Freq Control*, **47(3)**, 575–583.
- Rose, J L, & Zhao, X. 2001. Flexural mode tuning for pipe elbow testing. *Materials Evaluation*, 621–624.
- Rose, J L, Ditri, J J, Pilarski, A, Rajana, K, & Carr, F. 1994b. A guided wave inspection technique for nuclear steam generator tubing. *NDT& E International*, **27 (6)**, 307–310.
- Rose, J L, Jiao, D, & Spanner, J. 1996. Ultrasonic guided wave NDE for piping. *Materials Evaluation*, 1310–1313.

- Rudd, K E, Leonard, K R, Bingham, J P, & Hinders, M K. 2007. Simulation of guided waves in complex piping geometries using the elastodynamic finite integration technique. *J. Acoust. Soc. Am.*, **121**(3), 1449-1458.
- Salley, L, & Pan, J. 2002. A study of the modal characteristics of curved pipes. *Applied Acoustics*, **63**, 189-202.
- Sanderson, R. 2003. The application of finite element modelling to guided wave testing systems. *Pages 256–63 of: Review of Progress in Quantitative Nondestructive Evaluation*. AIP Conference Proceedings.
- Sanderson, R. 2007. Long range ultrasonic guided wave focusing in pipe with application to defect sizing. *In: ICU Conference*.
- Sanderson, R, & Catton, P P. 2011a. Flaw sizing in pipes using long-range guided wave testing. *In: Review of Progress in Quantitative Nondestructive Evaluation, Volume 30*.
- Sanderson, R, & Smith, S. 2002. The Application of Finite Element Modelling to Guided Ultrasonic Waves in Rails. *Insight*, **44**(6).
- Sanderson, R M, & Catton, P P. 2011b. An Analytical Model for Guided Wave Inspection Optimization for Prismatic Structures of Any Cross Section. *IEEE Trans Ultra Ferr Freq Control*, **58**(5), 1016–1026.
- Schafbuch, P J, Thompson, R B, & Rizzo, F J. 1993. Elastic scatterer interaction via generalized Born series and far-field approximations. *J. Acoust. Soc. Am.*, **93**(1), 295–307.
- Shin, H, & Rose, J. 1998. Guided Wave Tuning Principles for Defect Detection in Tubing. *Journal of Nondestructive Evaluation*, **17**(1), 27–36.
- Shin, H, & Rose, J. 1999. Guided waves by axisymmetric and non-axisymmetric surface loading on hollow cylinders. *Ultrasonics*, **37**, 355-363.
- Silk, M, & Bainton, K. 1979. The propagation in metal tubing of ultrasonic wave modes equivalent to lamb waves. *Ultrasonics*, 11–19.
- Siqueira, M, Gatts, C, da Silva, R, & Rebello, J. 2004. The use of Ultrasonic Guided Waves and Wavelets Analysis in Pipe Inspection. *Ultrasonics*, **41**(10), 785–797.
- Thompson, R B, Alers, G A, & Tennison, M A. 1972. Applications of Direct Electromagnetic Lamb Wave Generation to Gas Pipeline Inspection. *IEEE Ultrasonics Symposium*, 9194.

- Tiratsoo, J N H (ed). 1999. *Pipeline Pigging Technology*. Butterworth-Heinemann.
- Tucker, R, Kercel, S, & Varma, V. 2003 (September). Characterisation of Gas Pipeline Flaws using Wavelet Analysis. *In: Quality Control Using Artificial Intelligence*.
- Velichko, A, & Wilcox, P. 2009a. Excitation and scattering of guided waves: Relationships between solutions for plates and pipes. *J. Acoust. Soc. Am.*, **125**(6), 3623-3631.
- Velichko, A, & Wilcox, P D. 2009b. Post-processing of guided wave array data for high resolution pipe inspection. *J. Acoust. Soc. Am.*, **126**(6), 2973-2982.
- Viktorov, I. 1967. *Rayleigh and Lamb Waves - Physical Theory and Applications*. New York, NY: Plenum Press.
- Volker, A, & Bloom, J. 2011. Guided wave time travel tomography for bends. *In: Review of Progress in Quantitative Nondestructive Evaluation, Volume 30*.
- Wang, R-T. 2000. Vibration of straight-curved-straight hollow shafts. *Journal of Sound and Vibration*, **234**(3), 369-386.
- Wilcox, P. 1998. *Lamb wave inspection of large structures using permanently attached transducers*. Ph.D. thesis, Imperial College.
- Wilcox, P. 2003. A rapid signal processing technique to remove the effect of dispersion from guided wave signals. *IEEE Trans Ultra Ferr Freq Control*, **50**(4), 419 - 427.
- Wilcox, P, Evans, M, Diligent, O, Lowe, M, & Cawley, P. 2002. Dispersion and excitability of guided acoustic waves in isotropic beams with arbitrary cross section. *In: Review of Progress in Quantitative Nondestructive Evaluation*.
- Wilcox, P, Evans, M, Pavlakovic, B, Alleyne, D, Vine, K, Cawley, P, & Lowe, M. 2003. Guided wave testing of rail. *Insight*, **45**(6), 413-420.
- Wright, O. 2012. Gallery of Whispers. *Physics World*, **February**, 31-36.
- Zemanek, J. 1972. An experimental and theoretical investigation of elastic wave propagation in a cylinder. *J. Acoust. Soc. Am.*, **51**, 265 - 283.
- Zhang, Li, & Rose, J L. 2006. Ultrasonic guided wave focusing beyond welds in a pipeline. *In: Review of Quantitative Nondestructive Evaluation, Volume 25*.

- Zhou, W J, Ichchou, M N, & Mencik, J M. 2009. Analysis of wave propagation in cylindrical pipes with local inhomogeneities. *Journal of Sound and Vibration*, **319**, 335–354.
- Zhu, W. 2002. An FEM simulation for guided elastic wave generation and reflection in hollow cylinders with corrosion defects. *Journal of Pressure Vessel Technology*, **124**, 108–117.
- Zhuang, W, Shah, A H, & Datta, S K. 1997. Axisymmetric guided wave scattering by cracks in welded steel pipes. *Jornal of Pressure Vessel Technology*, **119**, 401–405.
- Zienkiewicz, O, & Taylor, R. 2000. *The finite element method, Volume 1: The basis*. 5 edn. Butterworth-Heinemann.